Inaugural dissertation

for obtaining the doctoral degree

of the

Combined Faculty of Mathematics, Engineering and Natural Sciences

of the

Ruprecht-Karls-University

Heidelberg

Presented by

M.Sc. Katja Baur

born in Bensheim, Germany

Oral examination: 03. August 2023

Apical Neural Stem Cells

and the Effect of Growth/Differentiation Factor 15

on their Primary Cilia and Proliferation

Referees:
Prof. Dr. Hilmar Bading
Dr. Francesca Ciccolini

Summary

The ventricular-subventricular zone (V-SVZ) is one of the two main neurogenic niches in the mouse brain that maintains neurogenesis throughout adulthood. However, a closer characterisation of the different subtypes of the neural stem cells (NSCs) residing there, their contribution to neurogenesis and the specifics of their regulation is yet to be performed.

In the first part of this thesis, using a mouse model to genetically tag NSCs, I could show the presence of apical and basal NSCs in the adult V-SVZ. The two groups of NSCs differ in terms of Nestin expression and presence of primary cilia, which are predominantly observed in apical NSCs. Moreover, in a collaborative effort, I determined that although they also are capable of quiescence, cycling basal NSCs divide more rapidly than the apical counterpart and contribute the most to olfactory bulb neurogenesis in the adult mouse.

In the second part of this thesis, I investigated the effect of growth/differentiation factor 15 (GDF15) on NSCs in the V-SVZ. Here, I found for the first time that its only recently discovered receptor GDNF-family receptor alpha-like (GFRAL) is expressed in NSCs in the E18 lateral ganglionic eminence (GE) and adult V-SVZ, as well as in primary cilia. Using immunofluorescence on homozygous Gdf15 knock-out / LacZ knock-in ($Gdf15^{-/-}$) mice, I found that ablation of GDF15 increased proliferation and cell cycle speed especially at the apical side of the niche, and that apical cells carried shorter primary cilia, a phenotype that could be rescued by application of exogenous GDF15 protein for 24 h.

To determine the mechanisms behind these changes, I first analysed epidermal growth factor (EGF) receptor (EGFR) signalling. In the mutant germinal niche, surface EGFR protein levels were lower and EGFR signalling dynamics were altered. Although exposure to GDF15 rescued EGFR surface expression, manipulation of EGFR signalling did not rescue the defect in proliferation. Instead, I found that ciliary length regulators adenylate cyclase 3 and histone deacetylase 6 were overexpressed in the mutant mice, and that their inhibition using pharmacological blockers led to a rescue of both ciliary morphology and proliferation similar to GDF15 application. Lastly, I found that sonic hedgehog signalling, a vital ciliary signalling pathway during development, was impaired but still responsive in $Gdf15^{-/-}$ mice, suggesting an impact of the altered ciliary morphology on organelle signalling.

All in all, in this thesis I show that apical NSCs represent a smaller subgroup of NSCs in the V-SVZ and I describe for the first time the effect of GDF15 on the development of the apical region of the V-SVZ. This effect encompasses cilia morphology and proliferation of apical progenitors affecting the generation of apical NSCs and ependymal cells in the V-SVZ.

Zusammenfassung

Die ventrikulär-subventrikuläre Zone (V-SVZ) ist eine der beiden wichtigsten neurogenen Nischen im Gehirn der Maus, die die Neurogenese während des gesamten Erwachsenenalters aufrechterhalten. Eine genauere Charakterisierung der verschiedenen Subtypen der dort ansässigen neuralen Stammzellen (NSCs), ihres Beitrags zur Neurogenese und der Besonderheiten ihrer Regulation steht jedoch noch aus.

Im ersten Teil dieser Arbeit konnte ich mithilfe eines Mausmodells zur genetischen Markierung von NSCs das Vorhandensein von apikalen und basalen NSCs in der adulten V-SVZ nachweisen. Die beiden Gruppen von NSCs unterscheiden sich in Bezug auf die Expression von Nestin und das Vorhandensein von primären Zilien, die vor allem bei apikalen NSCs zu beobachten sind. Darüber hinaus habe ich, in Kollaboration, festgestellt, dass sich die basalen NSCs, die sich im Zellzyklus befinden, schneller teilen als die apikalen NSCs und am meisten zur Neurogenese des Riechkolbens in der erwachsenen Maus beitragen, obwohl sie auch zur Ruhephase fähig sind.

Im zweiten Teil dieser Arbeit untersuchte ich die Wirkung von Growth/differentiation factor 15 (GDF15) auf die NSCs in der V-SVZ. Dabei habe ich erstmalig herausgefunden, dass sein erst kürzlich entdeckter Rezeptor GDNF-family receptor alpha-like (GFRAL) in NSCs in der E18 ganglionären Eminenz (GE) und der adulten V-SVZ sowie in primären Zilien exprimiert wird. Mit Hilfe der Immunfluoreszenz an homozygoten Gdf15-Knock-out/LacZ-Knock-in-Mäusen ($Gdf15^{-/-}$) konnte ich feststellen, dass die Ablation von GDF15 die Proliferation und die Geschwindigkeit des Zellzyklus vor allem an der apikalen Seite der Nische erhöhte und dass apikale Zellen kürzere primäre Zilien trugen, ein Phänotyp, der durch die Verabreichung von exogenem GDF15-Protein für 24 Stunden gerettet werden konnte.

Um die Mechanismen hinter diesen Veränderungen zu bestimmen, analysierte ich zunächst die Signalübertragung durch den epidermalen Wachstumsfaktor (EGF) Rezeptor (EGFR). In der Keimnische der genveränderten Mäuse war die Menge an EGFR-Protein an der Zelloberfläche geringer und die EGFR-Signaldynamik war verändert. Obwohl die EGFR-Oberflächenexpression durch Applikation von GDF15 wiederhergestellt werden konnte, führte die Beeinflussung der EGFR-Signalübertragung nicht zu einer Verbesserung der Proliferationsstörung. Stattdessen stellte ich fest, dass Adenylatzyklase 3 und Histondeacetylase 6, bekannte Regulatoren der Länge von Zilien, in den mutierten Mäusen überexprimiert waren und dass ihre Hemmung durch pharmakologische Blocker, ähnlich wie GDF15-Applikation, zu einer Wiederherstellung sowohl der ziliären Morphologie als auch der Proliferation führte. Schließlich fand ich heraus, dass der Sonic-Hedgehog-Signalweg, ein wichtiger ziliärer Signalweg während der Entwicklung, in $Gdf15^{-/-}$-Mäusen zwar beeinträchtigt, aber immer noch aktivierbar war, was auf eine Auswirkung der veränderten ziliären Morphologie auf die Signalweiterleitung in der Organelle hindeutet.

Insgesamt zeige ich in dieser Arbeit, dass apikale NSCs eine kleinere Untergruppe der NSCs in der V-SVZ darstellen, und ich beschreibe zum ersten Mal die Wirkung von GDF15 auf die Entwicklung der apikalen Region der V-SVZ. Dieser Effekt umfasst die Zilienmorphologie und die Proliferation apikaler Vorläuferzellen, die die Bildung apikaler NSCs und ependymaler Zellen in der V-SVZ beeinflussen.

Table of Contents

Table of Figures

Table of Tables

Contribution Statement

Except where stated otherwise by reference or acknowledgment, the work presented was generated by myself under the supervision of Dr. Francesca Ciccolini during my doctoral studies.
Whenever a figure or parts thereof are identical to a previous publication or a manuscript in preparation, it is stated explicitly in the figure description. Copyright of the publication is granted under the creative commons license.

The following parts of the thesis have been already published in Baur *et al*. (2022)[2]:

- Overall results in Chapter III-1
- Figs. III-1D; III-2C; IV-1

The following parts of the thesis are part of a published pre-print, Baur *et al.* (2023)[1]:

- Overall results in chapter III-2.1, III-2.3, III-3.4 to III-3.6, III-4.1, III-4.2
- Figs. III-3A, C, D; III-5; III-10 A-C, E, F; III-11 to III-13; III-14 B, C, E, F; III-15 to III-18

The following parts of the thesis are part of a manuscript in preparation:

- Overall results in Chapter III-2.2, III-3.1 to III-3.3, III-4.3 a-e
- Figs. III-6 to III-9; III-20 to III-25

The following parts of the thesis contain contributions of others:

- All experiments utilizing flow cytometry (in Figs. III-14, III-25, III-26) were performed with the help of Gabriele Hölzl-Wenig (FACS technician), who supported me with gate setting and sorting. All analyses based on this data were performed by me.
- Fig. III-6E: Sample preparation by Andrea Hellwig (electron microscopy technician) and Sebastian Weber of the Electron Microscopy Core Facility Heidelberg. Imaging was performed by Andrea Hellwig. Samples were provided and analysis was performed by me.
- Fig. III-26: Sample processing and mass spectrometry were performed by Ute Bach and Marcin Luzarowski at the Core Facility for Mass Spectrometry & Proteomics (CFMP) in Heidelberg. Final data analysis was performed by me.
- Figs. III-7 A, III-10 D, III-13 E: Sample preparation and imaging was performed by Şeydanur Şan under my supervision and guidance, as part of undergraduate training. Final data analysis was performed by me.
- Fig. III-16 D, F: Some of the analysed western blots were performed by Manja von Hahn under my supervision and guidance, as part of undergraduate training. Sample preparation, final analysis and the blots displayed were made by me.
- Fig. III-23 C: Some of the cultures displayed were made by Myriam Draï under my supervision and guidance, as part of undergraduate training. Final analysis was made by me.

Abbreviations

Abbreviation	Meaning
8w	8 weeks old
AA	Amino acid
AC3	Adenylate cyclase 3
acT	acetylated tubulin
ADP	Adenosine diphosphate
AMD	AMD3100, Plerixafor
AU	Arbitrary unit
Arl13b	ADP-ribosylation-like factor 13b
Ascl1	Achaete-scute family bHLH transcription factor 1
bp	Base pairs
BSt	Brain stem
cAMP	Cyclic adenosine monophosphate
Cbl	Cerebellum
CD133	Cluster of differentiation 133, Prominin-1
CFMP	Core Facility for Mass Spectrometry & Proteomics
Ctx	Cortex
CXCR4	C-X-C chemokine receptor 4
DCX	Doublecortin
DG	Dentate gyrus
Dlx2	Distal-less homeobox 2
DMSO	Dimethyl sulfoxide
Doxy	Doxycycline
E10-18	Embryonic day 10-18
EGF	Epidermal growth factor
EGFR	EGF-receptor
E^h	Expressing EGFR at high levels
EMCF	Electron Microscopy Core Facility
ERK	Extracellularly regulated kinase
FACS	Fluorescence-activated cell sorter/sorting
FCS	Foetal calf serum
FGF-2	Fibroblast growth factor 2
FGFR1	FGF-receptor 1
FOP	FGFR1 oncogene partner
G^+	hGFAP:H2B-GFP reporter expressing
GDF15	Growth/differentiation factor 15
GDNF	Glial-derived neurotrophic factor
GE	Lateral ganglionic eminence
GFAP	Glial fibrillary acidic protein
GFP	Green fluorescent protein
GFRAL	GDNF-family receptor alpha-like
GPCR	G-protein coupled receptor
h	Hour(s)
H2B	Histone 2B
HDAC6	Histone deacetylase 6
hGFAP	Human GFAP promoter
HP	Hippocampus
HTh	Hypothalamus
LC-MS	Liquid chromatography mass spectrometry
LV	Lateral ventricle

min	Minute(s)
MS	Mass spectrometry
NP-40	Nonidet P 40 (detergent)
NSC	Neural stem cell
OB	Olfactory bulb
P2, P7	Postnatal day 2, 7
PBS	Phosphate-buffered saline
PCP	Planar cell polarity
PDGFR	Platelet-derived growth factor receptor
PFA	Paraformaldehyde
phEGFR	phosphorylated EGFR
phERK	phosphorylated ERK
pHH3	phosphorylated Histone H3
P^+	Prominin-1-expressing
Prom	Prominin-1
Ptch1	Patched1
RG	Radial glia
RTK	Receptor tyrosine kinase
SAG	Smoothened agonist
SAP	Subapical progenitor
ScEM	Scanning electron microscopy
SDF-1	Stromal-derived factor 1
SDS	Sodium dodecyl-sulfate
SEM	Standard error of mean
SGZ	Subgranular zone
Shh	Sonic hedgehog
Smo	Smoothened
SNP	Short neural progenitor
Sox2, Sox9	SRY-box 2, 9
SRY	Sex determining region
SuFu	Suppressor of Fused
SVZ	Subventricular zone
TAP	Transit-amplifying progenitor
TBS	Tris-buffered saline
TBS-T	TBS containing 0.1% Triton X-100
TGF	Transforming growth factor
TSA	Tubastatin A
V	Ventricle
V-SVZ	Ventricular-subventricular zone

I. Introduction

1. Neural stem cells and neurogenesis in the mouse brain

1.1 The ventricular-subventricular zone

Throughout adulthood, neural stem cells (NSCs) generate new neurons in the brain[3], a process called neurogenesis, ensuring among others the ability to make new memories and repair brain tissue in case of injury[4,5]. In the adult murine brain, there are two main neurogenic niches that ensure adult neurogenesis: the ventricular-subventricular zone (V-SVZ) that lines the lateral wall of the lateral ventricles, and the subgranular zone (SGZ) in the dentate gyrus of the hippocampus[6-8] (Figure I-1).

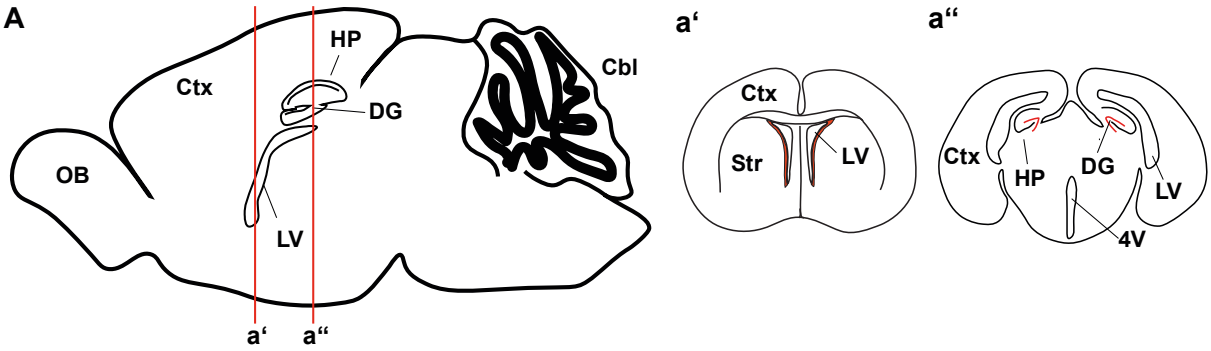

Figure I-1: Neurogenic niches in the adult mouse brain.
(A) Sketch of a sagittal section of the mouse brain. Red lines indicate where coronal sections in a' and a'' are located. (a') Location of the lateral V-SVZ, shown in red, in a sketch of a more rostral coronal section. (a'') Location of the SGZ, shown in red, in a sketch of a more caudal coronal section.
Cbl = cerebellum, Ctx = cortex, DG = dentate gyrus, HP = hippocampus, OB = olfactory bulb, LV = lateral ventricle, 4V = fourth ventricle.

The V-SVZ in adult animals is at its apical side, i.e. towards the ventricular lumen, lined with ependymal cells, or E-type cells, connected by tight junctions, which separate the cerebrospinal fluid (CSF)-filled lumen from the subventricular tissue[7,9] (for an overview of the niche, see Figure I-2 A, B). In between these ependymal cells, which are organized in a pinwheel-like fashion[10], there are the apical NSCs, also referred to as B1-type cells. These B1 cells display apical-basal polarity, i.e. they contact the ventricle with their apical membrane while a long basal process contacts the blood vessels deeper in the tissue. In adult animals, these apical NSCs are largely quiescent[11,12], i.e., they have temporarily exited the cell cycle and do not proliferate, but are capable of becoming activated via various signalling cascades (see also Chapter I-1.4), upon which they will again enter a proliferative state in which they undergo neurogenesis. Activated NSCs can then undergo symmetrical or asymmetrical cell division[13-16], giving rise to two NSC daughter cells or one NSC and one neural progenitor daughter cell, respectively. While NSC daughter cells will mostly enter quiescence again, neural progenitor cells will become transit amplifying progenitors (TAPs), also called C-type cells[12,17,18].

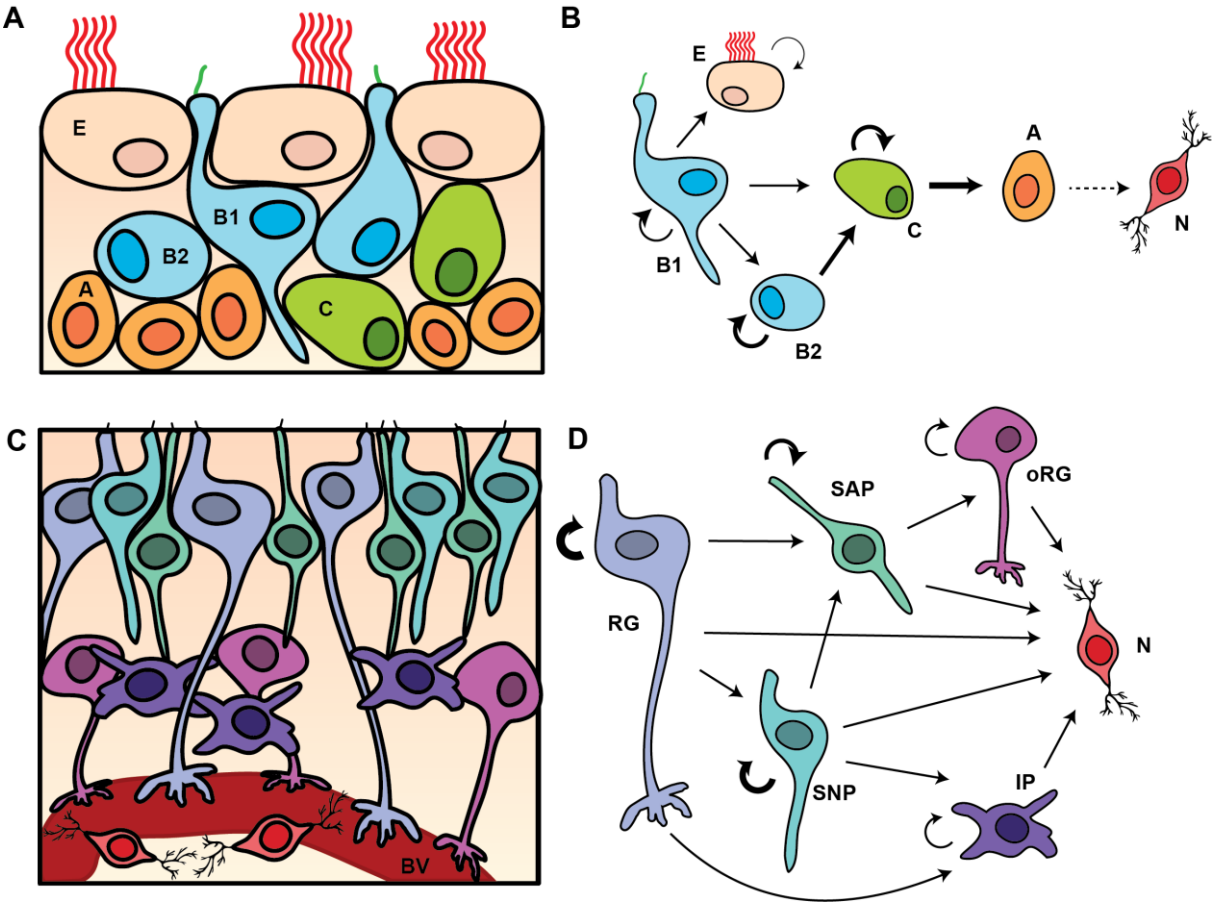

Figure I-2: Cellular organization in the adult V-SVZ and embryonic GE.
(A) Sketch of a cross-section of the adult V-SVZ showing the spatial organization of the different cell types in relation to the ventricle (above ependymal cell layer).
(B) Lineage progression from adult NSCs to neurons. A = neuroblast, B1 = apical NSC, B2 = basal NSC, C = transit amplifying progenitor, E = ependymal cell, N = neuron.
(C) Sketch of a cross-section of the embryonic GE showing the spatial organization of the different cell types in relation to the ventricle (top). BV = blood vessel
(D) Lineage progression from radial glia to neurons. RG = radial glia, SNP = short neural progenitor, SAP = subapical progenitor, oRG = outer radial glia, IP = intermediate progenitor, N = neuron.
Straight arrow = gives rise to, circle arrow = self-renewal/proliferation, dashed arrow = differentiation after migration. Thickness of arrows indicates relative frequency: thick arrow = frequently gives rise to, frequent self-renewal; thin arrow = rare self-renewal or differentiation.

When becoming a TAP, the progenitor daughter cell will move away from the apical surface[16] and proliferate quickly at the basal side of the SVZ, producing a high number of neuroblasts[19], also referred to as A-type cells. These neuroblasts are no longer capable of producing new cells and terminally differentiate into neurons after migrating along the rostral migratory stream to their target region, the olfactory bulb[20-22].

Furthermore, the basal side of the V-SVZ harbours basal NSCs, or B2-type cells, which have been termed niche astrocytes due to their expression of glial fibrillary acidic protein (GFAP) and perceived lack of neurogenesis[23-27]. However, recent studies have found evidence that there may be different pools of NSCs in the niche, including on the basal side[2,28,29]. The neurogenic potential of these cells is yet to be investigated.

1.2 The developing ventricular zone

Before birth, the lateral V-SVZ is not yet formed, and ependymal cells and mature, long-term quiescent NSCs are not yet present[30]. At embryonic day (E) 12, the ventricle is instead surrounded by the developing cortex on the dorsal side and on the lateral and ventral sides by the ganglionic eminences, namely the medial, caudal and lateral ganglionic eminence[31]. The lateral ganglionic eminence (GE), a pseudo-stratified epithelium, later gives rise to the adult lateral V-SVZ and forms the basal ganglia including the striatum. The GE is made up in large parts by highly proliferative radial glia cells which are derived from the initial neuroepithelial cells and emerge at E10[32]. Similar to apical NSCs, radial glia contact the lateral ventricle with their apical cell membrane while extending a basal process towards the pia and later, when the tissue becomes thicker, wrap around blood vessels in the tissue[33-35] (Figure I-2 C, D). Contrary to adult NSCs, while dividing, radial glia undergo interkinetic nuclear migration, during which the nucleus of the cell migrates towards the apical surface during M-phase and away from the ventricle during G- and S-phase[36,37]. Newly generated neuroblasts then migrate along the basal processes to differentiate into neurons in the striatum or other regions[32,38].

At E14, the lateral GE contains at the apical surface three types of progenitors: short neural progenitors (SNPs), subapical progenitors (SAPs) and radial glia, with radial glia giving rise to the other progenitor types during late embryonic development[33,39,40] (Figure I-2 D). SNPs are highly similar to radial glia, but instead have only a short basal process which does not contact basal blood vessels, while SAPs instead divide subapically, i.e., at a farther distance from the apical surface[33]. Therefore, from this age until birth[41-44], the different apical progenitor cells can be identified by the position of their nucleus during mitosis.

The niche at this age also contains outer radial glia, which like radial glia possess long basal processes but do not contact the apical surface and divide on the basal side of the niche only, and intermediate precursors, which do not possess apical-basal polarity[33,39]. Like adult NSCs, radial glia, SNPs and SAPs extend primary cilia into the ventricular lumen to receive signals present in the CSF[39] (see also Chapter I-2). Shortly before and after birth, NSCs in the embryonic GE increasingly begin to enter quiescence while ependymal cells start to differentiate[42,45]. Already 7 days post-partum (P7), the apical surface is largely covered by ependymal cells and during ageing, the number of NSCs as well as proliferation and neurogenesis steadily decrease until NSCs are largely depleted or in deep quiescence[46-49]. Already in adult animals (8 weeks old, 8w), neurogenesis is significantly reduced compared to P7 mice[2,20,47].

Lastly, ependymal cells in the V-SVZ also develop from radial glia shortly after birth[25,36,42] and are thought to be terminally differentiated; however, they are still capable of proliferation and produce more ependymal cells after injury[50].

1.3 Marker expression of NSCs and their progeny in the developing and adult V-SVZ

NSCs, radial glia and other cell types in the developing and adult V-SVZ can be identified by their distinct protein expression profiles (Figure I-3 A). Early radial glia cells show a clear expression pattern of Vimentin and Nestin[6,42], both intermediate filaments, as well as sex-determining region (SRY)-box (Sox) 2 and 9, transcription factors localized to the nucleus[27,51,52]. Radial glia in human embryos will express glial fibrillary acidic protein (GFAP), another intermediate filament, whereas this protein is expressed in these cells only shortly before birth in mice[53]. Currently, SNPs and SAPs cannot be differentiated from radial glia with any marker and can be solely identified by cell morphology and nuclear localization during mitosis.

When transitioning from radial glia to adult NSCs, radial glia in the lateral GE gain responsiveness to epidermal growth factor (EGF) around age E16, which is evidenced by the increased expression of EGF receptor (EGFR) and a further increase of the receptor after EGF application at this age[54]. After activation of the NSCs by EGF, they will increase EGFR expression, which will remain high until further differentiation into neuroblasts[18]. Thereby, both activated NSCs and TAPs can be identified by their high EGFR expression; however, while activated NSCs still show immunoreactivity to Nestin, Vimentin and GFAP, TAPs lose the expression of these proteins and instead upregulate achaete-scute family bHLH transcription factor 1 (Ascl1), previously known as Mash-1, and distal-less homeobox 2 (Dlx2), both of which promote neuronal differentiation by regulating notch signalling[55,56]. Due to their rapid proliferation, TAPs also can also be identified in their frequent expression the nuclear protein Ki67, which is only expressed throughout the active phases of the cell cycle, i.e., S-, M-, G_1- and G_2-phases, thereby also labelling activated NSCs[57]. Proliferation can also be detected via phosphorylation of histone H3 (phH3), a modification which is present during mitosis, thereby only labelling cells in M-phase[58]. The latter marker is therefore also suitable to distinguish between embryonic SNPs and radial glia, which divide close to the apical border, and SAPs, which divide further away.

Further along the neuronal lineage, TAPs give rise to neuroblasts, which still express Dlx2 but also start expressing neuroblast marker doublecortin (DCX) while migrating to their target destination, which, in adult mice, is the olfactory bulb. C-X-C chemokine receptor 4 (CXCR4) is expressed on the surface of these migrating cells as they migrate along a gradient of stromal-derived factor 1 (SDF-1), the ligand of CXCR4[59-62]. This migration along an SDF-1 gradient is also utilized upon injury[63]. However, while CXCR4 is vital for neuroblast migration, it is not only expressed on neuroblasts but also in NSCs and progenitor cells across the niche, in which it maintains stemness[64,65], as well as in NSCs in the SGZ of the hippocampus[66,67].

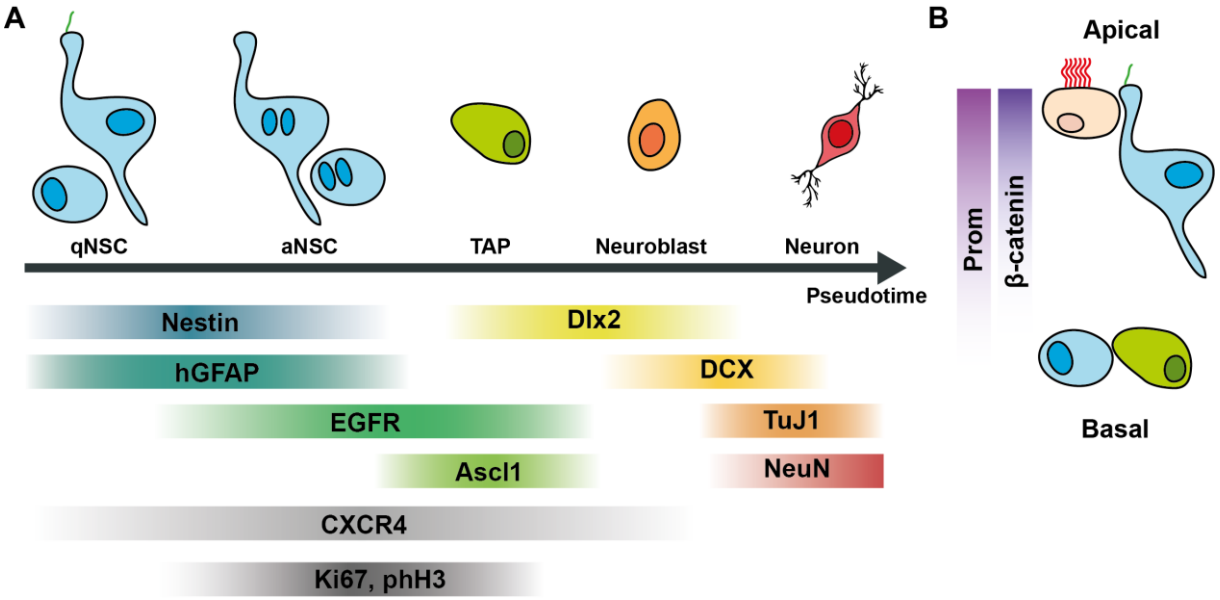

Figure I-3: Expression of marker genes during neurogenesis in the V-SVZ.
(A) Protein expression in quiescent (qNSC) and activated NSCs (aNSC) and their progeny along a pseudotime axis.
(B) Difference in protein expression in apical and basal cells.

In the olfactory bulb, the V-SVZ-derived neuroblasts terminally differentiate mainly into inhibitory interneurons, marked by the expression of neuronal proteins β-tubulin III (TuJ1) and DCX in immature neurons[7] and Neuronal Nuclei (NeuN) in fully differentiated neurons[68].

Lastly, as the organization of the V-SVZ is divided into apical cells, which contact the ventricle, and basal cells, which are further away from the ventricular lumen, apical and basal cells may also be distinguished by their protein expression (Figure I-3 B). To separate the brain tissue from the CSF of the ventricle, the apical cells are connected by tight junctions containing β-catenin, which can be used to highlight the apical surface and reveal cell-cell contacts. Apical cells such as B1-type NSCs and ependymal cells show expression of Prominin-1 (Prom), also frequently referred to as cluster of differentiation (CD) 133[69-71], a transmembrane glycoprotein localized mostly at the apical membrane, as well as at the tips of cilia[12,72]. Prom is not only a marker for apical cells but the protein is vital in preserving stem cell function[73] and cellular signalling, such as Wnt signalling[74]. While both ependymal cells and NSCs express Prom, ependymal cells can be distinguished from the latter by their morphology, as ependymal cells are larger with a larger apical surface and do not have basal processes, by their expression of the marker protein forkhead box protein J1 (Foxj1)[75], as well as by their multi-ciliated surface, which can be visualized by labelling cilia-related markers (see Chapter I-2).

1.4 Signalling pathways regulating neurogenesis in the V-SVZ

1.4 a) EGF signalling

EGF is a small, 53 amino acid (AA) polypeptide which regulates proliferation and differentiation in the V-SVZ via its receptor EGFR[19,54,76], a receptor tyrosine kinase (RTK) of the ErbB family and 1210 AA transmembrane glycoprotein. At age E14-E18, NSCs arise in the GE that respond to EGF application with increase of EGFR expression and neurosphere generation *in vitro*, while before that age, cells respond only to fibroblast growth factor 2 (FGF-2)[77]. *In vivo*, EGFR signalling promotes proliferation and stemness in NSCs and TAPS[18,78,79], as well as migration in the developing telencephalon[80]. Besides EGF, other ligands for EGFR are transforming growth factor (TGF) α, amphiregulin (AREG), epiregulin, betacellulin, epigen and heparin-binding EGF-like growth factor. TGFα, AREG and EGF are specific to EGFR only, whereas the other ligands may bind to other members of the ErbB family[79].

Upon binding a ligand, EGFR dimerizes and undergoes autophosphorylation of several C-terminal tyrosine residues; phosphorylated EGFR (phEGFR) then triggers various signalling cascades, such as the mitogen-activated protein kinase / extracellular signal-regulated kinase (MAPK/ERK) pathway, as well as the Janus kinase (JAK) and protein kinase B (Akt) pathways[79] (Figure I-4). In the MAPK/ERK pathway, the Ras GTPase (RAS) becomes activated by EGFR and recruits RAF to the membrane, which in turn activates and phosphorylates MAPK/ERK Kinase (MEK), resulting in the downstream phosphorylation of ERK[81]. This activates the kinase activity of ERK, leading to the phosphorylation of downstream target proteins in the nucleus, which promotes cell proliferation.

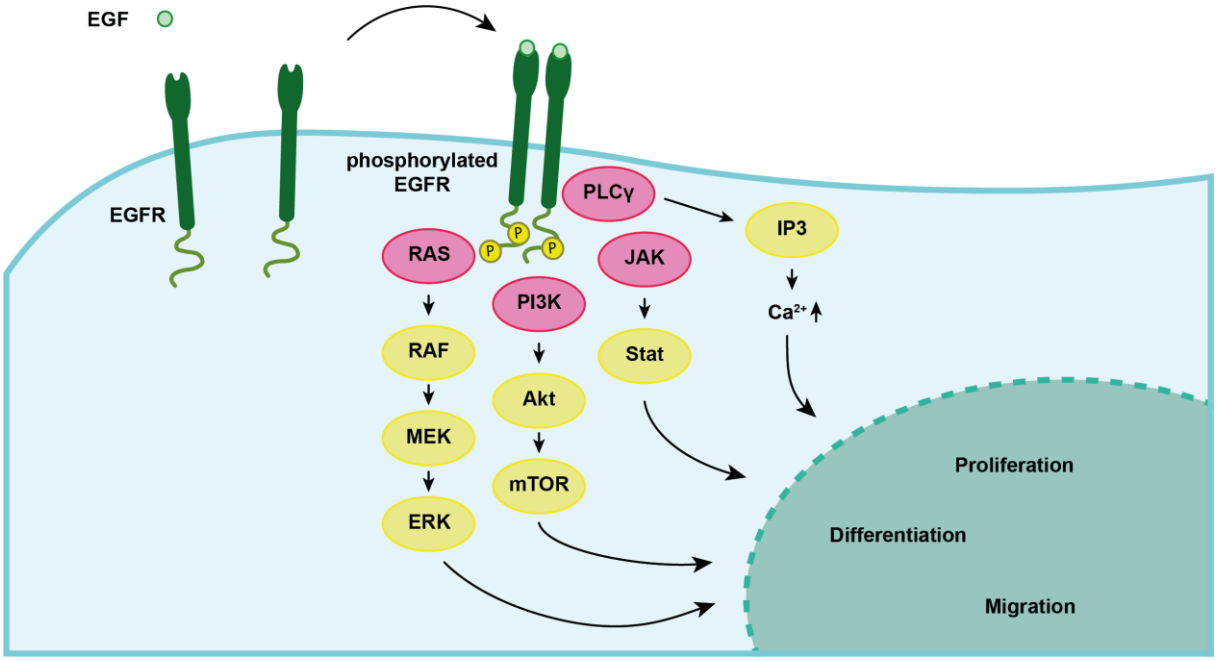

Figure I-4: EGFR signalling pathways.

The Akt pathway, triggered by interaction of phosphoinositide 3-kinase (PI3K) and resulting in mTOR activation similarly promotes cell proliferation while inhibiting differentiation. On the other hand, the JAK-STAT (signal transducer and activator of transcription proteins) pathway drives both differentiation and proliferation. Lastly, EGFR signalling may also affect intracellular Ca^{2+} levels via phospholipase C gamma 1 (PLCγ) and inositol 1,4,5-trisphosphate (IP3), a process that promotes proliferation as well as survival and motility[82]. Interference with these downstream pathways results in either overproliferation and cancer, or depletion of NSCs and lack of neurogenesis[19,78].

Besides the ligand concentration, EGFR pathway activation is regulated by the surface expression of EGFR molecules[83]. After activation and dimerization, EGFR undergoes a conformational change and is then internalized and degraded in a clathrin-dependent mechanism, which may attenuate the signal[84,85]. However, some studies suggest that the receptor internalization itself may contribute to and even be a requirement for downstream signalling[86].

The surface expression of EGFR and thereby sensitivity to EGF is upregulated in mice embryos between ages E14 and E18 where activation of EGFR by application of exogenous EGF results in increased surface expression of the receptor[54], suggesting a positive feedback loop.

1.4 b) Other pathways

After neurogenesis begins, early precursors in the niche are not responsive yet to EGF, but rather FGF-2[77], a growth factor which is necessary for differentiation of neurons as well as stem cell maintenance. FGF-2 *in vitro* promotes the expression of EGFR in E14 mouse cells, and thereby promotes also the formation of neurospheres[54].

Furthermore, the proliferation of NSCs is inhibited by bone morphogenetic protein 4 (BMP4), a member of the TGFβ superfamily which promotes NSC quiescence, thereby preventing NSC depletion, and in proliferating NSCs promotes a neurogenic cell fate[87].

Additionally, the Wnt/β-catenin pathway promotes proliferation in the niche, whereas the Wnt/planar cell polarity (PCP) pathway contributes to the establishment and maintenance of ependymal cells as well as to the differentiation, migration and maturation of new neurons in the OB[88].

Lastly, the proliferation and quiescence of NSCs can be regulated via soluble proteins in the CSF, e.g. by ciliary sonic hedgehog (Shh) signalling[89] and platelet derived growth factor (PDGF) signalling[90-92] (see Chapter I-2.2), as well as by cell-to-cell signalling such as Notch signalling, which is vital for the communication between apical and basal NSCs[2,93].

2. Primary cilia

2.1 Structure and function

Some signalling in NSCs, such as Shh and PDGFRa signalling, is dependent on primary cilia, which are closely associated with proliferation and cell cycle in these cells. Cilia, also known as flagella, are tiny, rod-shaped cellular organelles protruding from the cell membrane, which are supported by a tubulin cytoskeleton called the axoneme. These organelles were long thought to be vestigial, but were found in the recent decades to be vital for signalling and cell cycle regulation. Mutations in proteins contributing to ciliary signalling and structure lead to severe developmental defects called ciliopathies[94-96], or cancer[97,98]. In the V-SVZ, there are two types of cilia: primary cilia, generally a single one per cell, and motile cilia, which are only present on the apical surface of ependymal cells in groups of 10-30 cilia. These two types of cilia are not only different in length, where primary cilia are usually only about 1-5 µm long and motile cilia 10-15 µm, but also in structure and function. The main function of motile cilia is the movement of CSF[99,100]; therefore, the structure of motile cilia consists of a ring of 9 microtubule doublets, with a pair of single microtubules at the centre of the ring, termed 9+2 structure (Figure I-5). The outer microtubules have one their surface dynein arms and are connected to the inner pair by radial spokes, allowing the cilia to move in highly synchronized strokes to move CSF through the ventricles. Primary cilia, on the other hand, lack the inner microtubule pair, radial spokes and dynein arms (9+0 structure), rendering them immobile, a reason these organelles were in the past called “rudimentary” cilium and were believed to have no significant role in mammalian cells.

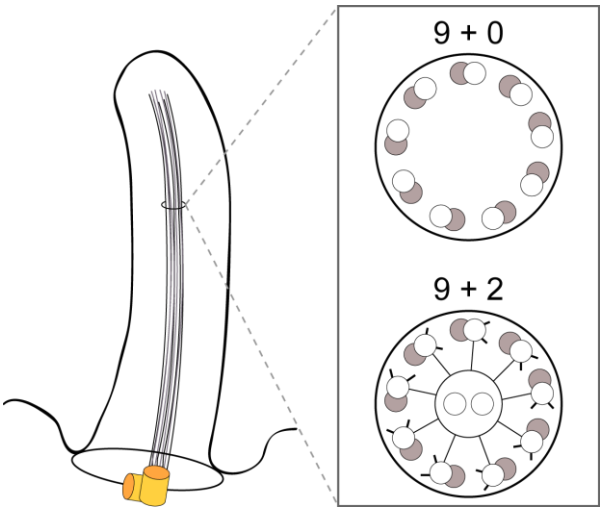

Figure I-5: Cilia structure.
Cilia consist of a membrane around a central axoneme made of 9 microtubule doublets in a circular arrangement, which extend from the basal body (yellow), a modified centrosome. Primary cilia have a 9+0 structure (top) of just the microtubule doublets, whereas motile cilia have two microtubule singlets in the middle, connected to the outer doublets by radial spokes (9+2 structure, bottom).

Independent of the tubule structure, all cilia are built – a process called ciliogenesis – from the basal body, a modified centrosome, which in primary cilia is usually the mother centriole[101,102]. In cells with motile cilia, on the other hand, the mother centriole multiplies to generate basal bodies for all cilia. These basal bodies can, in both primary and ependymal cilia, be identified by several markers, such as γ-tubulin, fibroblast growth factor receptor 1 oncogene partner (FGFR1OP, FOP), or centrins.

The ciliary membrane, while being part of the cell membrane, has a unique composition of lipids and proteins, with several transmembrane receptors and membrane-anchored proteins (see also Chapter 2.2), which are targeted to the cilia via various ciliary localisation sequences[103] but are still subject to local regulation. For example, both the specific amount of cholesterol in the ciliary membrane[104] and the transmembrane protein ADP-ribosylation factor 13b (Arl13b) regulate the presence of Shh signalling proteins in the cilium[105].

Ciliary membrane and cytoplasm are separated from the rest of the cell by the transition zone at the basis of the cilium. This division ensures that the cilia are a separate compartment of the cell that can have different concentrations of proteins, localized RNA translation and even differing calcium concentrations[106]. Especially in primary cilia, this is necessary for them to function as an independent sensory organelle, with proteins needed for several signalling pathways close together, thereby ensuring fast and efficient signal transduction.

The basal body of primary cilia is typically made up by the mother centriole of the cell. Therefore, during G_2/M phase transition, the cilium is retracted so the mother centriole can replicate and form, together with the daughter centriole, the mitotic spindle apparatus[107]. Hence, primary cilia are intrinsically linked to the cell cycle, and cilia are extended again in G_1 or G_0 phase[97,108]. While ciliary presence can therefore be used as an indicator of cell proliferation, it has previously been shown that the length of primary cilia rather than their overall presence is more indicative of the quiescence of a cell[12]. Furthermore, it has been shown that influencing the length or presence of a cilium directly affects cell cycle under physiological conditions and in cancer[109]; removing primary cilia was shown to increase proliferation and affect differentiation of precursor cells[97,109-111]. As the presence and length of primary cilia heavily relies not mostly on nuclear transcription but rather local translation and trafficking[106,112], modulating protein transport via overexpression of proteins such as intraflagellar transport (IFT) 88 causes cell cycle arrest after S-phase and subsequent apoptosis[113]. Besides trafficking, cilia length may also be regulated via local signalling and posttranslational modifications to the cytoskeleton, such as acetylation of α-tubulin at lysine (Lys) 40. Lys40 is acetylated by MEC-17[114], a relative of the Gcn5 histone acetyl transferases, and deacetylated by histone deacetylase (HDAC) 6[115] and sirtuin type 2 (SIRT2), both of which co-localize at the basal body and interact to regulate cilia length[116,117]. Therefore, activity and expression of HDAC6 have been found to be strongly involved in proliferation and differentiation behaviour of cancer cells as well as NSCs[118,119]. Moreover, via its interaction with Aurora A kinase (AurA), HDAC6 was shown to directly influence Wnt/β-catenin signalling in NSCs[74].

Lastly, local signalling such as cyclic adenosine monophosphate (cAMP) and Ca^{2+} signalling may influence regulation of cilia length and thereby proliferation and migration[120]. Activity of adenylate

cyclase 3 (AC3), a transmembrane enzyme which is commonly used as a marker for primary cilia[121-123], was found to regulate cilia length in mammalian cells *in vitro*[124], increase tumorigenic potential[125], and the lack of cAMP/protein kinase A (PKA) signalling resulting from the ablation of this activity was shown to result in defects in neuronal migration[126,127] and the development of a depression-like phenotype[128].

2.2 Ciliary signalling pathways

One of the most prominent primary cilia-dependent signalling pathways is Shh signalling. Shh signalling is a vital pathway during development, with roles in proliferation, differentiation, patterning and limb development in the early embryo (for a review, see Eggenschwiler and Anderson [129]). However, also in adult NSCs and neuroblasts, ciliary Shh signalling proved important for proliferation, stem cell maintenance and chemotaxis[89,130,131].

The receptor for Shh, a 12-span transmembrane protein named Patched1 (Ptch1), is expressed on the membrane of primary cilia and in an inactive state, represses Smoothened (Smo), a transmembrane G-protein coupled receptor (GPCR), which is thereby kept outside of the cilium[130,132-134] (Figure I-6). Upon binding of Shh to Ptch1, Ptch1 is endocytosed this repression is released; Smo then translocates into the primary cilium, where it in turn releases the repression of Gli proteins 1 and 2 by Suppressor of Fused (SuFu), and inhibits the formation of Gli3-repressor (Gli3-R). Gli 1 will then translocate into the nucleus to activate target genes, whereas Gli2 and Gli3 move toward the tip of the cilium[135-137]. Since the localization inside and outside of the cilium is inherently important in this pathway, ablation or defects in primary cilia or trafficking were found to significantly affect Shh signalling[104,105,138,139].

Besides Shh, there are also cilia-specific RTKs, such as platelet-derived growth factor receptor α (PDGFRa), a receptor commonly expressed in NSCs in the V-SVZ and associated with cancer[140-143], as well as other GPCRs, such as somatostatin receptor 3 and neuropeptide Y receptor 2, expressed in the primary cilia of neurons[144,145]. GPCRs in primary cilia activate adenylate cyclases, generally AC3, which then convert adenosine monophosphate into cAMP, activating PKA-signalling and the CREB pathway[125,126]. Active PKA however phosphorylates Gli3, which targets it for proteolytic processing into Gli3-R[146-148], thereby inhibiting Shh signalling (Figure I-6).

Lastly, while non-canonical Wnt/PCP signalling is still capable of functioning without a cilium, the primary cilium provides fine control over this pathway to prevent overactivation[149]. Additionally, β-catenin-independent Wnt/STOP signalling requires primary cilia to function and was shown to influence both size and protein content of dividing cells[150,151].

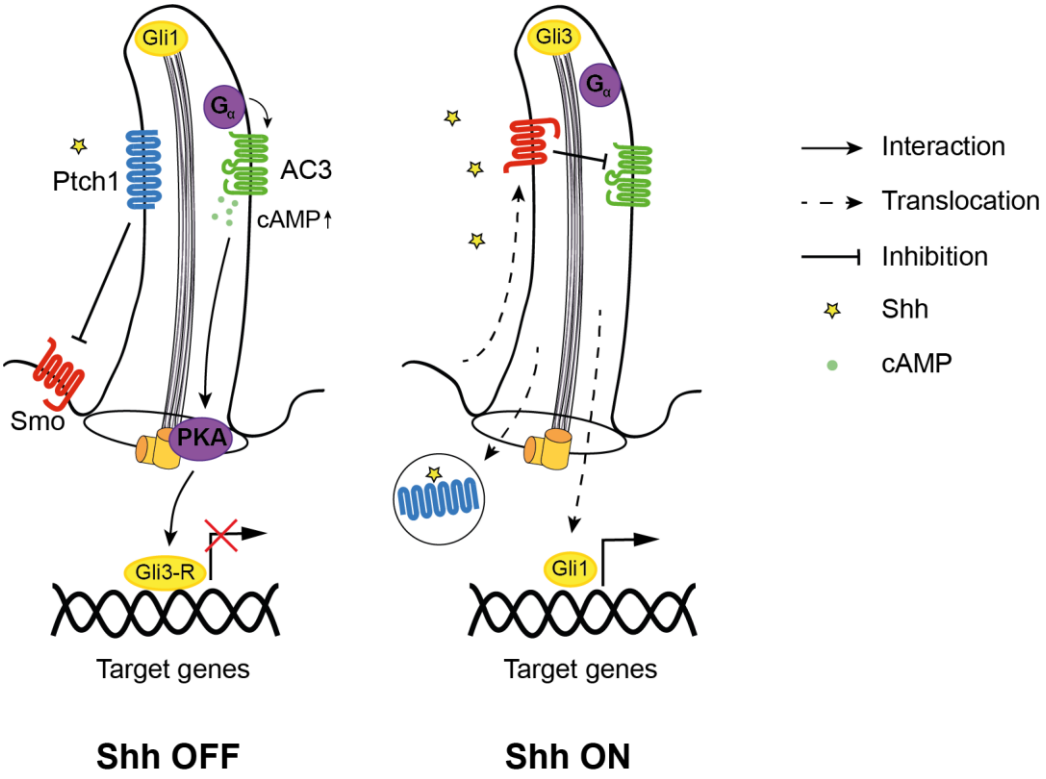

Figure I-6: Shh signalling in primary cilia.
When Shh signalling is off (left), Ptch1 represses Smo outside of the cilium. Meanwhile, GPCR activity activates AC3, which increases the ciliary levels of cAMP. This causes PKA to transform Gli3 into its repressor form. After Shh binds to Ptch1 (right), the receptor is internalized and degraded while Smo translocates into the cilium where it represses AC3 activity. Gli3 in its activator form translocates to the ciliary tip while Gli1 is trafficked to the nucleus, where it activates Shh target genes.

3. Growth/differentiation factor 15

Growth/differentiation factor 15 (GDF15) is a distant member of the TGFβ superfamily and a secreted protein with a size of 308 AA in humans and 303 AA in mice[152], and is, in contrast to other adult brain regions, expressed at the apical side of the V-SVZ and secreted by the choroid plexus[153], which suggests a role especially in apical NSCs. The protein is in its inactive form a size of 40 kDa and after cleavage of the N-terminus in its secreted form a 25 kDa disulfide-linked homodimer[154]. GDF15 was previously also known under the name macrophage inhibitory cytokine 1 (MIC-1) and its receptor, GDNF family receptor alpha-like (GFRAL), was not identified until recently[155-157].

GDF15 is widely expressed in and secreted by many tissues in the body; it was found in particularly high concentration in fat tissue, in the placenta and liver[154]. Additionally, it was found to be increased after injury, in inflammation and cancer, as well as in obese patients[153].

Many studies have therefore focused on the role of GDF15 in these pathologies, and it was found that GDF15 has both pro-apoptotic and proliferation-promoting roles in cancers[158-161], suggesting a highly complex working mechanism of this protein. Since the discovery of its receptor GFRAL, which was found to be only weakly expressed in most tissues, GDF15 was shown to play a larger role in obesity and food intake[155-157,162]. This effect of GDF15 is mediated by GFRAL-expressing neurons in the brain stem, which, upon binding GDF15, relay appetite-reducing signals, a mechanism which was found to lead to cachexia in cancers where the level of GDF15 was increased[161,163].

In the brain, GDF15 is only weakly expressed, but some expression was found at mRNA level in the murine V-SVZ, especially on the apical side of the niche as well as secretion by the choroid plexus[153], which suggests a role in neurogenesis. However, while a relevant expression of GFRAL in this region has not yet been confirmed, GDF15 was found to affect neurogenesis and regulate the proliferation of NSCs in the hippocampus, in a mechanism involving EGFR and CXCR4[164]. In this previous study, conducted by a former PhD student of my current laboratory, it was found that GDF15 is expressed in clonogenic Prom-expressing precursors, and that it is upregulated in the murine GE at E16 – the age when NSCs start to mature and gain responsiveness to EGF. The expression of the protein remains at a similar level until adulthood. Additionally, it was found that at E18, the level of *Gdf15* mRNA was higher in cells expressing high levels of surface EGFR ($EGFR^h$), both in the hippocampus and the GE, with a higher relative level in the latter region. Using GDF15 knock-out mice, they found that lack of GDF15 caused a reduction in the number of $EGFR^h$ cells as well as lower levels of *Egfr* mRNA in these cells. This GDF15 knock-out also led to a reduction of proliferation as well as migratory defects in neuroblasts and overall lower levels of DCX^+ neuroblasts. Lastly, they found that application of GDF15 increased the number of $EGFR^h$ cells, which was attenuated by inhibition of CXCR4, suggesting a mechanism involving a permissive role of the chemokine receptor.

4. Research question and aims for this thesis

While the expression of GDF15 in the V-SVZ has been known for over two decades, its receptor has only recently been identified and its role in this brain region is largely unknown. Since apical NSCs are present in the region where GDF15 is expressed and GDF15 has previously been shown to affect NSC proliferation in the SGZ of the hippocampus, I hypothesized that this protein might influence NSC proliferation in the V-SVZ as well.

In this thesis, I investigated the organization of NSCs in the V-SVZ and their contribution to neurogenesis, and I analysed the effect of GDF15 on NSCs and their primary cilia in this region. To elucidate the mechanism, I investigated the effect of GDF15 on EGFR signalling, as well as the involvement of CXCR4 and ciliary signalling such as Shh and the involvement of AC3 and HDAC6.

The main questions I wanted to answer in this thesis were:

1. What are the differences between apical and basal NSCs regarding ciliation, marker expression and proliferation?

2. Does GDF15 affect NSC behaviour in the V-SVZ?

3. Does GDF15 affect primary cilia signalling in the V-SVZ?

4. Which proteins are involved in the mechanism of action of GDF15 on NSC behaviour and ciliary signalling?

To answer these questions, I took advantage of the hGFAP:H2B-GFP reporter mouse model and Gdf15 knock-out mice, and manipulated proliferation and cilia morphology with a range of growth factors and pharmacological inhibitors.

II. Materials and Methods

1. Methods

If not otherwise indicated, all experimental steps are performed at room temperature. For detailed recipes for solutions and buffers as well as step-by-step protocols, please see VIII. Appendix.

1.1 Animals and tissue dissection

For this thesis work, I used time-mated pregnant (plug day = E1) and young adult (8-12 weeks old) C57BL/6 wild type (WT; Charles River) and Gdf15 knock-out/lacZ knock-in ($Gdf15^{-/-}$) mice, as well as P7 and adult hGFAP:H2B-GFP mice. Breeding and animal housing was provided by the Interfaculty Biomedical Research Facility (IBF) of Heidelberg University and organized by Gabriele Hölzl-Wenig. The $Gdf15^{-/-}$ line was generated by Jens Strelau *et al*.[165] and kept in the IBF with regular blood refreshments. The hGFAP:H2B-GFP line was kept and mated as described before[2,93]. Genotyping was performed by Gabriele Hölzl-Wenig as previously described[165].

For the experiments, the mice were rendered unconscious by CO_2 inhalation and subsequently killed by neck dislocation. Young mouse pups (P7) were killed by decapitation. The dissection of the embryonic GE was done to maximise the excision of the germinal region as described before[166] in ice-cold Euromed-N basal medium (Euroclone). Dissection and/or dissociation of the adult SVZ was performed as previously described[18]; the E18 GE was dissociated manually by 15x pipetting with a 200 µl pipette tip. The hippocampus, hypothalamus and brain stem were dissected as indicated in Figure II-1. All animal experiments were approved by the Regierungspräsidium in Karlsruhe, Germany.

1.2 Flow cytometry and fluorescence-activated cell sorting (FACS)

For a list of used antibodies, please refer to Table II-1.

1.2 a) For cells

Flow cytometry and cell sorting was performed as already described[2,12,18,167].

In short, dissociated cells were incubated with fluorophore-conjugated anti-Prominin (CD133) antibody for 30 min at 4°C in the dark, washed twice and then incubated with fluorophore-conjugated EGF to label surface EGFR levels. Propidium iodide (PI; Sigma Aldrich) was added at 1 µg/ml to label dead and damaged cells, and the cells were analysed and sorted using a FACSAria II flow cytometer (BD Biosciences). Unlabelled and single-labelled samples and, for EGFR stainings, a sample incubated with unlabelled recombinant EGF (EGF block) were used as controls for gate-setting. For full protocol and all used solutions, see Appendix (VII-1, VII-2).

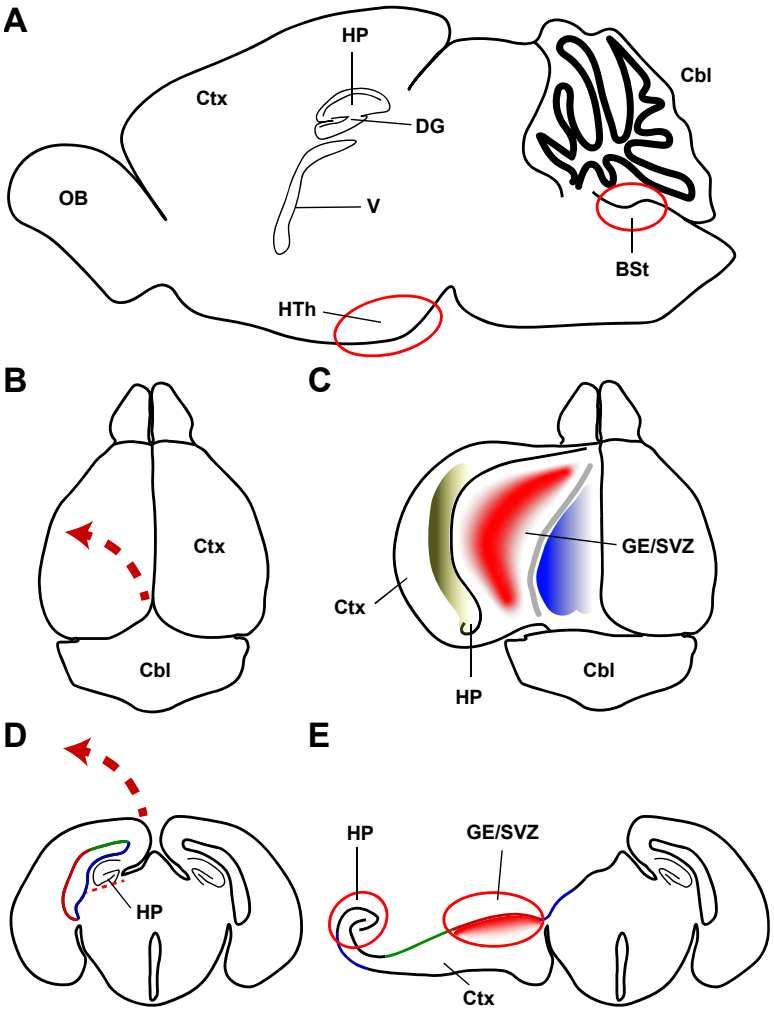

Figure II-1: Dissection of mouse brains.
(A) Sketch of a sagittal section of an adult mouse brain indicating regions for dissection of the hypothalamus (HTh) and brain stem (BSt).
(B-E) Workflow of dissection of the SVZ/GE and hippocampus (HP) on the example of an adult mouse brain looking onto the dorsal side (B, C) or in a coronal section (D, E). E18 and P2 brains were dissected likewise. Ventricles were opened sideways (B, D) to expose the SVZ/GE (C, red area), which was cut out whole and as thin as possible (E, red area). The medial wall (blue) and cortical ventricular zone (green) was not included. HP was cut caudal to rostral along the coloured gradient indicated in C.
Abbreviations: Cbl = cerebellum, Ctx = cortex, BSt = brain stem, DG = dentate gyrus, GE = ganglionic eminence, HP = hippocampus, HTh = hypothalamus, OB = olfactory bulb, SVZ = subventricular zone, V = ventricle.

1.2 b) For cilia

Flow cytometry for cilia and cilia sorting by FACS was performed as extensively described in Monaco, et al. [72] and Baur, et al. [168].

1.3 Whole mount preparations and incubation

For whole mount stainings, whole lateral walls of E18 or adult animals were dissected as described above and either directly fixed in a 3% paraformaldehyde, 4 % sucrose solution (3/4 PFA) for 24 h at 4°C, or incubated in a well of a 24-well-plate with 1 mL culture medium (see Appendix VII-1) containing blockers or growth factors for 24 h at 37°C, 5% CO_2, as indicated in the figures; for a full list of inhibitors and growth factors, refer to Table II-2.

After incubation, whole mounts were fixed in 3/4 PFA at 4°C for 24 h and then kept in phosphate-buffered saline (PBS) containing 0.01% sodium azide at 4°C until further experiments. If the samples were used for western blot, the whole SVZ was dissolved in RIPA buffer (see Chapter II-1.9 Western Blot).

1.4 Immunostaining

For a list of primary and secondary antibodies used and their concentration, refer to Table II-3 and Table II-4. For step-by-step protocols, see Appendix VII-3 and VII-4.

1.4 a) On slices

For brain sectioning, whole brains of E18, P7 or 8-12-weeks-old mice (adult) were divided into hemispheres with a razor and subsequently fixed by immersion in 4% PFA in PBS for 48 h at 4°C on a shaker. The PFA was refreshed once after 24 h. For cryoprotection, the brains were then put into a 30% sucrose in PBS solution, where they were kept until they sank to the bottom (around 24-48 h). The hemispheres were then cut in 20 µm sections at -20°C using a Leica CM1950 Cryostat. Sections of E18 animals were directly mounted onto Superfrost glass slides (Thermo Fisher Scientific), which were kept at -22°C until staining, while adult sections were stored free-floating at 4°C in a 48-well-plate containing PBS with 0.01% azide.

For immunostaining, all steps were performed on a shaker in a 48-well plate (adult and P7 free floating sections) or in staining dishes (E18 mounted sections) if not specified otherwise. The slices were first permeabilized with 0.5% NP-40 in PBS for 10 min, then the background fluorescence was quenched by incubation in 10 mM glycine in PBS for 10 min and the slices were blocked for 1 h in 5% foetal calf serum (FCS) in PBS; for E18 sections, this was performed in a damp slide chamber. Primary antibodies were incubated in PBS at 4°C overnight on a shaker or in the damp slide chamber, respectively.

After three 5 min washes in PBS, secondary antibodies together with DAPI (4',6-Diamidine-2'-phenylindole; 400 ng/ml, Roche Diagnostics) for nuclear staining were applied in 5% FCS in PBS for 2 h, in the damp slide chamber for E18 sections. After three 5 min washes in PBS and a short dip in distilled water, the adult and P7 sections were mounted on SuperFrost glass slides and all sections coverslipped with Mowiol 4-88 (Merck). The slides were dried overnight and then kept in a slide box at 4°C until imaging.

1.4 b) On whole mounts

For whole mount immunofluorescence, freshly dissected or overnight-treated whole lateral walls were fixed in 3/4 PFA at 4°C overnight. The fixed tissue was stored at 4°C in a 24-well-plate containing PBS with 0.01% azide until immunostaining.

If IdU was stained, the whole mounts were incubated in 2N HCl at 37°C for 30 min, followed by a neutralization step in 0.1 M sodium tetraborate pH 8.5 for 30 mins, followed by the standard protocol:

For the immunostaining, all steps were performed on a shaker. The whole lateral walls were permeabilized in 0.5% NP-40 for 15 min, then the background fluorescence was reduced by application of 100 mM glycine in PBS for 30 min. Afterwards, the tissue was blocked in 5% FCS, 0.1% NP-40 in PBS for 1.5 h and then incubated with primary antibodies in 0.1% NP-40 in PBS overnight at 4°C. The next day, the tissue was washed 3x 15 min, and secondary antibodies were applied in 0.5% FCS, 0.1% NP-40 for 2 h, with DAPI for nuclear counterstain. After 3x 15 min washes in PBS and a quick rinse in distilled water, the tissue was mounted in Mowiol 4-88 onto 12 mm coverslips with the apical surface of the SVZ facing the glass; excess Mowiol 4-88 was removed and the tissue was left to dry for 2-3 hours. When the tissue was dry and firmly stuck to the coverslip, the coverslip was then flipped and mounted on a glass slide in a drop of Mowiol 4-88 (~60-70 µl). The slides were left to dry overnight and then stored in a slide box at 4°C until imaging.

1.5 Imaging

All immunofluorescent stainings were imaged using a TCS SP8 confocal laser scanning microscope with LAS X software (Leica). Images were taken using a 63x oil-immersion objective, at 8-bit greyscale and a resolution of 1024x1024 pixels (for whole cells and nuclei) or 2048x2048 pixels (for cilia). Additionally, images were taken as z-stacks with 0.7-1 µm z-steps. For cell culture, the z-stack was around 4-6 µm thick, whereas whole mounts and slices were imaged in 18-22 µm stacks.

1.6 Scanning electron microscopy (ScEM)

Sample preparation for scanning electron microscopy was performed by Andrea Hellwig and Sebastian Weber. For this, whole E18 lateral walls, dissected as described above, were fixed in 2% glutaraldehyde in 0.1 M sodium phosphate buffer. Afterwards, the samples were washed in sodium phosphate buffer and postfixed with a 2% osmium tetroxide, 1.5% potassium ferrocyanide solution for 1 h. After additional washing and dehydration in ascending series of ethanol and finally pure acetone, the samples were critical point dried at the Electron Microscopy Core Facility (EMCF) at Heidelberg University, where they were mounted on sample holders and sputter-coated with an 80% gold, 20% palladium alloy. Finally, images were taken using a ULTRA 55 field-emission scanning electron microscope (ZEISS).

1.7 Mass spectrometry

After FACS sorting, Arl13b^{+}acT^{+} and Arl13b^{-}acT^{-} particles were collected in 100 µl PBS containing 10x cOmplete EDTA-free protease inhibitor (Merck). The samples were then frozen at -80°C until they were given to the Core Facility for Mass Spectrometry & Proteomics (CFMP) in Heidelberg, where further sample preparation and primary analysis was performed by Ute Bach and Marcin Luzarowski

as follows: The samples were digested using Single Tube Solid Phase Sample Preparation[169] (SP3; for protocol, see Appendix VII-5), desalted and then analysed using liquid chromatography mass spectrometry (LC-MS) using a Orbitrap-MS system (Thermo Fisher Scientific).

1.8 qPCR

For quantitative real-time PCR (qPCR), RNA was extracted using a Quick-RNA Microprep kit (Zymo Research). For this, tissue (SVZ or hippocampus from one hemisphere, or brain stem and hypothalamus, dissected as described in "Animals and tissue dissection", and incubated as described in "Whole mount preparation and incubation") was lysed in 300 µl lysis buffer; the RNA was extracted according to manufacturer's instructions, including a DNase digestion step. The RNA was eluted from the column in 20 µl RNase-free water, and then retrotranscribed into cDNA using M-MLV reverse transcriptase (Promega) and Oligo(dT)15 primers (Promega) according to manufacturer's instructions in a ProFlex PCR machine (Applied Biosystems). For the step-by-step protocol, see Appendix VII-6.

1 µl cDNA was used for qPCR in a volume of 20 µl, either using TaqMan GeneExpression Master Mix (Thermo Fisher Scientific) or Power SYBR Green PCR Master Mix (Thermo Fisher Scientific), according to manufacturer's instructions using a StepOne Plus Real-Time PCR System (Thermo Fisher Scientific). For a list of TaqMan probes and SYBR green primers, refer to Table II-5 and Table II-6, respectively.

For normalization, beta-actin was used as a housekeeping gene; fold change was calculated as $2^{-\Delta\Delta CT}$, where ΔC_T is the difference between cycle threshold (C_T) value of the gene of interest to its respective beta-actin C_T value, and $\Delta\Delta C_T$ is the difference between the ΔC_T value of a control sample (e.g. wild-type untreated) and that of the sample of interest. All samples were run as duplicates.

To visualize the qPCR products in Figure III-3 C, samples were mixed with 6x orange DNA loading dye (Thermo Fisher Scientific) and run on a 2 % agarose gel containing Midori Green (Nippon Genetics) in TBE buffer for 10 minutes. Afterwards, the DNA was visualized using ultraviolet light.

1.9 Western Blot

For a full protocol and solutions, see Appendix VII-7 and VII-8.

For EGF treatment in Figure III-16 C-E, dissociated GE cells were evenly distributed into 6 eppendorf tubes. For C-D, one tube was immediately centrifuged and cells lysed by resuspension in 30 µl RIPA buffer (baseline sample). The remaining tubes were incubated with 20 ng/ml EGF for 7 minutes and pelleted. They were then either directly lysed in 30 µl RIPA buffer (0 h sample) or further incubated in EGF-free medium for the time indicated in the figure. Afterwards, the cells were pelleted by centrifugation and resuspended in 30 µl RIPA buffer. For D-E, Eppendorf tubes were incubated either

without (0 ng/ml sample) or with EGF at the indicated concentrations for 7 min, then pelleted by centrifugation and lysed in 30 µl RIPA buffer.

For whole GE/V-SVZ experiments, the lateral ventricular wall was dissolved in 300 µl RIPA-buffer and 4x Laemmli buffer was added to a final concentration of 1x. Afterwards, 16 µl or 5 µg per sample was loaded onto a 7.5% polyacrylamide gel, which was then run in running buffer at a constant current of 30 mA per gel for 85 minutes on ice. Afterwards, the proteins were transferred onto a nitrocellulose membrane (Whatman Protran BA85, pore size 0.45 µm, Sigma-Aldrich) with a wet transfer system at a constant voltage of 20 V for 2h. To check for successful protein transfer, nitrocellulose membranes were stained with ponceau solution (Serva Electrophoresis GmbH) for 5 min on a shaker and then rinsed in water until bands were visible. The membranes were cut into separate parts, and separately blocked in 5% skim milk in TBS-T for 1h on a shaker; after a short rinse in TBS-T, membranes were incubated in primary antibodies (see Table II-7) in TBS-T at 4°C on a shaker overnight.

After 3x 5 min washes in TBS-T, secondary antibodies conjugated to horseradish peroxidase were applied (Table II-7) in 5% skim milk in TBS-T for 1h on a shaker. The membranes were then washed again 3x 5 min in TBS-T and chemiluminescent bands were detected with Amersham ECL Western Blotting Detection Reagent (GE Healthcare) and a Chemidoc Imaging System (Bio-Rad Laboratories). Exposure time was manually set between 30 s and 20 min.

1.10 Data analysis

1.10 a) Immunofluorescent samples

Cilia length on whole mounts, in slices and on cultured cells was measured along the central axoneme in Arl13b or acetylated tubulin channels using the straight- or segmented-line tools in Fiji/ImageJ[170], depending on size and shape of the cilium (Figure II-2 A, B). Thickness was measured orthogonally to the axoneme at the thickest point of the cilium, which was usually the base (see Figure II-2 C). All measurements per sample, with 3-5 images per sample, were used to calculate the average value. For cilium number in whole mounts, a representative square of 50 x 50 µm was selected on each image and all apical cilia inside where counted. Cilia number was then calculated as number per 1000 µm². In slices, cilia and nuclei were counted and cilia number was calculated as cilia per cell.

Cells were counted as positive for Ki67 and pHH3 when there was a visible nuclear staining; cells were counted as mitotic when the nucleus showed clear morphology of M-phase, namely meta-, ana- or telophase. Niche localization, i.e. apical or subapical, was determined by nuclear distance to the apical surface: a cell was considered apical if the nucleus was within two nuclei distance (~10 µm) to the ventricular wall; otherwise, it was considered subapical.

For fluorescence intensity analysis, all samples were stained simultaneously with the same antibody solutions, and images were taken with the same microscope settings (laser intensity, gain, offset) and the same z-stack size (22 µm). The average intensity was measured for each channel separately in a z-projection of maximum intensity in Fiji/ImageJ. The intensity was normalized by subtracting the average value of a region of interest that showed no specific staining.

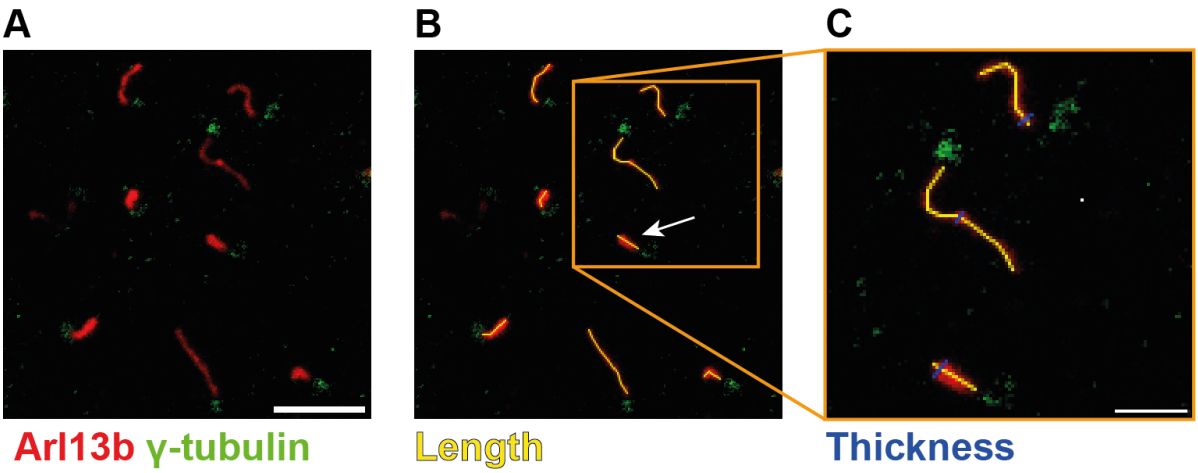

Figure II-2: Measuring primary cilia.
(A) Immunofluorescent image of primary cilia in the WT E18 GE, labelled with Arl13b and γ-tubulin. Scale bar = 5 µm. (B) Measuring of primary cilia length with Fiji/ImageJ using the segmented line tool (yellow line) or straight line tool (yellow line with white arrow). The length is measured along the centre of the cilium. (C) Measuring of primary cilia thickness using straight line tool (blue lines). Thickness was measured at the thickest point of the primary cilium, perpendicular to the length measurement. Scale bar = 2 µm.

1.10 b) Western blots

For densitometry analysis, a fixed-size rectangle the size of one band was selected on the raw TIFF-image and average pixel value measured with Fiji/ImageJ[170]. The value was then normalized to the WT untreated control for this protein on the same membrane and then to the respective normalized intensity of the housekeeping gene (i.e. β-actin, α-tubulin or GAPDH). GAPDH or β-actin were used to normalize acetylated tubulin intensity or other proteins in samples where tubulin acetylation was altered, to account for changes in overall tubulin intensity.

1.10 c) Flow cytometry

Flow cytometry analysis was performed as previously described[2,12,72,168]. In short, PI^+ cells were excluded from analysis; unlabelled samples were used as controls and gates were set to exclude these populations. Cells were regarded as positive for a marker if the fluorescence intensity was inside the gate that excluded the negative control. Positive cells were calculated as percentage of living (PI^-) cells; pharmacologically treated cells were normalized to respective untreated control or the same animal.

1.10 d) Graphs and statistics

Graph bars display the mean value from all animals per genotype and treatment group, with data points indicating the average value of each individual animal. Error bars indicate standard error of mean (SEM). Raw data was collected, and all calculations performed in Excel (Microsoft), and graphs and statistical tests were made with GraphPad Prism 8 (GraphPad). Two datasets were compared with two-tailed student's t-test, or paired t-test if the compared samples were derived from the same animal (e.g. untreated against treated sample). Datasets with more than two groups to compare were tested by two-way ANOVA with Dunnett's multiple comparisons test (different n per group) or with Sidak's multiple comparisons test (same n between groups). Significance was reached for *p<0.05, **p<0.01 and ***p<0.001 (this applies also to other symbols indicating significance, such as $^{+}$ and $^{\#}$).

1.10 e) Mass spectrometry

After LC-MS, proteins were identified by Marcin Luzarowski at the MPCF using a MASCOT database (Matrix Science) search, and the results were imported into the Scaffold software package (Proteome Software). After protein quantification and removal of proteins with less than two identified peptides, the results (proteins, peptides and their abundance) were compiled in an Excel file and returned to me. For heat maps, I log-transformed the abundance of proteins on a $\log_{10}$-base and displayed it on a heatmap using GraphPad Prism 8. For pathway analysis, I calculated the fold change of protein abundance in the $Gdf15^{-/-}$ cilia sample over the WT cilia sample and analysed enriched proteins (≥ 3-fold increase in mutant samples, and proteins not present in WT samples) using reactome[171,172] to identify overrepresented pathways.

2. Materials

Table II-1: Antibodies, fluorescently conjugated growth factors and conjugation kits used for flow cytometry.
N/A = not applicable. AF = Alexa Fluor. APC = Allophycocyanin. BV = Brilliant Violet. PE = R-Phycoerythrin.

Antigen	Conjugate	Host	Company, Catalog #	Lot #	Conc.
Prominin-1	APC	rat	Miltenyi Biotec, 130-102-197	5190517507	1:100
Prominin-1	PE	rat	Miltenyi Biotec, 130-102-210	5181126230	1:100
Prominin-1	BV 421	rat	BioLegend, 141213	B255870	1:1000
EGF	AF 488	N/A	Invitrogen, E13345	1802775	1:1000
EGF	AF 647	N/A	Invitrogen, 35351	1700382	1:1000
Adcy3 (AC3)	Manually; DyLight 488, Atto 633	rabbit	ThermoFisher Scientific, PA5-35382	UL2902981	1:3000
Arl13b	Manually; Dylight 488	mouse	UC Davis, 75-287 BioLegend, 857602	472-1JU-55 B323369	1:3000
Acetyl. tubulin	Manually; PE	mouse	Sigma Aldrich, T6793	017M4806V	1:1000
[Conjugation kit]	DyLight 488	N/A	Abcam, ab201799	GR3432271-1 GR3433329-1	1 µg/µl
[Conjugation kit]	PE	N/A	Abcam, ab102918	GR3218362-3	1 µg/µl
[Conjugation kit]	Atto 633	N/A	Abcam, ab269898	GR3422984-1	1 µg/µl

Table II-2: Growth factors, inhibitors and other compounds used in cell culture and whole mount incubations.
* *if not otherwise indicated in Figure of Figure legend.*

Name	Company	Order number	Concentration	Solvent/Buffer
Actinomycin D	AppliChem	A1489.0025	1 µM	DMSO
AMD3100 (Plerixafor)	MedChem Express	HY-50912	6 µM	H_2O
B27	Gibco	17504044	2%	-
DAPT	Sigma Aldrich	D5942	20 µM	DMSO
EGF (recombinant human)	Peprotech	AF-100-15	20 ng/ml*	Euromed-N
GDF15 (recombinant human)	R&D Systems	9279-GD-050	10 ng/ml	4 mM HCl
Iododeoxyuridine (IdU)	Sigma Aldrich	54-42-2	20 µM	0.2N NaOH
Matrigel	Corning	356230	1:100	Euromed-N
NKY80	MedChem Express	HY-103195	200 µM	DMSO
PD 158780	Cayman	13329	20 µM	DMSO
Smoothened Agonist (SAG)	Cayman	11914	200 nM	DMSO
Tubastatin A	Selleckchem	S8049	10 µM	DMSO
U0126	Calbiochem	270-237-M001	10 µM	DMSO

Table II-3: Antibodies used in immunofluorescence.
N/A = not available.

Antigen	Host	Company, Catalog #	Lot #	Concentration
Adcy3	rabbit	ThermoFisher Scientific, PA5-35382	UL2902981	1:500
Arl13b	mouse	UC Davis, 75-287 BioLegend, 857602	472-1JU-55 B323369	1:500
BrdU (for IdU)	mouse	Hybridoma Bank, G3G4	2/18/21	1:1000
β-catenin	mouse	Santa Cruz sc-7963	G0318	1:100
CXCR4 (CD184)	rat	Invitrogen, 14-9991-82	4339500	1:500
EGFR	mouse	Sigma, E2760	077M4783V	1:100
EGFR, phosphoryl.	rabbit	Abcam, ab40815	GR111622-5 GR3222717-5	1:500
FGFR10P (FOP)	mouse	Abnova, H00011116-M01	I9181-2B1	1:600
GFAP	rabbit	Molecular probes, AA11122	N/A	1:1000
GFAP	mouse	Molecular probes, A11120	N/A	1:1000
GFRAL	sheep	Invitrogen, PA5-47769	UH2824346A	1:200
HDAC6	rabbit	Proteintech, 12834-1-AP	00053805	1:500
phH3	rabbit	EMD Millipore, 06-570	3689895	1:500
Ki67	rabbit	Abcam, 16667	GR3313195-18 GR3375640-34 GR3375640-36	1:200
Nestin	mouse	BD-Pharmingen, 556309	8135889	1:100
Tubulin, acetylated	mouse	Sigma Aldrich, T6793	017M4806V	1:1000

Table II-4: Secondary antibodies used in immunofluorescence.
AF = Alexa Fluor. N/A = not available. WM = whole mounts.

Antigen	Host	Conjugate	Company, Catalog #	Concentration
Mouse	Goat	AF 488	Invitrogen, A11001	1:500 (WM), 1:1000 (Cells, slices)
Mouse	Goat	AF 594	Abcam, ab150116	1:500 (WM), 1:1000 (Cells, slices)
Mouse	Goat	AF 647	ThermoFisher Scientific, A21235	1:500 (WM), 1:1000 (Cells, slices)
Rabbit	Goat	AF 488	Invitrogen, A11008	1:500 (WM), 1:1000 (Cells, slices)
Rabbit	Goat	AF 594	Abcam, ab150080	1:500 (WM), 1:1000 (Cells, slices)
Sheep	Donkey	Cy3	Jackson ImmunoResearch, 713-165-003	1:200
Rat	Donkey	AF 488	Jackson ImmunoResearch, 112-165-003	1:500 (WM), 1:1000 (Cells, slices)
Rat	Goat	AF 647	ThermoFisher Scientific, A21247	1:500 (WM), 1:1000 (Cells, slices)

Table II-5: qPCR probes for TaqMan assays.
All assays from ThermoFisher Scientific, Catalog number 4331182. Fluorophore: FAM-MGB.

Gene	Organism	Assay #
Beta-actin	Mus musculus	Mm00607939_s1
Adcy3 (AC3)	Mus musculus	Mm00460371_m1
Gfral	Mus musculus	Mm02344882_m1
Gli1	Mus musculus	Mm00494654_m1
HDAC6	Mus musculus	Mm00515945_m1

Table II-6: qPCR primers for SYBR green assays.
**sequence from Origene, Cat# MP200232. #sequence from Kefaloyianni et al. [173].*

Gene	Forward	Reverse
Beta-actin*	5'-TGACGGGGTCACCCAACTGTG-3'	5'-CTAGAAGCATTTGCGGTGGACGAT-3'
EGFR#	5'-ACCTCTCCCGGTCAGAGATG-3'	5'-CTTGTGCCTTGGCAGACTTTC-3'
GFRAL	5'-GGGATGTTGGTTGGTGTCAG-3'	5'-AGGCAGGTGTCTTCCATTGA-3'
HDAC6	5'-GCCTCAATCACTGAGACCATCC-3'	5'-GGTGCCTTCTTGGTGACCAACT-3'

Table II-7: Antibodies used for western blot.
** = horseradish peroxidase-conjugated secondary antibody. N/A = not available.*

Antigen	Host	Company, Catalog #	Lot #	Concentration
Actin	rabbit	Cell signalling, 4970	N/A	1:10000
ERK	rabbit	Cell Signalling, 4695	8	1:1000
ERK, phospho	rabbit	Cell Signalling, 4370S	28	1:1000
GAPDH	mouse	Proteintech	60004-1-Ig	1:5000
Tubulin, acetylated	mouse	Sigma Aldrich, T6793	017M4806V	1:4000
α-Tubulin	mouse	Sigma Aldrich, T9026	N/A	1:10000
mouse*	goat	Jackson ImmunoResearch, 115-035-005	N/A	1:10000
rabbit*	goat	Jackson ImmunoResearch, 111-035-003	N/A	1:10000

III. Results

1. Characterization of apical and basal neural stem cells and their cilia

Some of the results in this chapter have already been published in Baur, et al. [2].

Apical neural stem cells (NSCs) have long been thought to be the major contributor to neurogenesis in the adult V-SVZ. However, previous studies have highlighted that adult NSCs are highly heterogeneous. Therefore, I examined the differences in neurogenesis and proliferation between apical and basal cells in the V-SVZ, and more closely investigated marker expression and ciliation of NSCs in adult mice (8 weeks old, 8w) and young mouse pups (7 days old, P7) of hGFAP:tTA;H2B-GFP (short: hGFAP:H2B-GFP) mice. These reporter mice express green fluorescent protein (GFP) fused to histone 2B (H2B) with a tet-off system, i.e., expression of the reporter is inhibited by administration of tetracyclines (here doxycycline, doxy). Since the tetracycline transactivator (tTA) is expressed under the control of the human GFAP (hGFAP) promoter, the nuclear signal labels NSCs and is visible already in embryonic radial glia progenitors from mid development and in NSCs in the adult brain. Due to this system, nuclear GFP-signal is diluted when cells divide during doxy administration, thereby enabling analysis of cell proliferation by comparing untreated to doxy-treated tissues.

1.1 Apical NSCs are more ciliated and express more Nestin then basal NSCs in the V-SVZ

Using NSC marker Nestin and primary cilia marker AC3, I labelled coronal sections of 8w hGFAP:H2B-GFP mouse brains and analysed co-expression of nuclear H2B-GFP (G) and these markers in untreated and doxycycline-treated animals (Figure III-1 A). Here I found that the majority of apical cells expressed Nestin (20.35 ± 6.9 % of total apical cells; Figure III-1 B), whereas fewer cells showed activity of the hGFAP promoter (G^+; 8.34 ± 2.2 %) or co-expression of both (6.37 ± 0.4 %). Cells in the basal layer of the niche, i.e., with a nuclear distance of > 20 µm to the apical surface, showed significantly less expression of Nestin, both alone (4.52 ± 0.8 % of total basal cells) and co-expressed with the G reporter (0.51 ± 0.5 %). However, here G^+ cells were more common than in the apical region (17.8 ± 4.9 %). To determine which cells are more proliferative, I compared the percentage of Nestin-expressing or G^+ NSCs in untreated mice to those in doxy-treated animals (Figure III-1 C). Here I found that both $Nestin^+G^-$ and $Nestin^-G^+$ apical NSCs did not decrease in numbers after treatment with doxy (18.5 ± 3.7 % and 12.64 ± 3.8 %, respectively), whereas $Nestin^+G^+$ cells were significantly decreased, implying proliferation. In the basal layer, both $Nestin^+$ and $Nestin^+G^+$ cells did not decrease (4.5 ± 1.5 % and 0.1 ± 0.1 %), whereas only $Nestin^-G^+$ cells showed a trend decrease (12.3 ± 1.6 %; $p = 0.1$). This suggests that in apical cells, only $Nestin^+G^+$ cells proliferate, whereas basal $Nestin^-G^+$ cells are more proliferative on the basal side while the rare $Nestin^+G^+$ cells do not contribute to neurogenesis there.

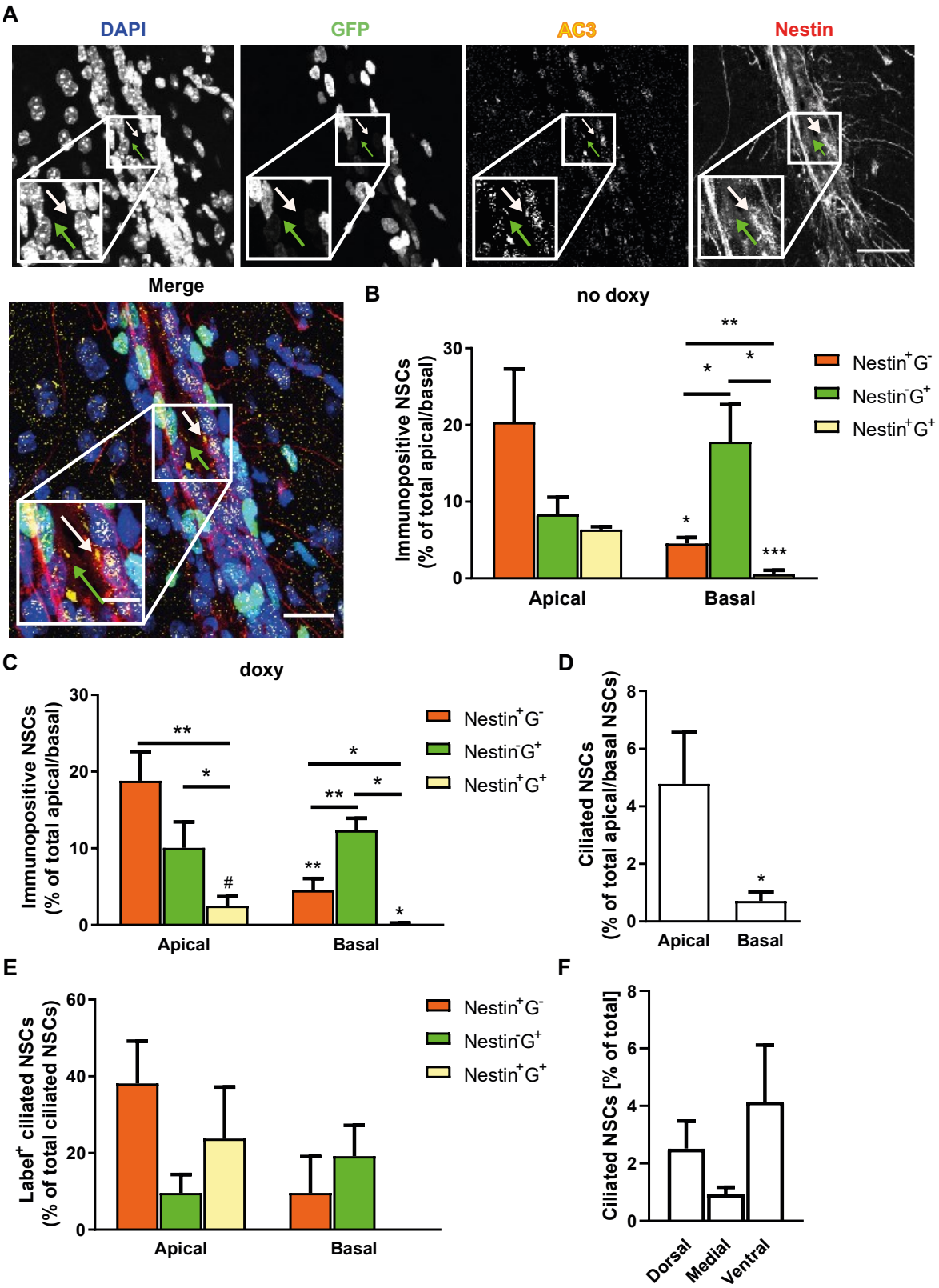

Figure III-1: Characterisation of NSCs and their cilia in the adult V-SVZ.
(A) Immunofluorescent micrograph of coronal brain sections of 8w hGFAP:H2B-GFP animals, labelled with Nestin (red) and AC3 (yellow). GFP fluorescence is displayed in green, DAPI (blue) was used as nuclear counterstain. White and green arrows indicate Nestin$^+$ and G$^+$ ciliated cells, respectively. Scale bar = 20 µm. (B, C) Quantification of label-expressing NSCs in untreated (B) and doxy-treated animals (C). (D-F) Quantification of ciliated NSCs, by layer (apical vs basal, D), label (E) and along the dorso-ventral axis (F). Some of the results in this Figure are already published in Baur, et al. [2].

Next, I analysed ciliation of Nestin/reporter-expressing cells (Figure III-1 D-F) by counting the number of cells displaying a primary cilium, which I labelled using primary cilia marker AC3 (Figure III-1 A, arrows). Here I found that while overall 4.78 ± 1.8 % of apical cells displayed a primary cilium, only 0.7 ± 0.3 % of basal cells were ciliated (Figure III-1 D). In the apical cell layer, Nestin-expressing cells were the most ciliated, with 38.06 ± 11.1 % of $Nestin^{+}G^{-}$ cells and 23.7 ± 13.4 % of $Nestin^{+}G^{+}$ cells extending primary cilia, while only 9.6 ± 4.7 % of $Nestin^{-}G^{+}$ cells were ciliated (Figure III-1 E). Among basal G^{+} cells, only 19.12 ± 8.0 % carried a cilium, while no basal ciliated $Nestin^{+}G^{+}$ cells could be detected in any analysed brain section. As ciliation is tightly associated with quiescence, these results overall might suggest that apical NSCs are more quiescent than basal NSCs in adult mice.

It has been previously shown that in adult animals, only NSCs in the ventral V-SVZ change their behaviour after constitutive cilia ablation[111]. This suggests that cells along the dorso-ventral axis might be differentially ciliated or regulated. Indeed, in the V-SVZ of 8w hGFAP:H2B-GFP animals, ventral cells were most ciliated, with 4.15 ± 1.97% of all cells carrying cilia (Figure III-1 F), while cells located in the middle of the lateral wall (medial) were least ciliated (0.92 ± 0.25 %). This indicates that differences in ciliation might be responsible for the differential response to cilia ablation.

To determine whether NSCs are already present in the neonatal brain, and since age decreases NSC number and increases ciliation[12], I investigated whether marker expression and ciliation in neonatal (postnatal day 7, P7) mice differ from adult mice (Figure III-2 A). Here I found that like in adult animals, at P7 $Nestin^{+}G^{-}$ and $Nestin^{+}G^{+}$ cells were already present mostly in the apical cell layer, while $Nestin^{-}G^{+}$ cells were present at similar percentages in apical and basal cell layers (Figure III-2 B). Similar to adult animals, P7 animals showed very high levels of ciliation in apical cells (20.99 ± 0.3 %; Figure III-2 C) and significantly less cilia were extended by basal cells (0.46 ± 0.2 %); the $Nestin^{+}$ cells regardless of H2B-GFP co-expression showed the highest rates of ciliation (Figure III-2 D). Lastly, I found that ventral cells are already more ciliated at P7, although still at much higher rates than adult animals (13.5 ± 0.6 %; Figure III-2 E), while cells located in the medial V-SVZ were more likely to carry cilia than their 8w counterpart. Meanwhile, ciliation seemed to remain similar in the dorsal region of P7 animals (1.5 ± 0.65 %) compared to 8w animals (2.8 ± 1.7 %).

Together, these results suggest that these differences between apical and basal NSCs as well as the ciliation of ventral NSCs is already established early in postnatal development, and that apical NSCs enter quiescence already shortly after birth. Furthermore, the low ciliation of basal NSCs may indicate higher proliferation and decreased quiescence in this cell group, while the higher ciliation of medial cells at P7 might suggest a slower maturation of this part of the niche.

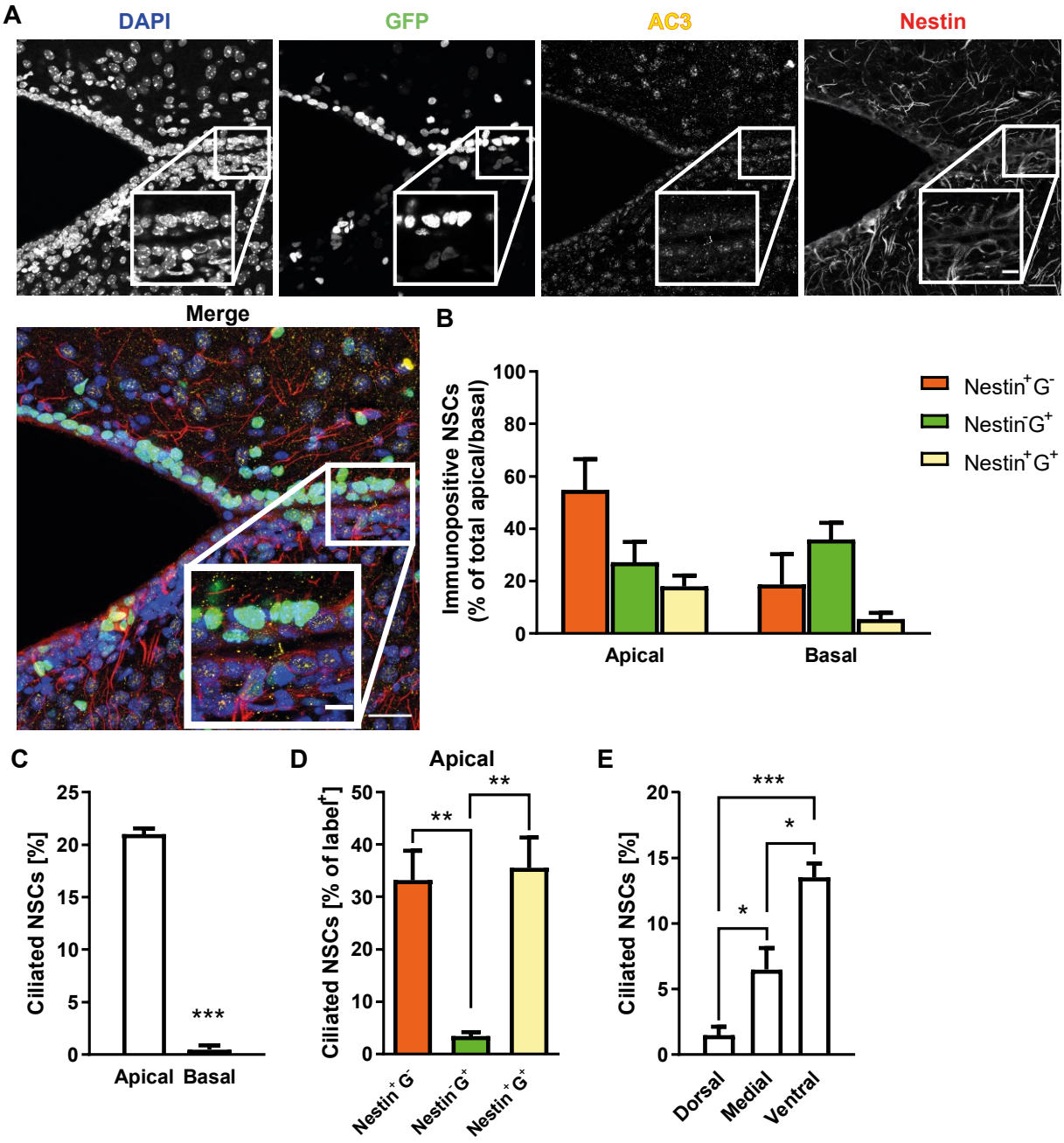

Figure III-2: Characterisation of NSCs and their cilia in the P7 V-SVZ.
(A) Immunofluorescent micrograph of coronal brain sections of P7 hGFAP:H2B-GFP animals, labelled with Nestin (red) and AC3 (yellow). GFP fluorescence is displayed in green, DAPI (blue) was used as nuclear counterstain. Scale bar = 20 µm.
(B) Quantification of label expressing NSCs.
(C-E) Quantification of ciliated NSCs, by layer (apical vs basal, C), label (D) and along the dorso-ventral axis (E). Some of the results in this Figure are already published in Baur, et al. [2].

2. Expression of GDF15-receptor GFRAL in the mouse neurogenic niches

Some of the results in this chapter and the following chapters are already published as pre-print[1], which is currently under peer review at *Development* and is aimed for publication later this year, or part of a manuscript in preparation.

2.1 GFRAL is expressed in NSCs in the V-SVZ but not in the hippocampus.

Growth/differentiation factor 15 (GDF15) has previously been shown to be expressed at the apical side of the V-SVZ[153] at mRNA-level and protein level[1,153,174], as well as secreted by the choroid plexus[152,174]. However, recent studies investigating the expression of its receptor GFRAL showed little to no expression in the brain using RNA analysis[155,156,162]. Since GDF15 expression in the GE is upregulated at E16 and then stays stable from E18 until adulthood[164], suggesting a role of the growth factor in the niche, I used an antibody against the GFRAL protein to detect the receptor expression in the GE/V-SVZ of E18 and adult wild-type (WT) animals.

Here I found that GFRAL, like GDF15, is highly expressed especially at the apical side of both the E18 GE and the 8w V-SVZ (Figure III-3 A). At E18, $GFRAL^+$ cells show a strong apical-basal polarity similar to radial glia-like cells, suggesting that the cells expressing GFRAL might be NSCs. In the hippocampus (HP), I however saw only very little expression of GFRAL at both embryonic and adult stages. To determine whether the cells expressing GFRAL are in fact NSCs, I used immunofluorescence on cryosections of brains of 8w old mice to label Nestin, which is expressed by NSCs and ependymal cells, glial cell marker GFAP, and CXCR4 to label neural progenitor cells. Here I found that in the dentate gyrus (DG), the neurogenic niche in the HP, GFRAL weakly co-localized with GFAP, but not with Nestin or CXCR4, while in the V-SVZ, GFRAL co-localized both with Nestin and GFAP, suggesting that GFRAL is expressed by ependymal cells and NSCs in this niche. Lastly, I did not see any co-expression of GFRAL with CXCR4 at the basal side of the niche, indicating that GFRAL expression is lower in basal cells farther in the neural lineage, while CXCR4-expression in apical cells was overall weaker.

NSCs In the V-SVZ highly depend on EGFR signalling for activation and proliferation; activated NSCs can be distinguished from quiescent NSCs by their higher levels of surface EGFR expression[54,77]. In a previous study, GDF15 was shown to regulate EGFR expression in the HP[164], however, since the receptor for GDF15 had not yet been discovered[155-157], it could not be determined whether this effect is direct, i.e. affecting the cells expressing the GDF15 receptor, or if this effect is relayed by different cells via distinct mechanisms. Therefore, I used immunofluorescence to label EGFR and GFRAL to investigate co-expression. Indeed, I found that GFRAL co-localizes in part with EGFR in the GE/V-SVZ of both embryonic and adult animals (Figure III-3 C, D), which could point towards a direct effect of GFRAL on EGFR expression or activation.

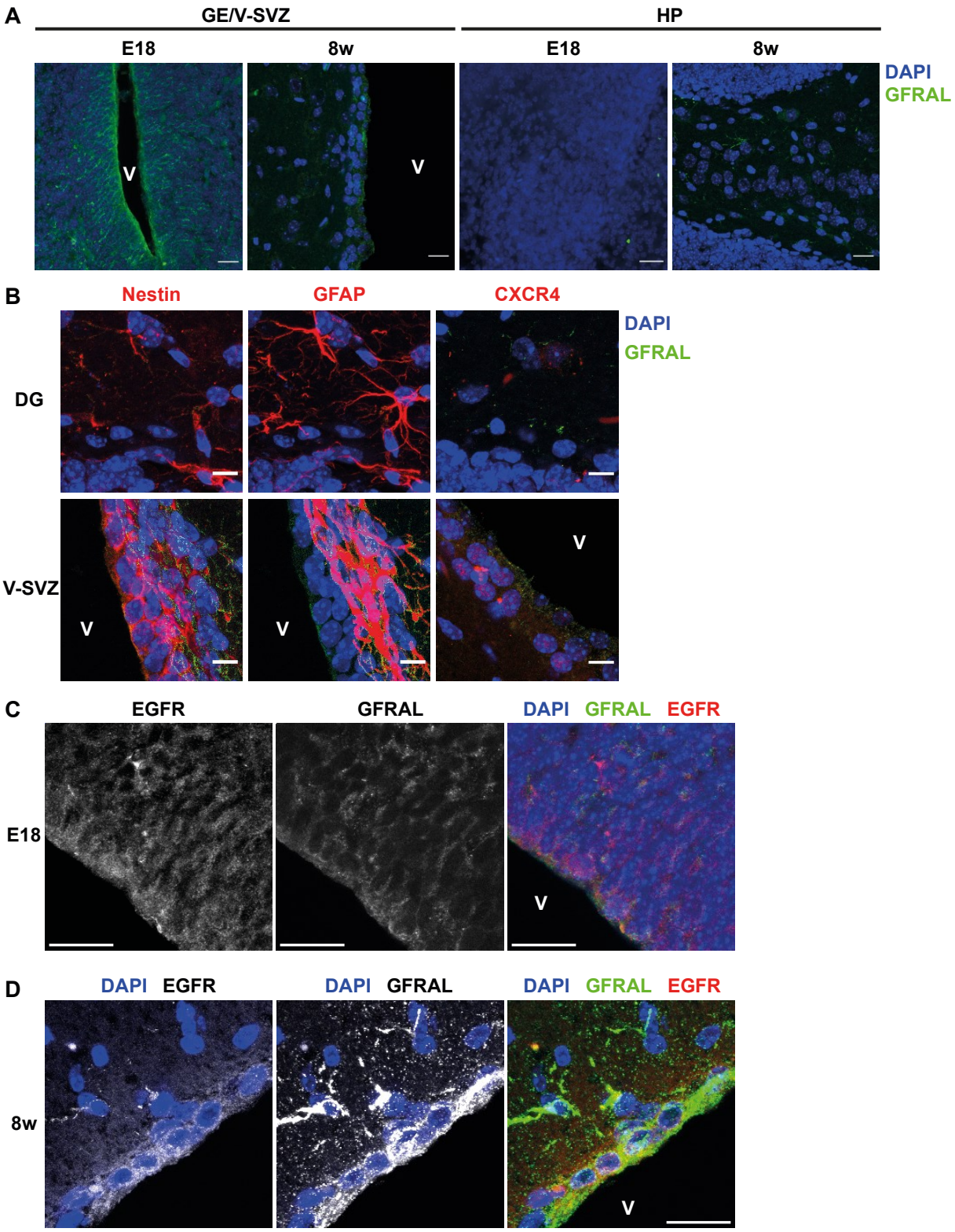

Figure III-3: Expression of GDF15-receptor GFRAL in the neurogenic niches.
(A) Immunofluorescent staining of GFRAL in the E18 and adult (8w) GE/V-SVZ and hippocampus (HP) as overview. Scale bars = 20 µm.
(B) Co-expression of GFRAL with NSC markers nestin and GFAP, as well as CXCR4, which is mainly expressed by neural precursors, in 8w old animals in the V-SVZ and the dentate gyrus (DG) in the HP. Scale bars = 10 µm.
(C, D) Immunofluorescent staining of GFRAL and EGFR in the E18 and adult (8w) GE/V-SVZ. Scale bars = 20 µm.
V = ventricle. Parts of this figure are already published in Baur, et al. [1] [pre-print].

2.2 GFRAL is expressed in primary cilia in the E18 GE, but not in the hippocampus.

Since I found a high expression of GFRAL in apical NSCs, particularly those expressing Nestin, and I previously found that apical Nestin-expressing cells are highly ciliated, I hypothesized that GFRAL might interact with or affect primary cilia. Therefore, I labelled GFRAL together with primary cilia in the embryonic GE and HP using Arl13b, which labels multiple types of cilia in the GE, and NSC primary cilia in the HP[123], and AC3, which labels only primary cilia, and exclusively neuronal primary cilia in the HP[121,122] (Figure III-4). Since there are more ciliated cells in the GE before birth, as well as less ependymal cells to obstruct analysis, I performed this analysis in GE whole mounts and coronal sections of the HP in mice at E18. Here I found that in the E18 GE, GFRAL accumulated in primary cilia and co-localized with both Arl13b and AC3 (white arrows). However, not all primary cilia expressed GFRAL, as some only expressed Arl13b (blue arrows) or Arl13b and AC3 (green arrows). In the HP, not only was the overall expression of GFRAL lower, but also no co-localization with cilia markers was visible. This suggests that the working mechanism of GFRAL in the embryonic GE might be different from that in the HP, and that in the former region, primary cilia may be important to GDF15 signalling.

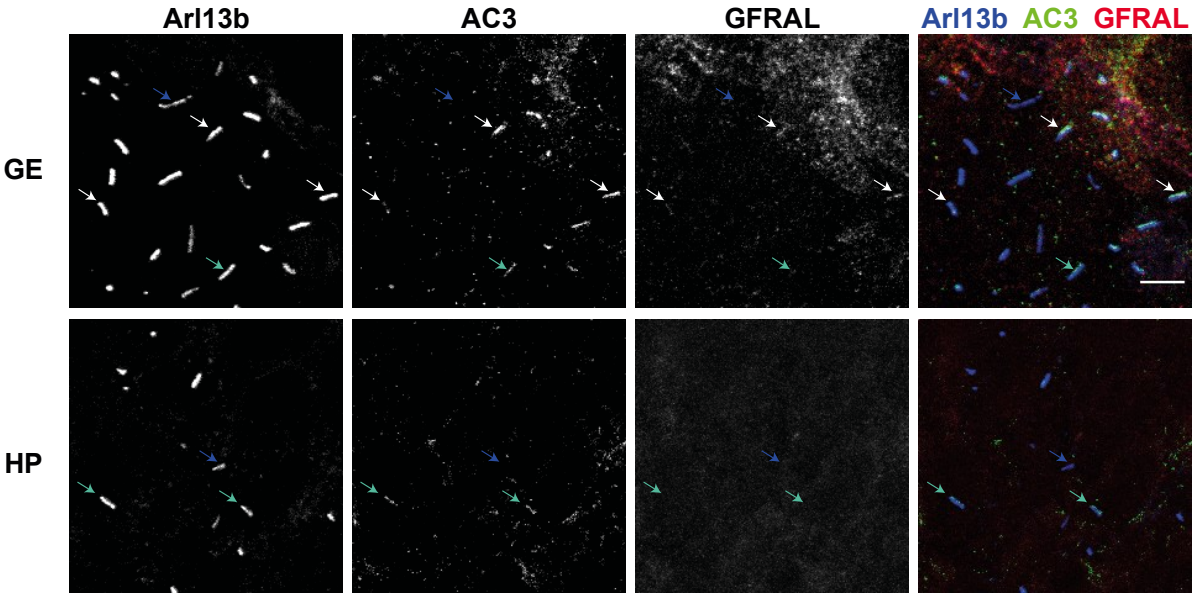

Figure III-4: GFRAL localizes to primary cilia in the GE, but not in the HP at E18.
Immunofluorescent staining of a whole mount of the WT E18 GE (top) and a coronal section of the E18 hippocampus. Primary cilia were visualized with cilia marker Arl13b (blue) and primary cilia marker AC3 (green). Co-localization of GDF15-receptor GFRAL with ciliary markers is visible (white arrows), although some cilia show immunoreactivity only to Arl13b (blue arrows) or Arl13b and AC3 (green arrows). Scale bar = 5 µm.
This figure is part of a manuscript in preparation.

2.3 GFRAL is only weakly expressed at mRNA level, but expression is not affected by GDF15 knock-out.

To closer examine the role of GDF15 in the GE, I investigated molecular changes in mice without GDF15 protein expression (Gdf15$^{-/-}$). These mice have a C57BL/6 genetic background and a LacZ-knock-in at the locus of the endogenous *Gdf15* gene; therefore, homozygous mice express only LacZ under the endogenous *Gdf15* promoter and have no copy of the *Gdf15* gene, and thereby no GDF15 protein.

Commonly after gene knock-out, compensatory mechanisms are activated to ensure a functional organism in spite of the missing protein, leading to a reduced visible phenotype. For secreted signalling proteins, one of the most common compensatory mechanisms is receptor overexpression or downregulation. Therefore, I used quantitative real-time PCR (qPCR) to measure levels of GFRAL mRNA transcripts in the GE and HP of E18 WT and Gdf15$^{-/-}$ animals (Figure III-5 A, B). Brain stem (BSt) samples were used as a positive control, as the effect of GDF15 on body weight is relayed by neurons in the BSt displaying high levels of GFRAL expression[156]. I used both a commercially available TaqMan assay as well as self-designed primers for SYBR Green assay; with both approaches, I found that there are similar levels of *Gfral* transcripts in the GE and DG, and that both are much lower than in the BSt. With these low levels of *Gfral* transcripts, the receptor may not be considered expressed in the V-SVZ. However, my finding that GFRAL protein is also present in these regions does not support this conclusion. In all analysed brain regions, I could not find any differences between WT and Gdf15$^{-/-}$ animals. To confirm that the amplification product is of expected length (i.e. 213 bp), I analysed the product of the SYBR Green assay on a 2% agarose gel (Figure III-5 C). I found that in all brain regions analysed, the PCR product was of the expected length of 213 bp; a negative control with water instead of cDNA showed no amplification, excluding primer dimers, and since the primers were selected to be exon spanning, a contamination of the sample with genomic DNA can be excluded. All in all, these results suggest that GFRAL is expressed at low levels, but consistently, in both the GE and the HP at E18, and that GDF15 knock-out is not compensated by receptor overexpression.

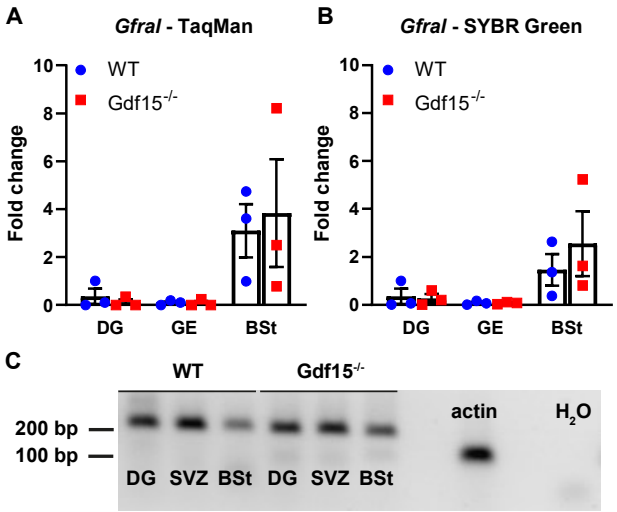

Figure III-5: Gfral mRNA level in the DG, GE and BSt.
(A, B) Fold change of mRNA in WT and Gdf15$^{-/-}$ mice using TaqMan (A) and SYBR Green (B) assays.
(C) Agarose gel showing qPCR products of SYBR green assay. Expected product size: 213 bp. Primers for actin (113 bp) were used as positive control, and primers for Gfral with H_2O instead of cDNA as negative control.
This figure is already published in Baur, et al. [1] [pre-print].

3. Effects of GDF15 knock-out on the V-SVZ

3.1 Ablation of GDF15 changes cilia length in the E18 GE and adult V-SVZ

Primary cilia are vital signalling organelles that govern NSC activation and quiescence, especially in apical cells in the V-SVZ; due to the expression of GFRAL in these cells and its localisation to primary cilia in the niche, I hypothesized that primary cilia and their signalling may be affected in Gdf15$^{-/-}$ animals. To investigate cilia morphology and number, I used immunofluorescence for cilia marker Arl13b on E18 GE whole mounts, since there are more cilia and NSCs in the GE before birth (Figure III-6 A). Here I found that primary cilia in the GE of E18 Gdf15$^{-/-}$ animals are on average shorter (Figure III-6 B), thicker (Figure III-6 C) and more numerous (Figure III-6 D) than age-matched WT controls. On average, primary cilia in the WT GE were 3.67 ± 0.45 µm long, whereas Gdf15$^{-/-}$ cilia were only

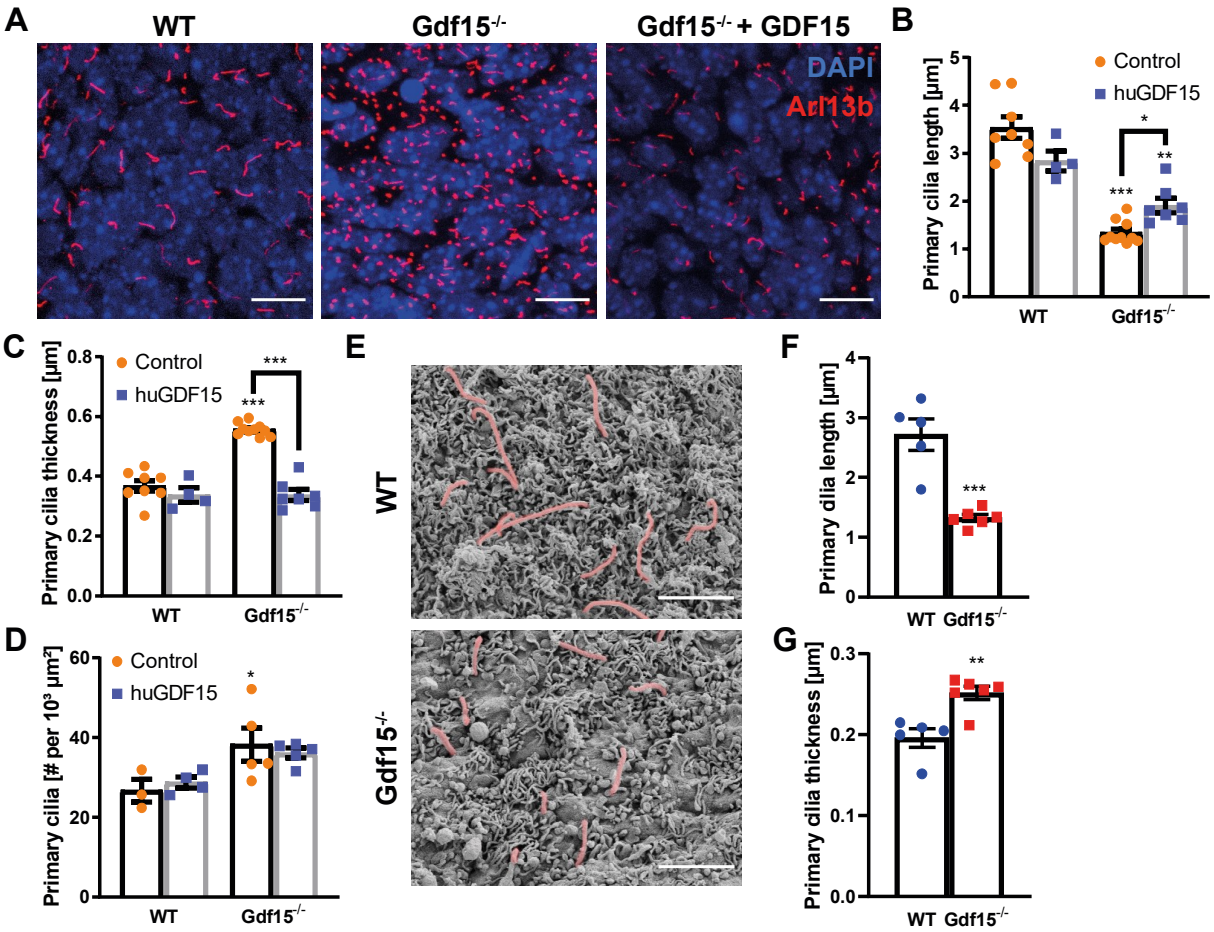

Figure III-6: Gdf15$^{-/-}$ animals have shorter, thicker and more primary cilia in the apical E18 GE.
(A) WT and Gdf15$^{-/-}$ E18 GE whole mounts immunofluorescently labelled with Arl13b (red). DAPI (blue) was used as nuclear counterstain. + GDF15 = incubated with exogenous GDF15 for 24 h pre-fixation. Scale bars = 10 µm.
(B-D) Quantification of primary cilia length (B), thickness (C) and number (D) based on immunofluorescence in WT and Gdf15$^{-/-}$ E18 whole mounts with or without GDF15 application overnight.
(E) Scanning electron microscopic images of the WT and Gdf15$^{-/-}$ E18 GE. Primary cilia are highlighted in red. Scale bars = 5 µm.
(F, G) Quantification of primary cilia length (F) thickness (G) based on electron micrographs.
The panels in this figure are part of a manuscript in preparation.

1.29 ± 0.11 µm long. Thickness, as measured at the thickest part of the cilium perpendicular to the axoneme, was 0.39 ± 0.02 µm in WT and 0.54 ± 0.01 µm in Gdf15$^{-/-}$ animals (Figure III-6 C), and with 23.44 ± 3.89 cilia per 1000 µm², the GE of Gdf15$^{-/-}$ animals contained more cilia than that of WT animals, which on average contained only 14.96 ± 1.98 cilia in the same area (Figure III-6 D).

To determine whether this difference is a by-product of GDF15 knock-out in early development or rather a direct effect of lack of GDF15 on cilia, I incubated whole lateral GEs of WT and Gdf15$^{-/-}$ animals in medium with recombinant human GDF15 for 24 h (Figure III-6 A-D). This treatment increased primary cilia length in Gdf15$^{-/-}$ samples by half (to 1.9 ± 0.14 µm), and reduced thickness to WT level, while the number of cilia in the niche was not significantly changed consistently. During multiple rounds of experiments, I found that, even though the number of primary cilia per area was consistently higher in the Gdf15$^{-/-}$ samples than in the WT samples, their absolute number was very variable between experiments and thus, not a good indicator of overall cilia phenotype; therefore, I did not analyse this parameter in subsequent experiments. In WT animals, treatment with GDF15 showed no significant effect on primary cilia in any of the measured parameters (Figure III-6 B-D).

Here I visualised primary cilia by immunolabelling Arl13b, a protein which is not universally expressed in all cilia, and whose expression levels may change due to various factors like intracellular trafficking, ciliary signalling or cell proliferation. To confirm that the ciliary measurements made in the Arl13b channel reflect true changes in ciliary morphology, I used scanning electron microscopy (ScEM) to assess the shape of primary cilia in the niche without the use of marker proteins (Figure III-6 E-G). This analysis confirmed that cilia length measured with Arl13b fluorescence reflected true cilia length as measured from the cell membrane, with WT cilia measuring an average length of 2.7 ± 0.3 µm and cilia in the Gdf15$^{-/-}$ GE only 1.3 ± 0.05 µm (Figure III-6 F), which did not significantly differ from the values measured in fluorescence. However, the thickness of cilia measured only around 0.2 µm compared to 0.39 µm in fluorescence, although there was still a significant increase in cilia thickness in Gdf15$^{-/-}$ samples (Figure III-6 G). This difference may be explained by the dehydration necessary for electron microscopy, which may shrink organelles only contained by a membrane, or the resolution limit of light microscopy, which may artificially increase thickness of structures by a radial glow. Lastly, increased fluorescence in the Arl13b channel may be caused by differential expression of the protein, or locally higher concentration of the protein due to shorter cilia. Since, however, a difference in thickness between WT and Gdf15$^{-/-}$ cilia is still visible in scanning electron microscopy, I conclude that cilia in the Gdf15$^{-/-}$ GE are indeed thicker than in WT age-matched controls.

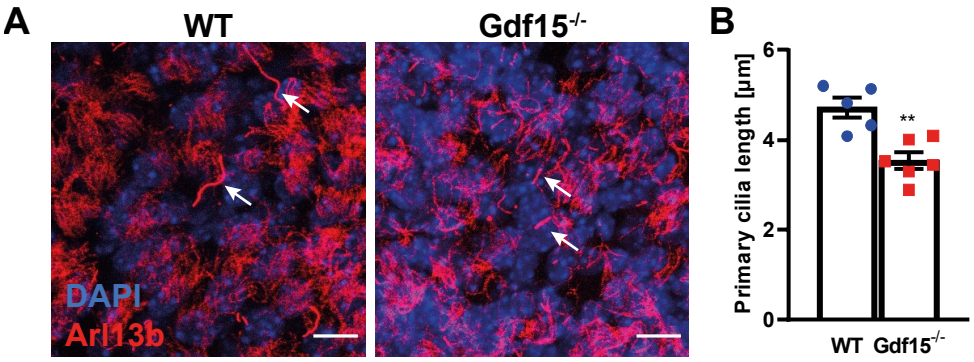

Figure III-7: Primary cilia length in the adult V-SVZ.
(A) Micrograph of whole mounts of the V-SVZ of 8w WT and Gdf15$^{-/-}$ animals labelled with Arl13b to visualise primary cilia (white arrows). DAPI was used as nuclear counterstain. Scale bars = 10 µm. Images courtesy of Şeydanur Şan.
(B) Quantification of primary cilia length.
This figure is part of a manuscript in preparation.

During ageing, NSCs in the V-SVZ increasingly enter quiescence[49]. Since primary cilia extension is closely correlated with cell cycle[12,108,110], NSCs in deep quiescence carry longer cilia than more proliferative cells, leading to an increase in average cilia length in adult animals[12]. To investigate whether the change in cilia morphology at E18 is a transient effect on the highly proliferative embryonic NSCs or a long-lasting change that persists into adulthood, I measured cilia length in the V-SVZ of adult (8-weeks-old, 8w) WT and Gdf15$^{-/-}$ animals with the help of master student Şeydanur Şan (Figure III-7). As expected, cilia length was increased in 8w animals compared to E18, with WT cilia averaging to 4.71 ± 0.22 µm, but cilia in the knock-out animals were still significantly shorter (3.54 ± 0.18 µm; Figure III-7 B).

Taken together, these data show that lack of GDF15 affects cilia morphology, which is not transient and persists into adulthood, and that this effect is reversible by application of exogenous GDF15.

3.2 Cilia length is not changed in other brain regions at E18 or 8w

While I found GFRAL localization to the primary cilia only in the GE, GDF15 was previously shown to play a role in progenitors in the subgranular zone of the HP[164]. To determine whether ciliary localization of GFRAL is correlated with the effect on cilia morphology, I measured cilia length in coronal sections in the E18 and 8w HP, as well as the hypothalamus (HTh) and the brain stem (BSt) of 8w animals, regions where GFRAL was shown to more highly expressed[156] (Figure III-8). Since Arl13b is differentially expressed in some brain regions[123], I used also primary cilia marker AC3 to label e.g. neuronal cilia in the HP, where Arl13b is only expressed in cilia of NSCs and glia. In both E18 and adult (8w) animals, I did not find a difference in length in neuronal ($AC3^+$) and other primary cilia ($Arl13b^+$) in the $Gdf15^{-/-}$ HP compared to that of a WT control (Figure III-8 A-D). Furthermore, there was no difference in the percentage of ciliated cells (Figure III-8 E). However, while at E18, multiple cilia still showed immunoreactivity to both AC3 and Arl13b (double positive, DP), no such cilia were found in the adult HP (Figure III-8 B, D), and $Arl13b^+$ cilia overall increased in length with age. This change in ciliary protein expression and length is most likely an effect of maturation of the niche, with DP cilia belonging to immature neurons or neuroblasts that lose Arl13b-expression upon maturation. Additionally, I found that at E18, $AC3^+$ cilia were longer than $Arl13b^+$ cilia, likely reflecting the high proliferation of NSCs in the niche at this time[12], while neurons extending $AC3^+$ cilia are already fully differentiated and therefore, their cilia are at their mature length (E18: 2.4 ± 0.3 µm; 8w: 2.1 ± 0.1 µm). As previously mentioned, primary cilia length is closely associated with quiescence[12]; therefore, $Arl13b^+$ primary cilia of NSCs are significantly longer in the adult than in the E18 HP (E18: 1.6 ± 0.1 µm; 8w: 3.3 ± 0.1 µm; $p<0.0001$). These parameters are the same in the WT as in the $Gdf15^{-/-}$ HP, which indicates that ciliogenesis, as well as neuronal and NSC maturation, are not heavily affected by lack of GDF15 in this niche.

In the HTh and BSt, where GDF15-receptor GFRAL is more highly expressed, I could also not find any differences in the length of primary cilia in the mutant compared to the WT control (Figure III-8 F, G, I, J). In the HTh, there was a trend increase in the number of cells containing $Arl13b^+$ cilia in $Gdf15^{-/-}$ animals, which might suggest an increase in glial cells in this region, however, the difference was not statistically significant (Figure III-8 H). In the BSt, like in the HP, there was no discernible difference in the number of ciliated cells (Figure III-8 K).

Taken together, these data indicate that cilia morphology is altered only in the GE/V-SVZ, where I previously found that GFRAL localises to primary cilia. This suggests that ciliary GFRAL localisation is a necessary factor for the shortening of primary cilia due to lack of GDF15.

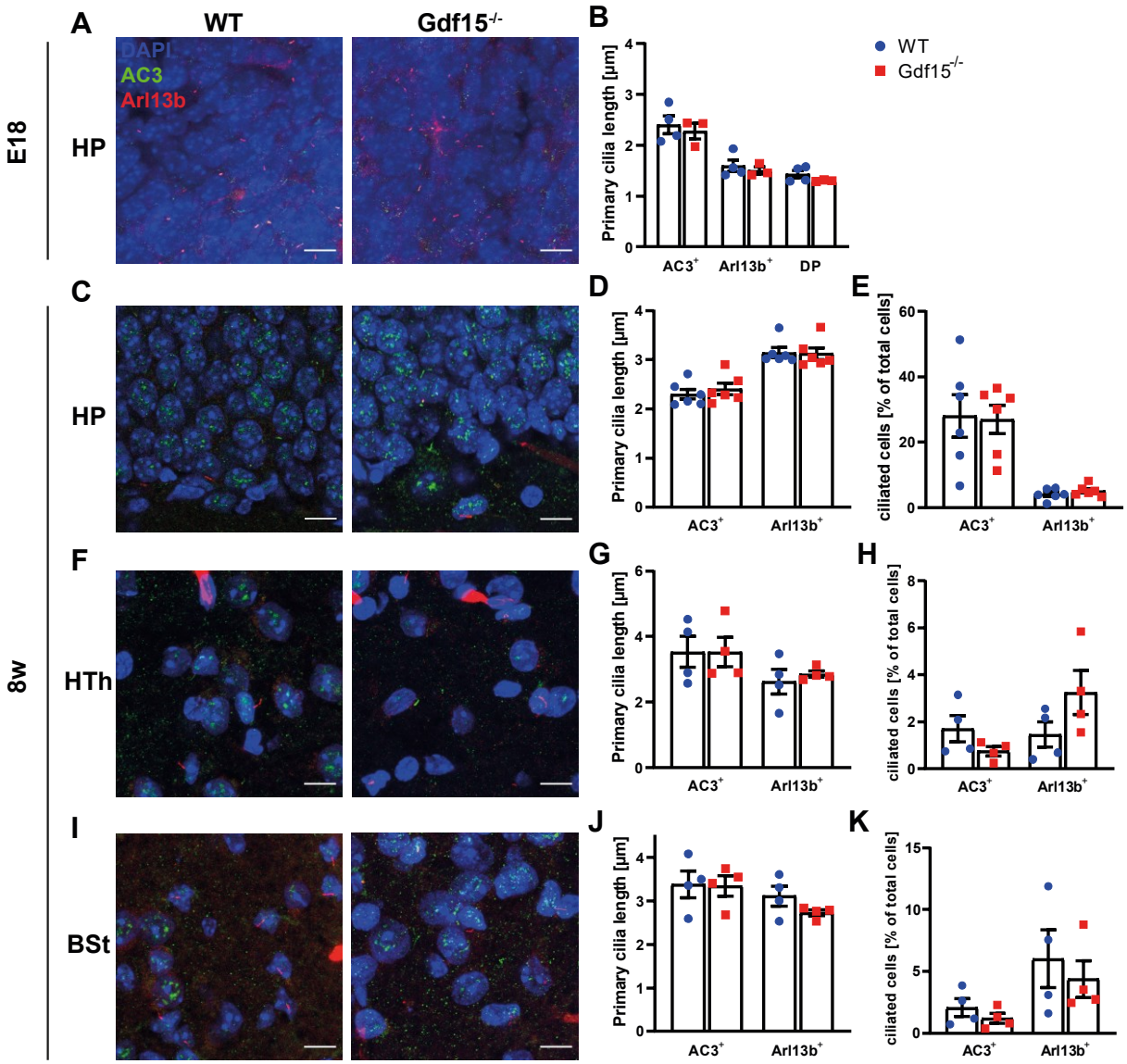

Figure III-8: Primary cilia length and number is not changed in other brain regions.

(A, C, F, I) Immunofluorescent staining of coronal sections of the E18 HP (A), and the 8w HP (C), HTh (F) and BSt (I) for Arl13b and AC3. DAPI was used as nuclear counterstain. Scale bars = 10 µm.

(B, D, G, J) Average cilia length in the E18 HP (B), and the 8w HP (D), HTh (G) and BSt (J). DP = Double positive, Arl13b$^+$ AC3$^+$.

(E, H, K) Average number of cilia per nucleus in the 8w HP (E), HTh (H) and BSt (K). Due to the high cell density at E18, nuclei were not counted in the E18 HP.

This figure was already published in a preprint[1].

3.3 Cilia elongation upon GDF15 application requires MAPK/ERK signalling

Incubation of Gdf15$^{-/-}$ E18 whole lateral wall explants with exogenous GDF15 overnight increased cilia length (see Chapter III-3.1). To determine whether this mechanism is local, i.e. requiring only intra-ciliary signals, or if it requires further downstream signalling and transcriptional activation, such as MAPK/ERK signalling, I blocked ERK signalling during application of GDF15. For this, I used U0126, a MEK1/2 inhibitor, which prevents phosphorylation and thereby activation of ERK, and measured primary cilia in the presence and absence of the inhibitor and GDF15. As a control, I used EGF, which activates ERK signalling via EGFR, but its receptor is not localized to primary cilia.

First, I confirmed MAPK/ERK activity and inhibition by U0126 by western blot. Here, I found that both application of EGF and GDF15 increased ERK phosphorylation in the WT and Gdf15$^{-/-}$ GE at E18, while U0126 blocked ERK phosphorylation entirely (Figure III-9 A). When measuring primary cilia in the Gdf15$^{-/-}$ GE, I found that ERK pathway activation by EGF alone did not elongate cilia or reduce thickness (Figure III-9 B-D), however, when ERK phosphorylation was inhibited by U0126, cilia elongation and reduction in thickness in response to GDF15 application was also blocked.

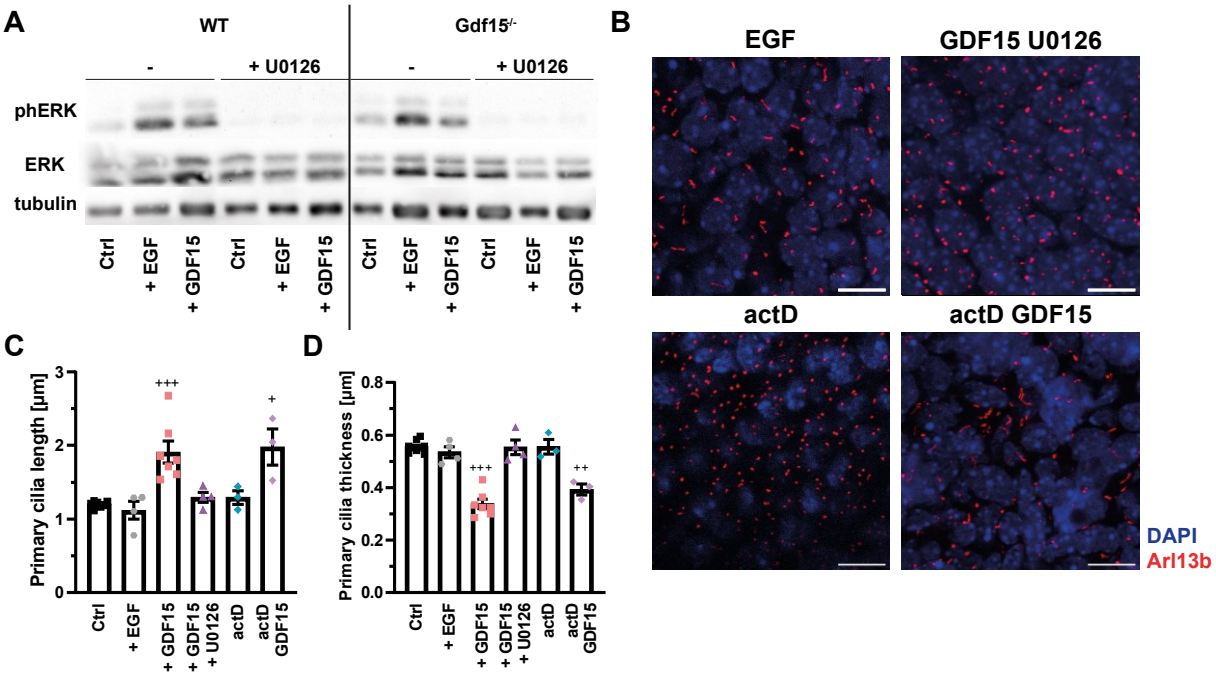

Figure III-9: Rescue of ciliary morphology requires MAPK/ERK signalling but no transcription.
(A) Western blot showing phosphorylated ERK (phERK) and ERK levels in samples of the WT and Gdf15$^{-/-}$ E18 GE, treated with EGF, GDF15, or GDF15 with U0126 overnight. α-tubulin was used as endogenous control.
(B) Immunofluorescent images of Gdf15$^{-/-}$ E18 whole mounts treated with EGF, GDF15 with U0126, actinomycin D (actD), and actD with GDF15 overnight. Scale bars = 10 µm.
(C, D) Quantification of primary cilia length (C) and thickness (D) in the GE of E18 embryos, after treatment with EGF, GDF15 with U0126, actD, and actD with GDF15.
Parts of this figure are part of a manuscript in preparation.

These data indicate that ERK phosphorylation downstream of GFRAL, but not EGFR activation, is necessary for the mechanism mediated by GFRAL; however, this implies that other mechanisms caused by GDF15 apart from ERK pathway activation are also vital for ciliary length regulation.

Lastly, to determine whether the cilia elongation requires transcriptional activation, or if local translation and trafficking are sufficient, I used actinomycin D (actD) to block transcription while treating whole GEs of E18 Gdf15$^{-/-}$ mice with GDF15 for 24 h, and subsequently analysed ciliary length and thickness (Figure III-9 B-D). Lack of any staining for Ki67 (not shown), a protein which has a half-life of only 1-1.5 h and thereby requires permanent transcriptional activation to remain detectable[57], showed that inhibition of transcription by actD was successful. Here I found that actD itself did not change ciliary shape and did not inhibit the rescue of length and thickness caused by GDF15. This suggests that this rescue does not depend on transcriptional activity and can be sustained by other means.

3.4 GDF15-knock-out leads to increased proliferation in the E18 GE and 8w V-SVZ

Primary cilia are closely linked to the cell cycle and NSC quiescence[12,108]. Therefore, it is likely that differences in cilia morphology either cause or reflect changes in cell cycle dynamics or stem cell activation in the ciliated, i.e., apical NSCs. To investigate this issue, I used Ki67, a nuclear protein expressed in cycling cells[57], to visualize actively proliferating cells in the GE of E18 WT and Gdf15$^{-/-}$ embryos, as well as in the V-SVZ of adult animals (Figure III-10). Here I found that at E18, Gdf15$^{-/-}$ embryos have significantly more Ki67^{+} cells in the GE than WT age-matched controls (Figure III-10 A, B), and that more cells could be identified as mitotic, i.e. showing a nuclear morphology of ana-, meta- or telophase (Figure III-10 C). In the latter analysis, I distinguished between apically and subapically dividing progenitors, where cells dividing with ≤ 10 µm distance towards the ventricle lumen were considered apical, and cells dividing further away were considered subapically dividing cells (see also illustration in Figure III-10 A). Since the distance of the nucleus to the ventricle at the time of mitosis is indicative of the NSC subtype, e.g. radial glia and SNPs, which divide in the apical cell layer, or SAPs, which divide subapically[31], this approach allows me to determine if diverse NSC subtypes are differentially affected by GDF15-knock-out. However, here I found that dividing cells were increased in both apical and subapical cell layers, indicating that multiple different populations of NSCs might be affected by the increase in proliferation.

GDF15 expression is upregulated in late embryonic development (E16), and the expression remains on a similar level well into adulthood[164]. To determine whether the increase in proliferation at E18 is a temporary effect of acute lack of GDF15, e.g. that NSCs enter quiescence at a later timepoint, I investigated proliferation also in the V-SVZ of adult animals (Figure III-10 D-F) with the help of master student Şeydanur Şan.

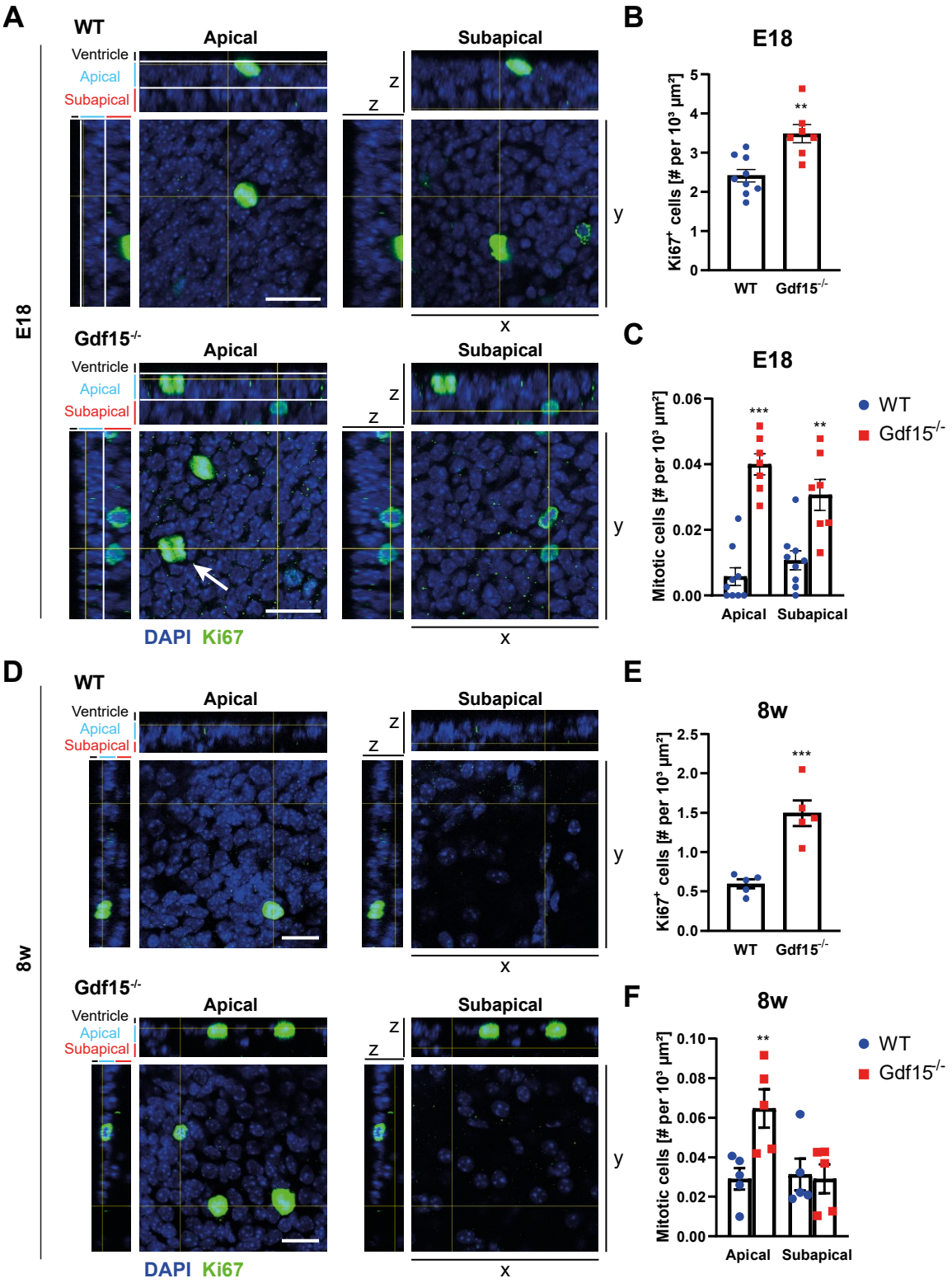

Figure III-10: Lack of GDF15 leads to increased proliferation in the GE and V-SVZ.
(A, D) Immunofluorescence micrographs of WT and Gdf15$^{-/-}$ whole mounts at E18 (A) and 8w (D), labelled with proliferation marker Ki67, at apical and subapical cell layers. Smaller images are orthogonal projections based on z-planes. Yellow lines indicate location of the respective cross-section, x, y and z indicate image axes. DAPI was used as a nuclear counterstain. Images displayed in panel D courtesy of Şeydanur Şan. Scale bars = 20 µm. (B, C, E, F) Quantification of Ki67^{+} cells (B, E) and cells in mitosis (C, F) in the E18 GE (B, C) or the adult V-SVZ (E, F).
Parts of this figure are already published in Baur, et al. [1] [pre-print].

Although proliferation was overall lower in the adult V-SVZ compared to the E18 GE (WT_{adult}: 0.6 ± 0.05 cells / 10^3 µm², WT_{E18}: 2.4 ± 0.2 cells / 10^3 µm², $p<0.001$; compare Figure III-10 B and E), the V-SVZ of $Gdf15^{-/-}$ animals still contained significantly more proliferating cells than the WT control (Figure III-10 E). When analysing the dividing cells, however, I found that there were significantly more mitotic cells in the apical, but not in the subapical cell layer in the $Gdf15^{-/-}$ V-SVZ compared to WT animals (Figure III-10 F). This indicates that apically dividing cells are continuously proliferating more in adult $Gdf15^{-/-}$ animals, suggesting a stronger effect of the lack of GDF15 on this side of the niche.

Higher numbers of $Ki67^+$ and mitotic cells in the $Gdf15^{-/-}$ GE could be due to two reasons: either there are more progenitors, i.e. more cells are cycling and not exiting the cell cycle to differentiate, or the cell cycle progression is increased, leading to more cells in M-phase at any point in time. To determine which of these applies to the $Gdf15^{-/-}$ E18 GE, I incubated whole mount explants of WT and $Gdf15^{-/-}$ embryos with 5'-Iodo-2'-deoxyuridine (IdU), a thymidine analogue which is incorporated into the DNA during S-phase, for 1.5 h and either directly fixed the tissue or further incubated it in IdU-free medium for a 12 h chase period (Figure III-11 A). Here I found that after 1.5 h of exposure to IdU, significantly more cells in the $Gdf15^{-/-}$ GE had incorporated the nucleoside analogue into their DNA than in the WT control (Figure III-11 B), suggesting that in the $Gdf15^{-/-}$ GE, more cells were in S-phase during the 1.5 h time period. Using phosphorylated histone H3 (phH3) as a mitosis marker, I found that in both apical and basal niche regions, more IdU^+ cells were also $phH3^+$ (Figure III-11 C, D), suggesting that they had already entered M-phase after being in S-phase no more than 1.5 h before, which is indicative of a faster cell cycle. Meanwhile, there were slightly less IdU^-phH3^+ cells in mutant mice compared to WT controls, suggesting that most IdU^+ cells were also $phH3^+$, and therefore experiencing faster cell cycles.

After a 12 h chase period, the number of IdU^+ cells was decreased in the GE of both genotypes (Figure III-11 E), suggesting a dilution of the labelled DNA due to subsequent divisions; however, the $Gdf15^{-/-}$ GE still contained more IdU^+ cells compared to the WT control. In both apical and subapical $Gdf15^{-/-}$ cells, the number of IdU^-phH^+ cells was now increased in relation to the WT control, which further points to faster label dilution due to more divisions (Figure III-11 F, G). Furthermore, after the 12 h chase, the number of IdU^+phH^+ in the subapical side of the WT GE had increased, so no significant difference could be found between WT and $Gdf15^{-/-}$ samples; this may be due to faster cell cycle of subapical cells compared to apical cells in WT animals.

To determine whether lack of GDF15 affects not only the number of progenitors but also cell cycle exit and re-entry, I labelled E18 GEs incubated with IdU as above with cell cycle marker Ki67 (Figure III-11 H). As expected from the previous experiment, after 1.5 h, there were more cycling cells ($Ki67^+$) and more cells that had replicated their DNA during this time (IdU^+) in the $Gdf15^{-/-}$ GE than in the WT

control; these differences were statistically significant for the IdU$^+$Ki67$^-$ and IdU$^+$Ki67$^+$ groups (Figure III-11 I). After the 12 h chase period, the number of IdU$^+$Ki67$^+$ in the knock-out samples had decreased to WT levels (Figure III-11 J) while the number of IdU$^+$Ki67$^-$ remained high, suggesting that some of the cells that had been in S-phase during the incubation period had exited the cell cycle after 12 additional hours.

All in all, these results suggest that there are more cycling NSCs in the GE of Gdf15$^{-/-}$ embryos, which also cycle faster than those in WT age-matched controls, but that these cells still exit the cell cycle after several rounds of proliferation and do not represent constitutively cycling progenitors.

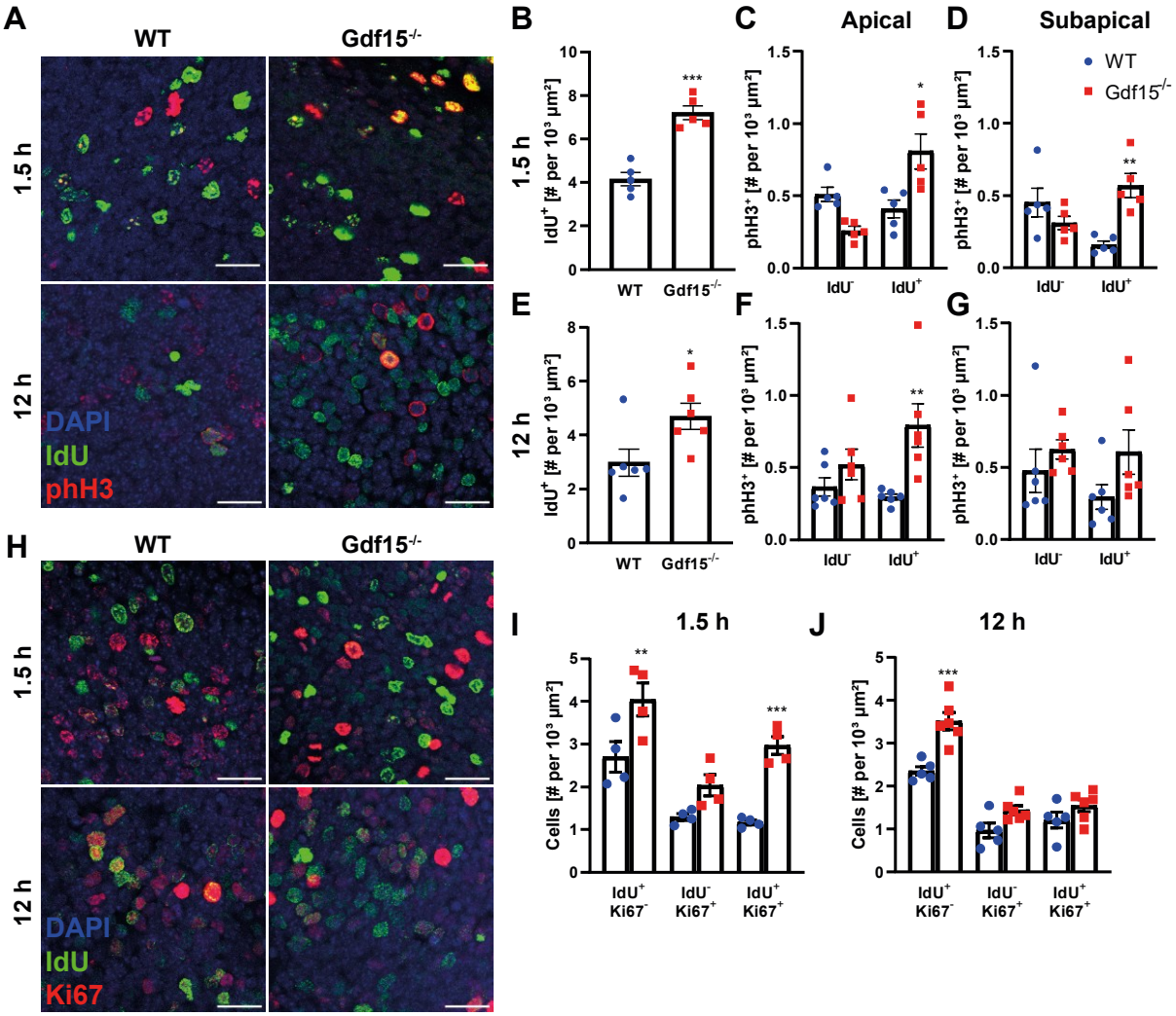

Figure III-11: GDF15 knock-out leads to increase in number of cycling cells and cell cycle speed.
(A, H) Representative micrographs of the apical side of whole mounts of E18 WT and Gdf15$^{-/-}$ GEs fixed directly after 1.5 h IdU application (1.5 h) or after a further 12 h chase period (12 h), immunofluorescently labelled for IdU (green) and either phosphorylated histone H3 (phH3; red; A) or Ki67 (red; H). DAPI was used as nuclear counterstain. Scale bars = 20 µm.
(B-G) Quantification of total IdU cells (B, E) and apical (C, F) and subapical phH3$^+$ cells (D, G) directly after IdU incubation (B-D) or after an additional 12 h chase period (E-G).
(I, J) Quantification of total IdU$^+$ and Ki67$^+$ cells after directly after IdU incubation (I), or after a 12 h chase period (J).
Parts of this figure are already published in Baur, et al. [1] [pre-print].

3.5 Increased proliferation is reversible by application of exogenous GDF15

GDF15 is upregulated in the mouse GE at E16-E18[164], a time where NSCs mature, which is reflected in their heightened responsiveness to EGF[54,167] as well as the increased entering of quiescence[43]. Since I found that lack of GDF15 leads to a greater number of proliferative cells in the E18 GE, it is possible that GDF15 affects this transition from immature to mature NSCs. To determine whether GDF15 application directly affects cell cycle or if the increased proliferation in the niche is the consequence of a more systemic effect caused by the synergy of multiple pathways, I tested whether application of exogenous GDF15 can rescue the phenotype and regulate NSC proliferation to WT levels. For this, I incubated the GEs of WT and Gdf15$^{-/-}$ E18 embryos in medium containing recombinant human GDF15 for 24 h and counted the number of cycling (Ki67^{+}) and mitotic cells (Figure III-12). Here I found that exposure to GDF15 significantly reduced the cycling cells in the Gdf15$^{-/-}$ GE while not affecting Ki67^{+} cells in WT animals (Figure III-12 B). When analysing the number of mitotic cells, i.e. the cells in ana-, meta- or telophase based on nuclear morphology, I found that while in the knock-out GE, GDF15 application significantly reduced their number in both apical and subapical regions, mitosis actually increased in apical WT cells (Figure III-12 C). This suggests that while GDF15 does seem to have a role in suppressing progenitor overproliferation, as apparent from the overproliferation of the knock-out cells, the regulation of proliferation by GDF15 may be context-specific. Additionally, these data indicate that GDF15 has a stronger effect on apical NSCs compared to their subapical counterpart.

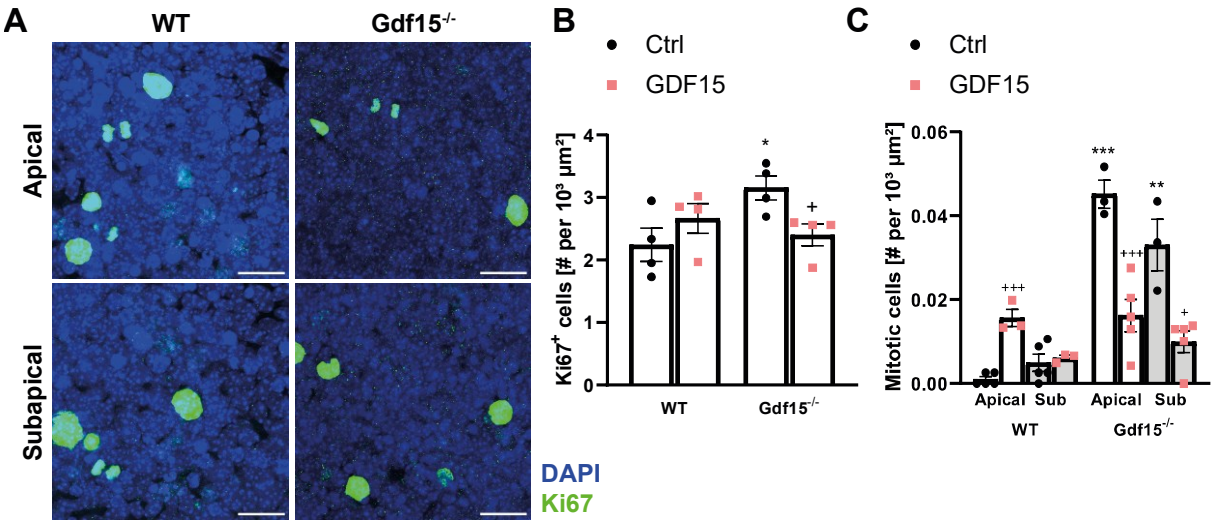

Figure III-12: Application of exogenous GDF15 rescues proliferation in Gdf15$^{-/-}$ embryos.
(A) Representative micrographs of the apical and subapical cell layers of WT and Gdf15$^{-/-}$ GEs treated with GDF15 for 24 h, labelled with Ki67 (green). DAPI was used as nuclear counterstain. Scale bars = 20 µm.
*(B, C) Quantification of Ki67^{+} (B) and mitotic cells (C) in samples without (Ctrl) and with GDF15-treatment (GDF15) for 24 h. * indicates significance to WT, $^{+}$ indicates significance to Ctrl group of the same genotype.*
This figure is already published in Baur, et al. [1] [pre-print] in a modified version.

3.6 GDF15 ablation persistently increases number of ependymal cells and adult NSCs

Previously, I presented evidence showing that ablation of GDF15 leads to an increase in NSCs in the E18 GE, but also that while these cycling cells proliferate faster than those in a WT control, they nevertheless exit the cell cycle after a few divisions. After proliferation, NSCs either enter quiescence, i.e. remaining NSCs while not proliferating for a prolonged time period, or differentiate, i.e. becoming other cell types such as neurons or glia. In a her PhD thesis[175], Carmen Carrillo García already demonstrated that NSCs in the embryonic GE produce increased numbers of neuroblasts, a mechanism which is compensated by apoptosis, whereas there is no effect on the amount of oligodendrocytes and astrocytes (see also Baur, et al. [1]). Since I found here that especially apical progenitors are affected by ablation of GDF15, and since some of these apical proliferating progenitors, besides NSCs, also give rise to ependymal cells[9,176], I hypothesized that the increased proliferation of progenitors in the GE of $Gdf15^{-/-}$ mice may lead to an increase in ependymal cells or apical NSCs. Therefore, I analysed the number of ependymal cells in newborn WT and $Gdf15^{-/-}$ mice (postnatal day 2, P2) using whole mounts of the lateral walls labelled with antibodies against β-catenin and FGFR1 oncogene partner (FOP). With this approach, I was able to distinguish ependymal from single-ciliated (SC) cells since β-catenin labels cell-cell contacts while FOP is localized to the basal bodies of cilia, thereby making it possible to distinguish SC cells (≤ 2 FOP dots) from ependymal cells (> 2 FOP dots; see also Figure III-13 A). This analysis revealed that at P2, the $Gdf15^{-/-}$ GE contained more ependymal cells in the same area than WT controls (Figure III-13 B, C) while the number of SC cells remained the same. As the overall number of cells in the niche was also increased in $Gdf15^{-/-}$ animals (Figure III-13 D), the additional ependymal cells are likely not produced at the expense of SC cells but rather represent surplus cells.

To determine whether this is a transient effect that is compensated for in later development, I, with the help of master student Şeydanur Şan, analysed the number of ependymal cells and NSCs in the 8w V-SVZ using cilia marker Arl13b and NSC marker GFAP (Figure III-13 E). Here I found that at 8w, $Gdf15^{-/-}$ mice had significantly more ependymal cells, as determined by the number of multiciliated cells, as well as more SC $GFAP^{+}$ NSCs (Figure III-13 F). These data suggest that the increased proliferation rate in the E18 GE leads to persistently higher numbers of both ependymal cells and NSCs, which is not compensated by cell death.

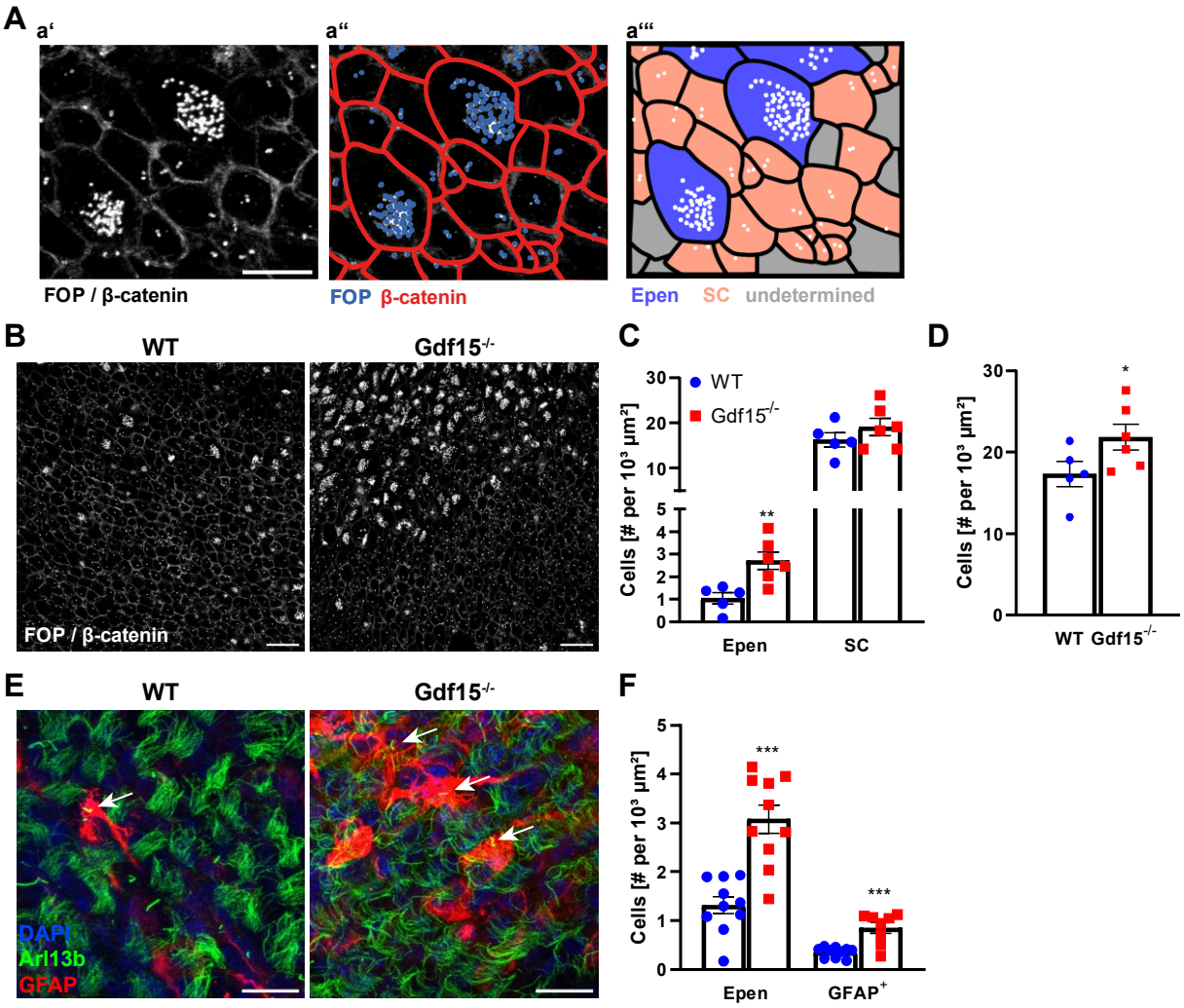

Figure III-13: Gdf15$^{-/-}$ animals have persistently increased number of ependymal cells and GFAP^{+} apical NSCs.
(A) Schematic showing counting of ependymal (Epen) and single-ciliated (SC) cells using FOP and β-catenin as markers. (a') Closeup of WT image in (B), showing β-catenin, indicating cell-cell contacts, and FOP, indicating ciliary basal bodies/centrosomes, in a single channel. Scale bar = 10 µm. (a'') β-catenin and FOP labels are distinguished by location, morphology and label intensity, with FOP being single dots that are more intense than β-catenin and located within the cell boundaries. (a''') Cells containing one or two centrosomes were considered SC cells (red), while cells with more than two centrosomes were considered multiciliated and therefore Epen (blue).
(B) Whole mounts of the E18 GE immunofluorescently labelled with FOP and β-catenin. Scale bars = 20 µm.
(C, D) Quantification of cells in (B) that were determined as Epen or SC cells (C) as well as total cells (D).
(E) Whole mounts of the adult V-SVZ immunofluorescently labelled with Arl13b, to label cilia, and GFAP, to label radial glia-like cells. White arrow indicates SC NSC. Scale bars = 20 µm. Images courtesy of Şeydanur Şan.
(F) Quantification of cells in (E) displaying multiple cilia (Epen) or displaying GFAP immunoreactivity (GFAP^{+}).
This figure and legend have already been published in Baur, et al. [1] [pre-print] in a modified version.

4. Mechanisms underlying GDF15 function

4.1 EGFR signalling

4.1 a) Lack of GDF15 leads to changes in surface EGFR expression

As mentioned before, responsiveness to EGF is increasing at the same time as the expression of GDF15. Since GDF15 was already found to promote EGFR signalling in the HP[164], I hypothesized that changes in EGFR signalling might also be a reason for the proliferation phenotype in the V-SVZ. Therefore, I used flow cytometry to assess the levels of surface EGFR protein by tagging the cells with fluorophore-conjugated EGF, namely EGF-Alexa488 (EGF-488) and EGF-Alexa647 (EGF-647; Figure III-14). Using EGF-488, I found that that significantly less cells seemed to express EGFR at the cell surface in the $Gdf15^{-/-}$ GE than in the WT control (Figure III-14 A top row, B); however, no such difference was found using EGF-647 (Figure III-14 A bottom row, C). This difference may be due to a lower sensitivity of EGF-488, as evidenced by overall lower numbers of positive cells, meaning that more EGFR molecules are necessary for the fluorescence to cross detection threshold, while when using EGF-647, lower levels of surface EGFR suffice. These data suggest that whereas there are not less cells in the $Gdf15^{-/-}$ GE that express EGFR, the surface levels of the receptor are reduced in the NSCs and progenitors of mutant mice.

To determine whether GDF15 directly affects surface EGFR levels, I incubated whole E18 GEs of WT and $Gdf15^{-/-}$ animals in medium with and without GDF15 (one hemisphere for each treatment per animal) for 24 h and then measured surface EGFR-levels with EGF-488 (Figure III-14 D). While overall EGFR levels in these cells were different compared to those of cells not incubated overnight (compare Figure III-14 D, Ctrl to A, top row), application of GDF15 significantly increased the number of detected $EGFR^{high}$ (E^{h}) cells compared to the control samples in both WT and mutant animals (Figure III-14 E).

Lastly, I investigated whether the differences in detectable surface EGFR reflect transcriptional changes in mRNA levels, or if they are rather caused by other factors like local translation, trafficking, or targeted degradation. Therefore, I measured the levels of *Egfr* mRNA in the E18 GE, with and without treatment with GDF15 for 24 h, by qPCR (Figure III-14 F). Here I found that neither knock-out nor application of GDF15 affected mRNA levels of *Egfr*, suggesting that regulation of *Egfr* levels by GDF15 is due to a direct mechanism that does not include transcriptional regulation.

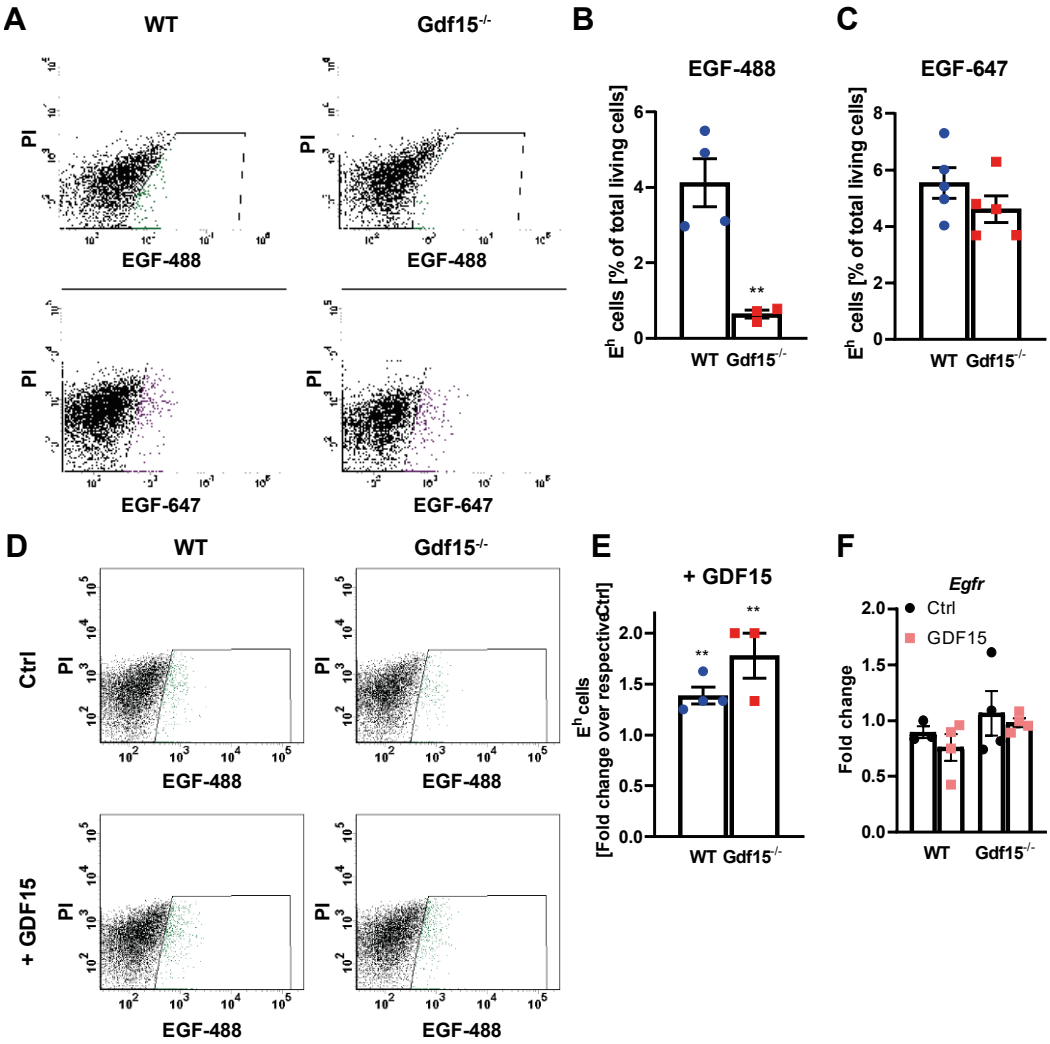

Figure III-14: Surface EGFR expression is reduced in the GE of E18 Gdf15$^{-/-}$ animals.
(A, D) FACS dot plots displaying WT and Gdf15$^{-/-}$ E18 GE cells low (black, E^{l}) and high in EGFR expression (green, E^{h}), using EGF-Alexa488 (A top, D) or EGF-Alexa647 (A bottom). Whole lateral walls were either dissociated directly after dissection (A) or first incubated in medium containing GDF15 or not (Ctrl) for 24 h (D). PI = propidium iodide, labelling dead cells. PI^{+} cells were excluded from analysis.
(B, C) Quantification of cells E^{h} cells detected with EGF-488 (B) and EGF-647 (C).
(E) Quantification of E^{h} cells after GDF15 treatment for 24 h, normalized to untreated cells of the same respective animal.
(F) Quantification of Egfr mRNA level in whole E18 GEs after 24 h without (Ctrl) or with exposure to GDF15.
Parts of this figure are already published in Baur, et al. [1] [pre-print].

4.1 b) Lack of GDF15 changes EGFR activation and signalling dynamics

Changes in surface EGFR level accompanied by constant mRNA expression might be caused by differences either in trafficking of the receptor to the cell membrane, in activation, or degradation. Therefore, I used immunofluorescence on coronal sections of the E18 and 8w brains of WT and mutant mice to detect intracellular levels of EGFR, as well as EGFR phosphorylated at Tyr^{1092} (phEGFR) to determine receptor activation (Figure III-15). At E18, I found that the EGFR fluorescence intensity was slightly weaker in the GE of Gdf15$^{-/-}$ animals compared to WT controls, especially at the apical border (Figure III-15 A, B). Activation, as evidenced by phEGFR levels, was not significantly different between

the genotypes (Figure III-15 C), however, some punctuate phEGFR was visible at the apical border of the Gdf15$^{-/-}$ GE but not at that of the WT (Figure III-15 A, arrows). This suggests a change in EGFR activation pattern as a response to lack of GDF15. Lastly, I found that immunofluorescent labelling of EGFR and phEGFR rarely overlapped, which indicates that the antibody for EGFR does not recognise the phosphorylated receptor.

In sections of 8w mice, I found significantly lower levels of EGFR fluorescence intensity in the Gdf15$^{-/-}$ V-SVZ compared to that of WT animals (Figure III-15 D, E); in WT animals especially showed

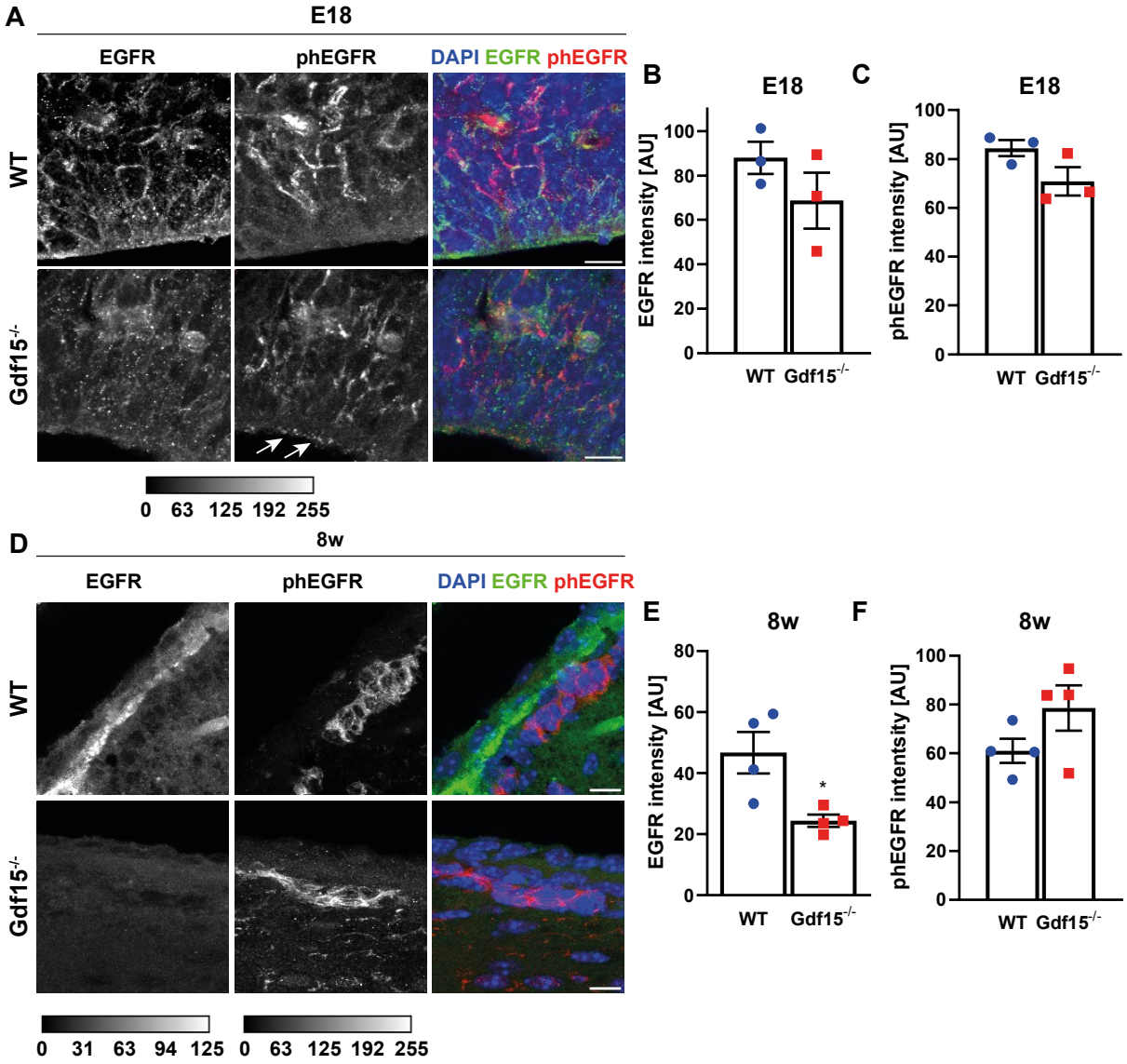

Figure III-15: Expression and activation of phEGFR in the E18 GE and adult V-SVZ.
(A, D) Coronal sections of WT and Gdf15$^{-/-}$ animals aged E18 (A) or 8w (D), immunofluorescently labelled with antibodies against EGFR (green) and pTyr^{1092} EGFR (phosphorylated EGFR, phEGFR; red). DAPI was used as nuclear counterstain. Pictures display the ventral regions of the GE / V-SVZ. Scale bars = 10 µm. Calibration bars display numerical values assigned to grey values in pictures placed above.
(B, C, E, F) Measured fluorescence intensity of EGFR (B, E) and phEGFR (C, F) in E18 (B, C) and 8w sections (E, F). AU = Arbitrary unit.
This figure is in a modified version already published in Baur, et al. [1] [pre-print].

high levels of the receptor at the apical border. As already observed at E18, the pattern of phEGFR fluorescence barely overlapped with that of EGFR, with phEGFR^{+} cells located in subapical clusters, while intensity showed a trend increase in Gdf15$^{-/-}$ animals compared to WT controls, especially at the apical surface (Figure III-15 D, F). This indicates that the lower surface EGFR expression found in Gdf15$^{-/-}$ mice at E18 might in fact be caused by a higher receptor activation, as activated EGFR is internalized and degraded and would not be detected by surface EGF binding.

To investigate whether the activation pattern of EGFR is truly changed in Gdf15$^{-/-}$ embryos, I used western blot analysis of phosphorylated ERK (phERK), a downstream target of EGFR signalling, to determine the levels of EGFR activation (Figure III-16).

First, I investigated whether the general levels of phERK were higher in the whole GE of Gdf15$^{-/-}$ E18 embryos, and if the levels were affected by exposure GDF15 and EGF similarly in both genotypes (Figure III-16 A, B). Surprisingly, I found that the base levels of phERK did not differ between the genotypes, and that both exposure to GDF15 and to EGF caused similar increases in ERK phosphorylation over control untreated samples (Figure III-16 B). Additionally, within 7 minutes of exposure, EGF caused a higher level of ERK phosphorylation than GDF15 after 24 h, suggesting that GDF15 is a weaker activator of MAPK/ERK signalling than EGF.

However, as EGFR signalling is highly complex and not only affected by overall activation, but also by the individual activation kinetics, i.e. activation time and concentration of EGF needed for downstream signalling, I more closely investigated these parameters using western blot (Figure III-16 C-F), with the help of master student Manja von Hahn. First, to investigate differences in temporal response, I incubated dissociated GE cells of WT and Gdf15$^{-/-}$ E18 embryos with EGF at a high concentration (20 ng/ml) for 7 min, then removed the medium and either directly lysed the cells (0 h) or further incubated them in EGF-free medium for 0.5, 1, 2 or 4 h, and analysed the level of phERK using western blot (Figure III-16 C, D). A sample that was not treated with EGF was used as baseline (b). Here I found no difference between WT and Gdf15$^{-/-}$ cells in their direct response to EGF (data not shown); however, when response to the signal was normalized to the highest response, i.e. to the 0 h timepoint (Figure III-16 D), I found that in Gdf15$^{-/-}$ cells, the phERK intensity was already reduced to baseline levels 1 h after EGF application, whereas this reduction was only visible after 2 h in WT animals, suggesting faster EGF signalling kinetics in the mutant mice. When testing the response to increasing levels of EGF, i.e. 0.1, 1, 5, 10 and 20 ng/ml (Figure III-16 E, F), I found that WT animals already showed a significant increase in phERK at only 1 ng/ml, whereas Gdf15$^{-/-}$ animals reached their maximum response at 5 ng/ml, which was then not further amplified by increasing concentrations of EGF. Cells of WT animals, however, showed another trend increase in ERK phosphorylation at a concentration of 20 ng/ml, suggesting a more sensitive response to differing EGF concentrations.

Taken together, these results suggest that while cells in the GE of Gdf15$^{-/-}$ embryos are able to receive and transmit EGFR signalling, their response dynamics are altered.

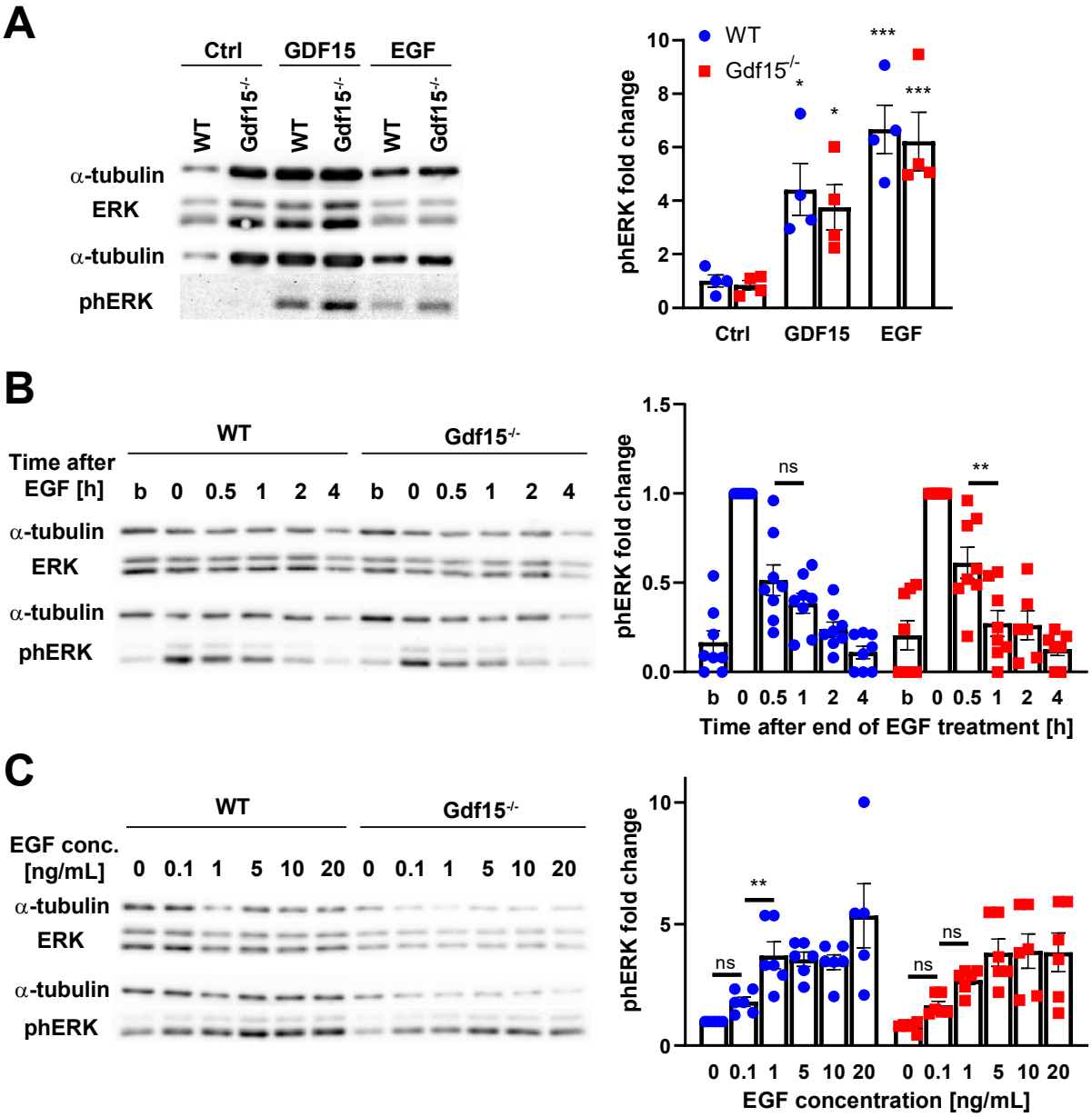

Figure III-16: WT and Gdf15$^{-/-}$ GE cells show differences in EGFR activation kinetics.
(A, B) Western blot (A) and quantification of phERK levels (B) in whole E18 GEs incubated with GDF15 for 24h or EGF for 7 minutes, or not incubated (Ctrl). Since ERK and phERK could not be detected on the same membrane, α-tubulin is used as loading control for both separately.
(C, D) Western blot (C) and quantification of phERK levels (D) in dissociated E18 WT and Gdf15$^{-/-}$ cells incubated without (baseline, b) or with EGF for 7 minutes and then further incubated without EGF for 0, 0.5, 1, 2 or 4 hours as indicated. To ensure comparability, cells from each single animal were dissociated and were subjected to every treatment. ns = not significant.
(E, F) Western blot (E) and quantification of phERK levels (F) in WT and Gdf15$^{-/-}$ cells incubated with 0, 0.1, 1, 5, 10 or 20 ng/ml EGF for 7 minutes as indicated. To ensure comparability, cells from each single animal were dissociated and were subjected to every treatment. ns = not significant.
This figure, including the legend, is in a modified version already published in Baur, et al. [1] [pre-print].
Some western blots included in the analysis displayed in panels D and F were performed by Manja von Hahn.

4.1 c) EGFR activation or inhibition does not rescue the Gdf15$^{-/-}$ proliferation phenotype

I previously presented evidence supporting the hypothesis that EGFR signalling is altered in Gdf15$^{-/-}$ mice. Since EGF is a vital mitogen in the embryonic GE as well as in the adult V-SVZ, it is possible that changes in EGFR signalling may be responsible for the increased proliferation that I observed in these mutant animals. Therefore, I treated whole mount explants of the E18 GE of WT and knock-out mice with either EGF or EGFR inhibitor PD158780 (PD) to determine if increasing or decreasing EGFR signalling can rescue the overproliferation in Gdf15$^{-/-}$ mice (Figure III-17).

Here I found that pharmacologically inhibiting EGFR with PD led to a significant reduction in cycling progenitors (Ki67^{+} cells) in both WT and Gdf15$^{-/-}$ animals (Figure III-17 A, B). This effect was even more strongly visible when analysing the number of cells in mitosis: no mitotic cells could be found among WT apical and Gdf15$^{-/-}$ subapical cells, and the mitosis in apical Gdf15$^{-/-}$ cells was significantly reduced (Figure III-17 C, D). When exposed to recombinant EGF, however, only WT apical cells responded with an increase in mitosis, whereas the number of overall cycling cells remained the same in both genotypes and mitosis was even reduced in subapical cells of the Gdf15$^{-/-}$ GE. These results suggest that while EGFR signalling is altered in Gdf15$^{-/-}$ mice, active EGFR is still necessary for proliferation and mitosis in these animals, hence GDF15 may have a role in regulating EGFR surface expression and signalling, but is not needed for the overall effect of EGF.

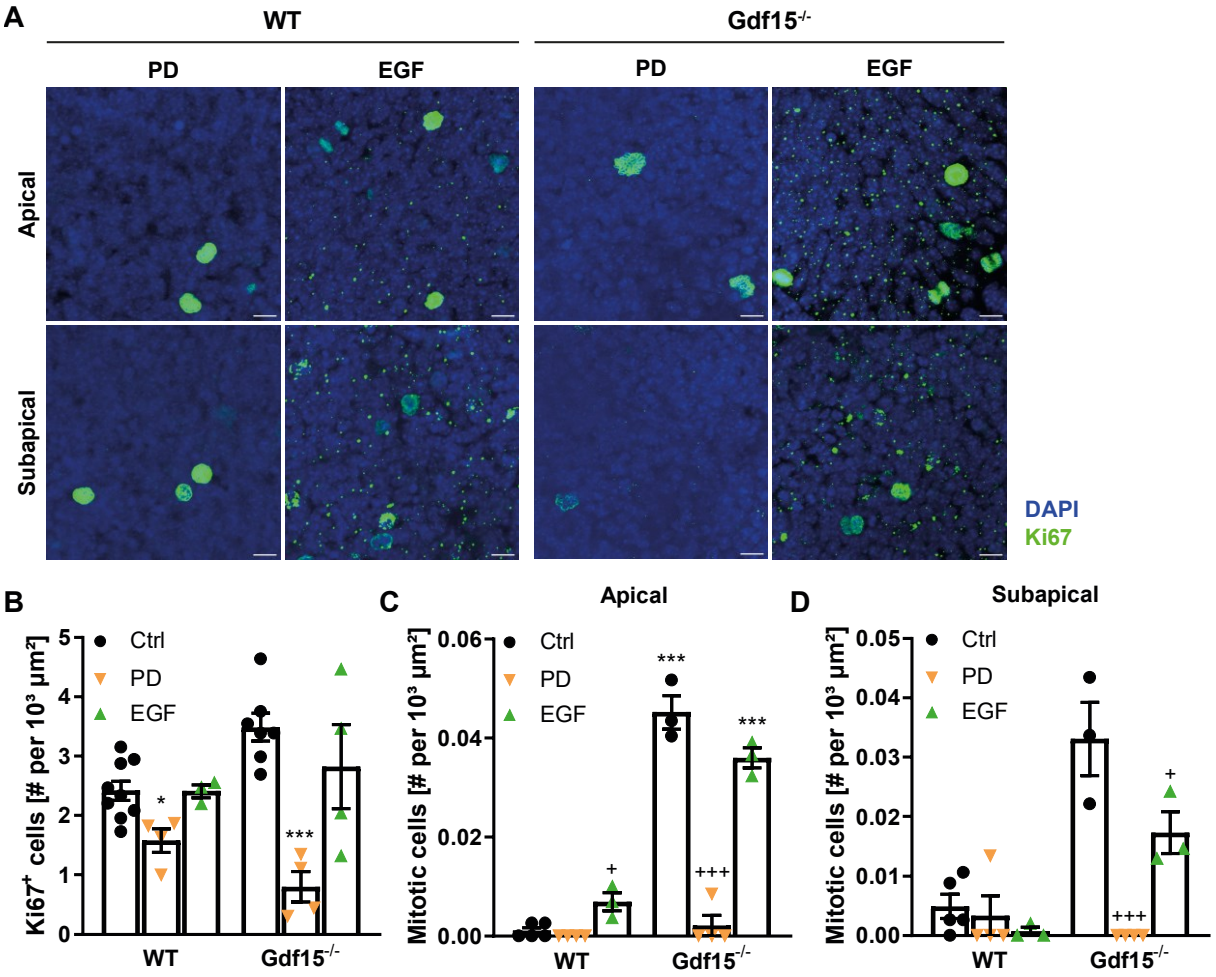

Figure III-17: Effect of EGFR signalling activation or inhibition on cycling cells in the E18 GE.
(A) Representative micrographs of the apical and subapical cell layers in WT and Gdf15$^{-/-}$ GE E18 whole mounts, which were treated with EGF or EGFR inhibitor PD158780 (PD) for 24 h and then immunostained for Ki67 (green). DAPI was used as nuclear counterstain. Scale bars = 10 µm.
*(B-D) Quantification of cycling (Ki67^{+}) cells (B) or cells undergoing mitosis in the apical (C) or subapical cell layer (D) after EGF or PD treatment. * indicates significance to WT, $^{+}$ indicates significance to Ctrl group.*
This figure is, in a modified version, already published in Baur, et al. [1] [pre-print].

4.2 CXCR4 signalling

4.2 a) Active CXCR4 signalling is not needed for the effect of GDF15 in the embryonic GE

Above, I have presented evidence that in the embryonic V-SVZ, EGFR expression and signalling is affected by lack of GDF15. A previous study conducted by this laboratory found that in the subgranular zone of the HP, GDF15 needs active CXCR4 to modulate EGFR[164].

To determine if this mechanism of action is similar in the V-SVZ, where CXCR4 is more expressed by basal cells and more differentiated progenitors[62,65,177], whereas I saw a more prominent change in EGFR expression in apical cells, I used the small molecule inhibitor AMD3100 (AMD, also known as Plerixafor), a CXCR4 antagonist, to block the receptor in the embryonic GE. For this, I incubated whole dissected lateral GEs of E18 WT and Gdf15$^{-/-}$ mice in medium containing 6 µM AMD, and then analysed the effect on proliferation using proliferation marker Ki67 (Figure III-18). Here I found that independent of genotype, AMD reduced the number of Ki67^{+} cycling cells (Figure III-18 B), and in WT animals, no dividing cells could be found after AMD treatment in both apical and subapical cell layers (Figure III-18 C, D). In the Gdf15$^{-/-}$ GE, AMD significantly reduced mitosis in apical cells, and slightly reduced mitosis in subapical cells. In combination with GDF15, both proliferating and mitotic cells were even more decreased in knock-out animals, whereas in the WT GE, more mitotic cells were found in apical and basal layers. This suggests that GDF15 and CXCR4-inhibitor affect separate pathways that can be activated or inhibited simultaneously without changing the effect of either, as GDF15 and AMD alone lead to mitosis reduction in Gdf15$^{-/-}$ animals, causing a complete loss of apical mitosis in combination in this genotype, whereas GDF15 increases mitosis in apical WT cells, thereby counteracting the effects of CXCR4 blockage when applied in combination.

4.2 b) CXCR4 inhibition does not affect cilia length or rescue thereof by GDF15

In Chapter III-2, I demonstrated that cilia morphology in the Gdf15$^{-/-}$ GE can be rescued by applying recombinant GDF15 to the culture medium. To determine whether this mechanism, separately from the overproliferation, is affected by CXCR4 signalling, I treated whole GEs with AMD or AMD in combination with GDF15 and measured length and thickness of primary cilia on the apical surface using Arl13b as a cilia marker (Figure III-19). Treatment with AMD only did not affect cilia phenotype in WT or Gdf15$^{-/-}$ GEs, neither regarding length (Figure III-19 B) nor thickness (Figure III-19 C). Furthermore, when applied together with GDF15, it did not significantly alter the lengthening or thickness reduction of cilia in the GE of Gdf15$^{-/-}$ animals in response to the growth factor. The only difference I found was that the reduction in thickness in response to GDF15 did not reach WT levels when AMD was present, although the differences to either the WT control or the GDF15-treated sample were not statistically significant.

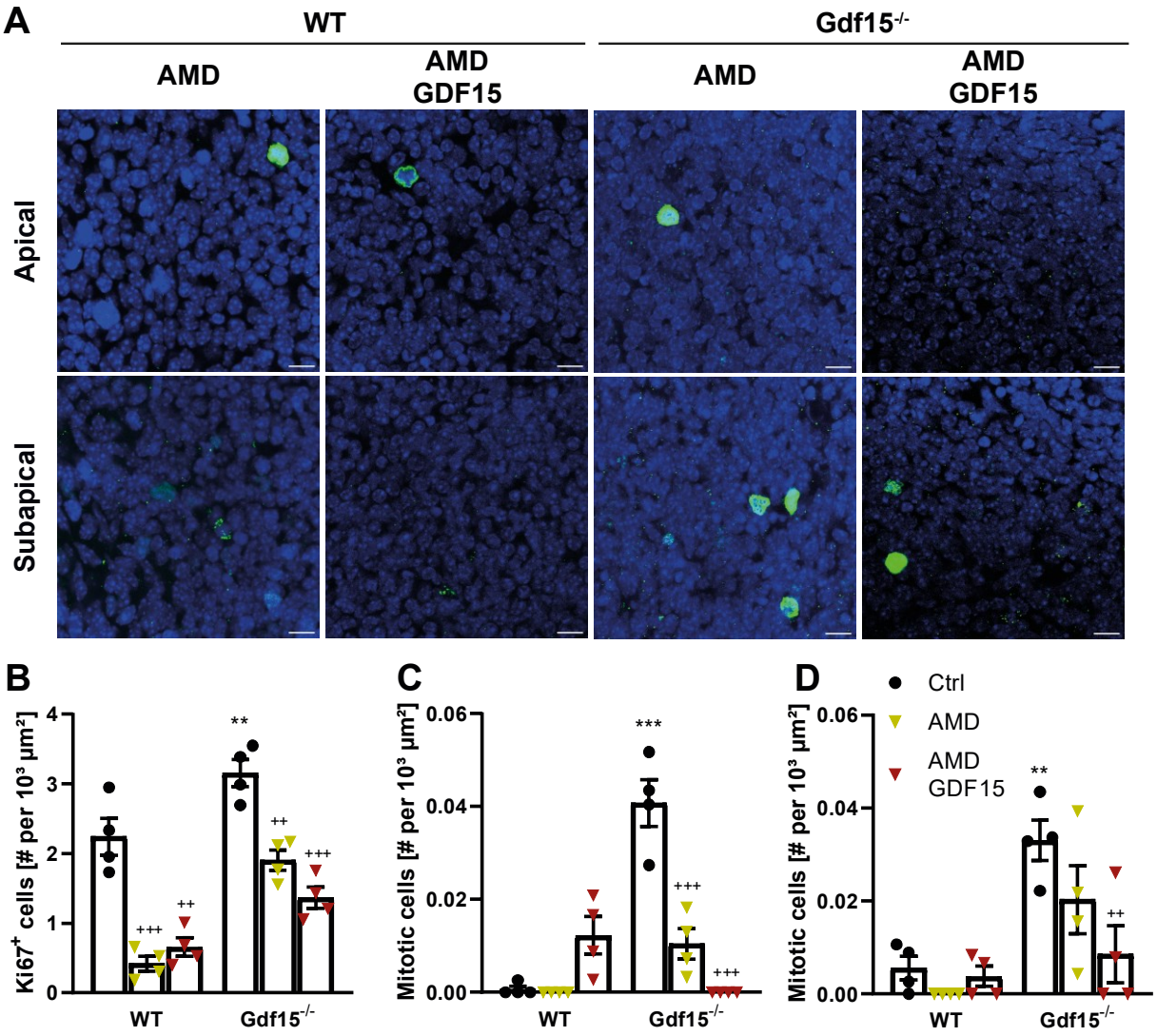

Figure III-18: Blocking CXCR4 inhibits proliferation separately from GDF15.
(A) Representative micrographs of the apical and subapical cell layers in WT and Gdf15$^{-/-}$ GE E18 whole mounts, which were treated with AMD3100 (AMD) or AMD together with GDF15 for 24 h and then immunostained for Ki67 (green). DAPI was used as nuclear counterstain. Scale bars = 10 µm.
*(B-D) Quantification of cycling (Ki67^{+}) cells (B) or cells undergoing mitosis in the apical (C) or subapical cell layer (D) after AMD treatment, or AMD together with GDF15. * indicates significance to WT, $^{+}$ indicates significance to Ctrl group.*
Part of this figure is already published in Baur, et al. [1] [pre-print].

These results indicate that either active CXCR4 is not needed for the effect of GDF15 on the same cells, or that CXCR4 and GDF15 receptor GFRAL are not expressed on the same cells, but rather separate cell populations, such as quiescent NSCs and migrating neuroblasts. The latter is also supported by the fact that I did not find any co-expression of CXCR4 and GFRAL in the basal GE of E18 WT brains (see Chapter III-2.1, Figure III-3 B).

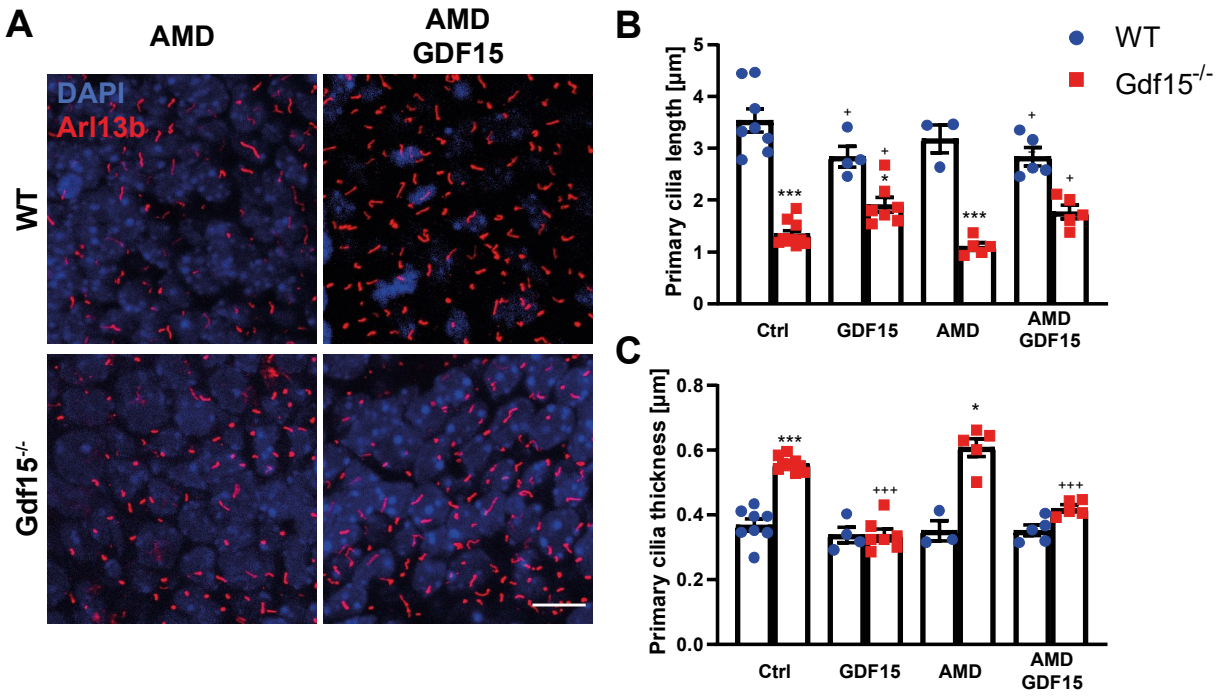

Figure III-19: AMD3100 does not affect cilia morphology.
(A) Representative micrographs of the apical surface of WT and Gdf15$^{-/-}$ E18 GEs after treatment with AMD3100 (AMD) or AMD in combination with GDF15 for 24 h, labelled with Arl13b to visualise cilia. DAPI was used as nuclear counterstain. Scale bar = 10 µm.
*(B, C) Quantification of cilia length (B) and thickness (C) in WT and Gdf15$^{-/-}$ E18 GEs with no treatment (Ctrl) or after incubation with GDF15, AMD, or AMD in combination with GDF15. * indicates significance to WT, $^{+}$ indicates significance to Ctrl group.*

4.3 Ciliary signalling

Activation and proliferation of NSCs is regulated not only by receptors on the whole cell surface, such as EGFR, but also by signals transmitted by primary cilia, where numerous receptors and downstream signalling proteins are in close proximity. In Chapter III-3, I found that cilia length is changed in the GE of Gdf15$^{-/-}$ mice, and that simultaneously their proliferation is increased. While there are several ciliary pathways that may influence cell proliferation and cilia length, I found that the regulation of cilia length did not require gene transcription and was not always linked to changes in cell cycle. Therefore, I here focused on the ciliary transmembrane enzyme AC3 and the nuclear protein HDAC6, which are direct modulators of cilia length that do not require gene transcription for their mechanism of action.

4.3 a) AC3 and HDAC6 are overexpressed in the GE of Gdf15$^{-/-}$ mice

AC3 is a transmembrane adenylate cyclase expressed mainly in neuronal primary cilia throughout the mouse brain[121,122,178], but is also expressed in the primary cilia of adult and embryonic NSCs in the V-SVZ[72,168,178]. Furthermore, AC3 was found to control primary cilia length[124], influence neuronal and progenitor survival and migration[127,128,179], and affect proliferation in cancer cells[125].

To investigate whether AC3 is involved in the mechanism that causes cilia shortening in Gdf15$^{-/-}$ mice, I first tested whether the expression of the protein and its RNA was changed (Figure III-20 A, B). When immunofluorescently labelling AC3, I found that the intensity and co-expression with cilia marker acetylated tubulin (acT) was increased in the GE of Gdf15$^{-/-}$ mice compared to a WT control and that incubation with recombinant GDF15 for 24 h led to a decrease of the visible protein levels (Figure III-20 A). Additionally, using qPCR, I found that the level of mRNA transcripts of AC3 gene *Adcy3* was significantly increased to about five times the WT level in the whole mutant GE (Figure III-20 B).

Another protein that is involved with regulating ciliary length is HDAC6, which catalyses deacetylation of ciliary tubulin, thereby destabilizing it and reducing cilia length[74,115,180]; due to its interaction with Wnt signalling via Aurora A kinase and β-catenin[181], HDAC6 is also involved with cell cycle control[117,118]. Since this also makes it a possible effector of the GDF15 mode of action, I also investigated transcript levels of *HDAC6*, which were also significantly increased in Gdf15$^{-/-}$ animals, although only about 2.5 times (Figure III-20 C).

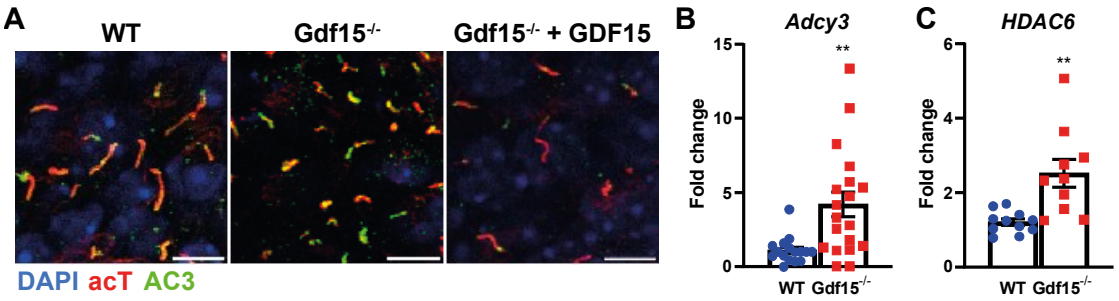

Figure III-20: AC3 and HDAC6 are overexpressed in the E18 Gdf15$^{-/-}$ GE.
(A) Representative micrographs of the apical surface of the WT and Gdf15$^{-/-}$ GE, labelled with acetylated tubulin (acT) and AC3. DAPI was used as a nuclear counterstain. Scale bars = 5 µm.
(B, C) Quantification of mRNA transcripts of Adcy3 (AC3 gene, B) or HDAC6 (C) using qPCR, displayed as fold change over WT control.

4.3 b) Inhibition of AC3 or HDAC6 increases cilia length and decreases proliferation

First, to determine whether the overexpression of AC3 and/or HDAC6 is contributing to the ciliary or proliferation phenotype of E18 Gdf15$^{-/-}$ animals, I used the antagonists NKY80 and Tubastatin A (TSA) to inhibit the catalytic activity of AC3 and HDAC6, respectively (Figure III-21). When analysing cilia using the marker Arl13b (Figure III-21 A) I found that both treatment with NKY80, inhibiting AC3, and TSA, inhibiting HDAC6, for 24 h caused significant increase in cilia length (Figure III-21 B) and decrease in cilia thickness (Figure III-21 C) in Gdf15$^{-/-}$ mice compared to a DMSO-treated control, a trend that was highly similar to the effect of recombinant GDF15. In WT mice, where GDF15 alone does not affect cilia length or thickness, treatment with NKY80 caused a 1.6-times increase in cilia length (DMSO: 3.3 ± 0.1 µm, NKY80: 5.2 ± 0.5 µm) with no change in thickness, whereas surprisingly, TSA caused a decrease in cilia length (2.2 ± 0.2 µm) and thickness (DMSO: 0.37 ± 0.02 µm, TSA: 0.27 ± 0.01 µm). This suggests that while the effects of inhibiting AC3 and HDAC6 are similar in the Gdf15$^{-/-}$ GE, the underlying mechanisms are different, as shown by the difference in effect on WT compared to Gdf15$^{-/-}$ animals.

Additionally, to investigate whether AC3 or HDAC6 overexpression might also influence the proliferation dynamics of progenitor cells in the Gdf15$^{-/-}$ GE, I used proliferation marker Ki67 to assess the number of cycling and mitotic cells (Figure III-21 D). Here I found that, similar to the effects on cilia, both NKY80 and TSA reduced the number of Ki67^{+} cells throughout the entire GE (Figure III-21 E) as well as the number of apically dividing cells (Figure III-21 F) in a similar fashion as application of GDF15 in Gdf15$^{-/-}$ mice. In WT cells, however, neither inhibitor showed an effect on the total number of cycling cells, while inhibiting the catalytic function of AC3 with NKY80 leads to a trend decrease in apically dividing cells. Since this treatment also causes drastic elongation of primary cilia and longer cilia have been shown to indicate quiescence, it is likely that the cilia length may be the cause of this change in proliferation. TSA on the other hand, which caused a small decrease in both cilia length and thickness, did not seem to induce any change in proliferation dynamics in the apical GE of WT E18 animals.

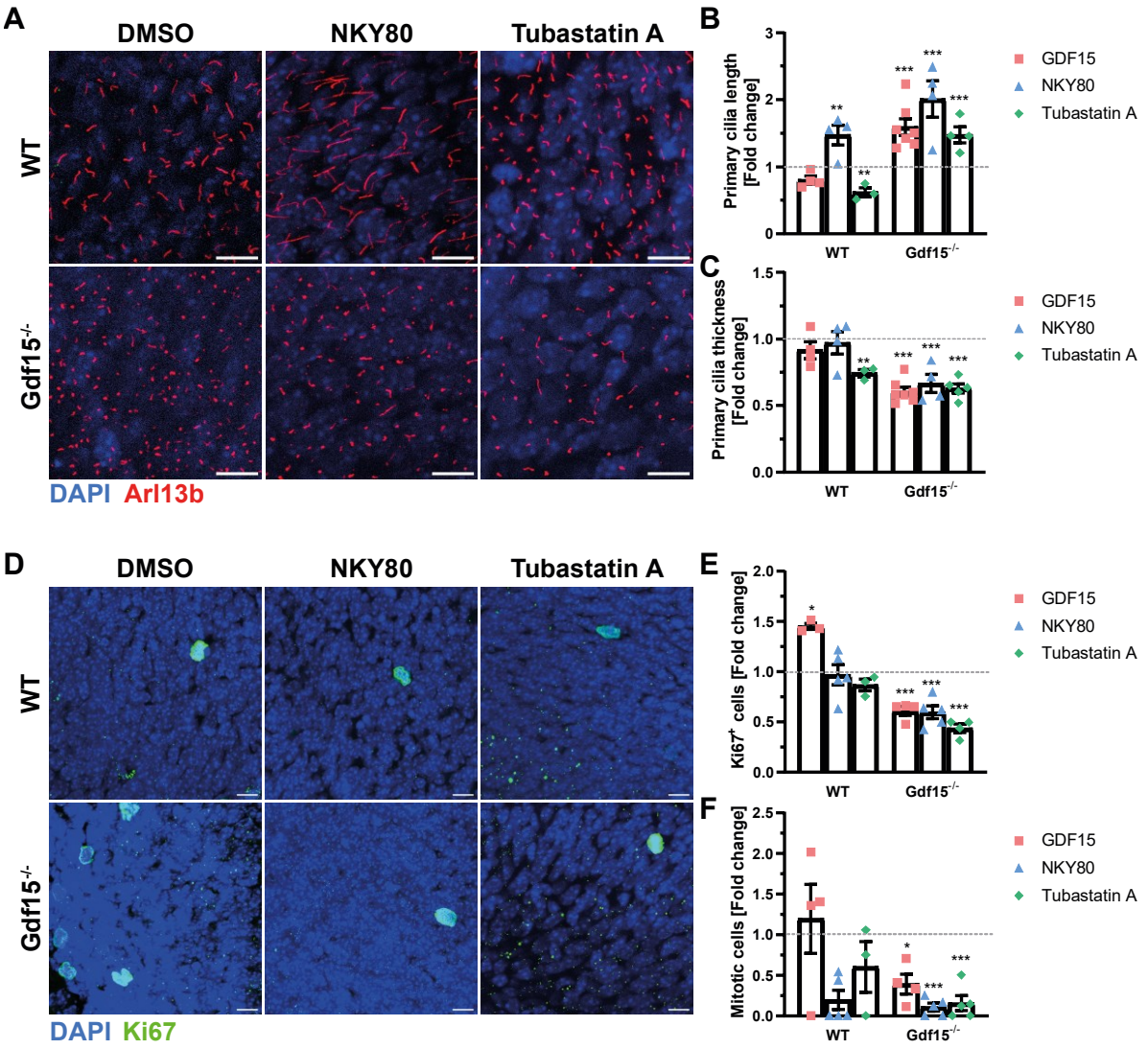

Figure III-21: Effect of inhibition of AC3 and HDAC6 on cilia morphology and proliferation.
(A, D) Representative micrographs of the apical surface of the WT and Gdf15$^{-/-}$ E18 GE after treatment with AC3-inhibitor NKY80 or HDAC6-inhibitor Tubastatin A for 24 h, or with solvent DMSO as control, stained for cilia marker Arl13b (A) or proliferation marker Ki67 (D). DAPI was used as nuclear counterstain. Scale bars = 10 µm. (B, C, E, F) Fold change of primary cilia length (B) and thickness (C), as well as of proliferating Ki67^{+} cells (E) and apically dividing cells (F), after treatment with NKY80 or Tubastatin A, normalized to the average of the DMSO-treated control (dotted line) of the same genotype.
** indicates significance to DMSO control.*

Lastly, I asked whether AC3 and HDAC6 interact with each other's expression, i.e. if either AC3 or HDAC6 inhibition or GDF15 application may lead to a change in expression in either of the genes. Therefore, I incubated whole GEs of E18 WT and Gdf15$^{-/-}$ mice in GDF15, NKY80 or TSA for 24 h and then assessed the levels of mRNA transcripts of *Adcy3* and *HDAC6* using qPCR (Figure III-22). Here I found that levels of *Adcy3* transcripts were significantly reduced in the GE of mutant mice by application GDF15 and NKY80, but especially when inhibiting HDAC6 with TSA (Figure III-22 A). This suggests that HDAC6 activity might control expression of AC3. In WT mice, GDF15 did not affect the mRNA levels of either *Adcy3* or *HDAC6*, and both inhibitors only caused a trend decrease in *Adcy3*

levels while not affecting *HDAC6* levels (Figure III-22 B). In Gdf15$^{-/-}$ mice, however, GDF15 and NKY80 caused a strong trend decrease in *HDAC6* mRNA levels (GDF15: p = 0.05, NKY80: p = 0.08), however only inhibition of HDAC6 using TSA caused a statistically significant reduction of *HDAC6* transcript levels.

Overall, these results suggest that in mutant mice, HDAC6 overexpression and activity may influence both the level of AC3 mRNA and protein as well as cilia length and proliferation both by itself and via AC3. In WT mice on the other hand, where GDF15 is present and HDAC6 is not overexpressed, additional inhibition of HDAC6 did not show similar effects on both cilia and proliferation, suggesting that GDF15 is involved in this mechanism.

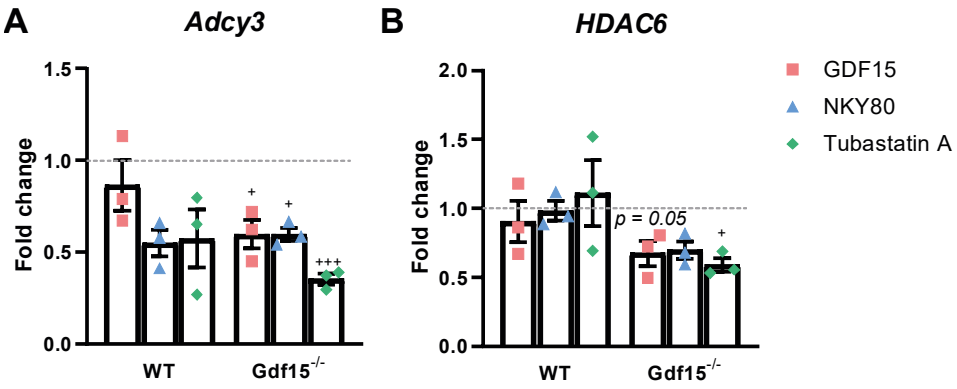

Figure III-22: qPCR analysis of* Adcy3 *and* HDAC6 *transcript levels after inhibition by NKY80 and Tubastatin A. *Fold change of mRNA levels of* Adcy3 *(A) and* HDAC6 *(B) in the whole GE of WT and Gdf15$^{-/-}$ embryos at E18 after* ex vivo *treatment with recombinant GDF15, NKY80 or Tubastatin A for 24 h, determined by qPCR and normalized to respective DMSO-treated controls. $^{+}$ indicates significance to respective DMSO-treated control. This figure is part of a manuscript in preparation.*

4.3 c) Gdf15$^{-/-}$ animals have distinct tubulin acetylation dynamics

In the previous chapter, I found that HDAC6 inhibition affected cells and cilia differently in the WT and Gdf15$^{-/-}$ GE. This may be due to either differences in localization (soma, nucleus or cilium) or general activity of the protein. Since HDAC6 catalyses tubulin deacetylation, I first investigated whether overall levels of acetylated tubulin (acT) were changed in the GE of WT and Gdf15$^{-/-}$ E18 embryos using western blot (Figure III-23 A). I found that there was no difference in the overall levels of acT, and that not GDF15 but only TSA led to an increase in tubulin acetylation in both WT and Gdf15$^{-/-}$ mice. Upon quantification of four separate western blots, however, I found that while acT luminescence intensity was significantly increased in the WT GE after TSA treatment for 24 h, mutant mice showed only a much lower trend increase that was not statistically significant (Figure III-23 B).

Since cilia in the GE are present and act mostly at the apical surface of the niche, I then used immunofluorescence to closer investigate tubulin acetylation on the apical surface as well as HDAC6 expression and possible differences in localization in either of these proteins, with and without treatment with TSA (Figure III-23 C). These images clearly show a difference in the organization of acT in WT and Gdf15$^{-/-}$ control samples, as well as different patterns of HDAC6 expression. When analysing overall apical acT fluorescence, there was no significant difference detectable between WT and Gdf15$^{-/-}$ animals in control samples (Figure III-23 D); however, when treated with TSA, WT samples showed a significant increase in acT intensity, while this effect was not visible in the Gdf15$^{-/-}$ GE, mirroring the results of the western blot.

Lastly, I analysed HDAC6 protein levels: qualitatively, the appearance of the protein is spotty in both WT and mutant animals, but in the latter, the localization seems to be more evenly distributed. Quantitatively, I could not find any significant difference in HDAC6 intensity between the two genotypes (Figure III-23 E), although a trend increase in mutant mice was visible. Inhibition of HDAC6 activity by TSA application did also not alter the protein levels in either WT or Gdf15$^{-/-}$ samples.

These results point towards a difference in HDAC6 localization, which may lead to changes in tubulin acetylation and thereby cilia length, as well as cellular stability.

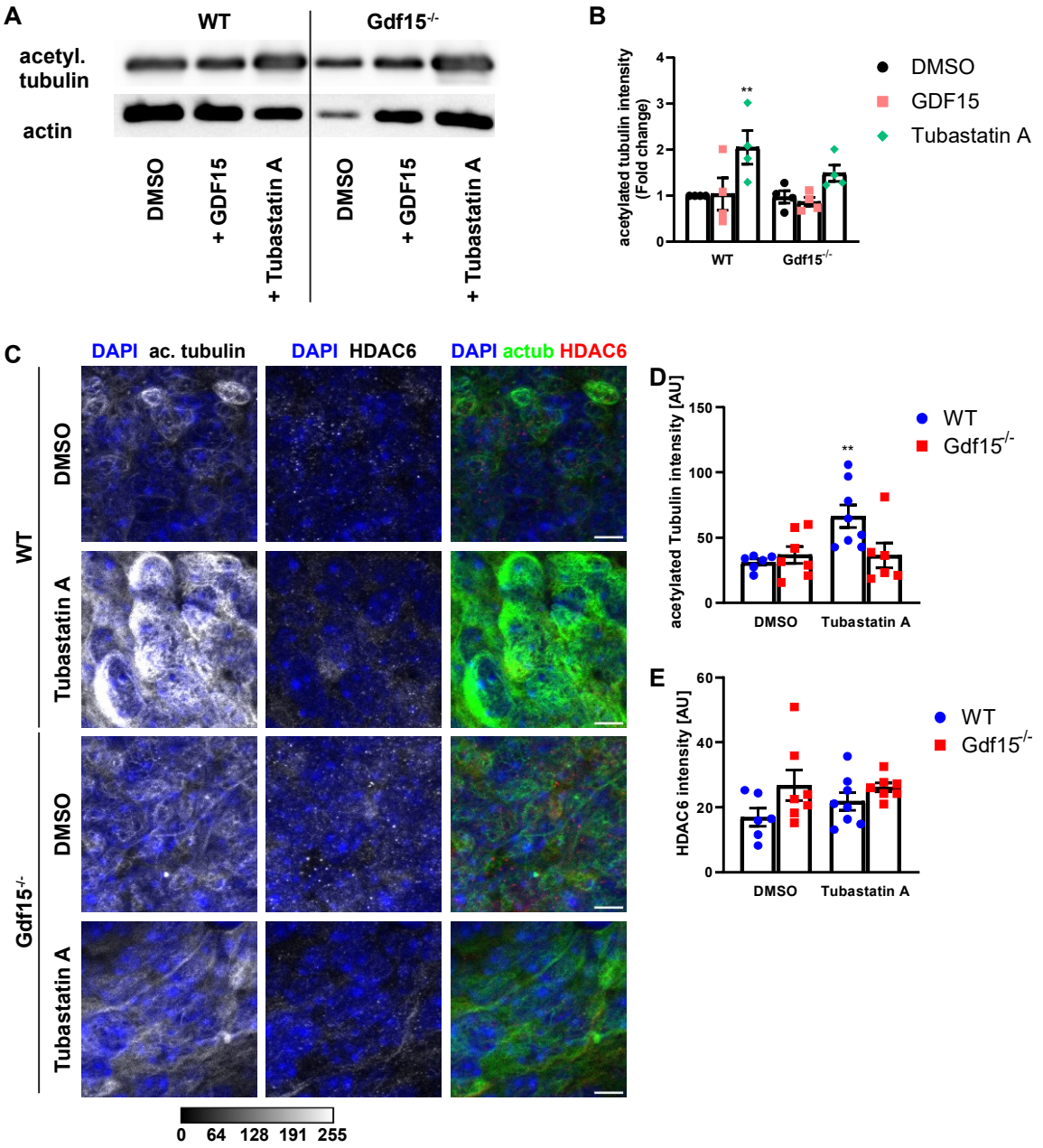

Figure III-23: Gdf15$^{-/-}$ mice show different tubulin acetylation and dynamics.
(A) Western blot of acetylated tubulin (acT) in whole E18 WT or Gdf15$^{-/-}$ GE treated with either DMSO as control or recombinant GDF15 or Tubastatin A (TSA) for 24 h. Actin was used as endogenous control.
(B) Quantification of acT luminescence intensity on western blot, normalized to actin, displayed as fold change over DMSO-treated control.
(C) Representative micrographs of the apical surface of the GE of WT and Gdf15$^{-/-}$ mice at E18, after 24 h treatment with either DMSO as control or TSA, immunofluorescently stained for acT and HDAC6. DAPI was used as nuclear counterstain. Scale bars = 10 µm. Calibration bar displays fluorescence intensity value of greyscale channels.
(D, E) Analysis of fluorescence intensity of acT (D) and HDAC6 (E) at the apical surface of the GE of WT and Gdf15$^{-/-}$ mice at E18, after 24 h treatment with either DMSO as control or TSA. AU = Arbitrary unit, as displayed in calibration bar in C.
This figure is part of a manuscript in preparation.

4.3 d) Sonic Hedgehog signalling is affected by GDF15 knock-out, but is not the cause of divergent cilia morphology

One of the most important ciliary pathways in stem cells is the Sonic Hedgehog (Shh) pathway, which contributes to the regulation of proliferation in adult NSCs and is vital for patterning in the early embryo[89,109,131]. Activation of Shh signalling increases expression of Shh effector Gli1, a mechanism that can also be triggered by Smoothened agonist (SAG), which acts directly on a downstream effector of Shh, Smoothened, instead of the Shh receptor Patched1[132,133]. As ciliary malformations have been linked to defects in Shh signalling[105,138], I hypothesized that Shh signalling may also be affected in the GE of Gdf15$^{-/-}$ mice. Therefore, I analysed the level of *Gli1* mRNA transcripts in the GE of WT and Gdf15$^{-/-}$ E18 embryos with and without treatment with SAG to determine the endogenous Shh activity as well as the response to Shh pathway activation (Figure III-24 A). In Gdf15$^{-/-}$ mice, I found that the level of *Gli1* transcripts was significantly lower than in WT mice, suggesting a lower activity of the pathway in these mice; however, the transcript levels were increased after exposure to SAG, showing that despite the different ciliary morphology, Shh signals could still be transduced by the cilia.

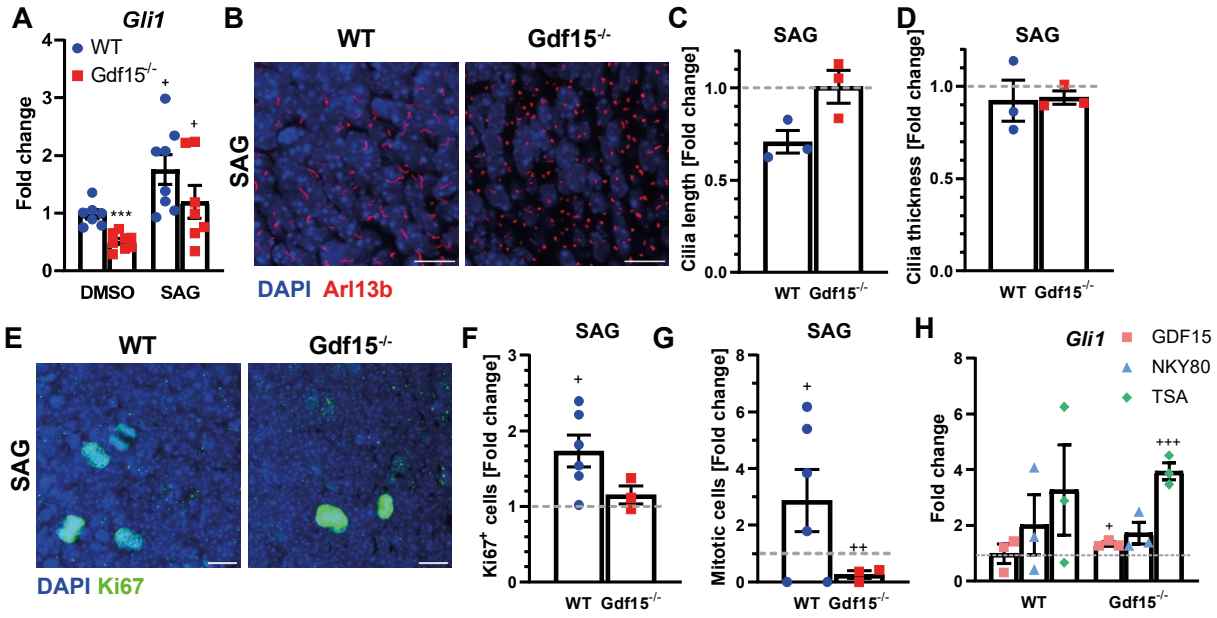

Figure III-24: Shh signalling is impaired in Gdf15$^{-/-}$ mice, but this is not the cause for the cilia phenotype.
(A) Quantification of Gli1 transcripts in whole GEs of E18 WT and Gdf15$^{-/-}$ animals after treatment with Smoothened agonist (SAG), or solvent DMSO as a control, for 24 h. Data is displayed as fold change over the average of the WT DMSO group.
(B, E) Representative micrographs of whole mounts of the apical GE of E18 WT and Gdf15$^{-/-}$ animals after treatment with SAG for 24 h and labelling for cilia with Arl13b (B) or cycling cells with Ki67 (E). Scale bars = 10 µm.
(C, D, F, G) Fold change of cilia length (C) and thickness (D) as well as total Ki67^{+} cells (F) and apical mitotic cells (G) in SAG-treated whole mounts over their respective DMSO-treated controls (grey line). $^{+}$ indicates significance to respective DMSO-treated controls.
(H) Quantification of Gli1 transcripts in whole GEs of E18 WT and Gdf15$^{-/-}$ animals after treatment with GDF15, NKY80, TSA or solvent DMSO as a control (grey line), for 24 h. Data is displayed as fold change over the average of the WT DMSO group.

As I demonstrated in the previous chapters, activation or inhibition of ciliary-localized enzymes (e.g. AC3) may lead to changes in ciliary morphology. Thus, as Shh signalling showed decreased activation in the mutant mice, I used GE whole mounts to test whether activation of the pathway via SAG might rescue ciliary phenotype similar to the effects of blocking AC3 or HDAC6 (Figure III-24 B). In the $Gdf15^{-/-}$ GE, SAG application did not cause changes in either cilia length (Figure III-24 C) or thickness (Figure III-24 D), while length was slightly decreased in WT animals, although this difference was not significant. This suggests that while Shh signalling may be impaired in the GE of mutant mice, it does not seem to cause the altered ciliary morphology in the region.

Next, I investigated if Shh activation had the same effect on proliferation in both WT and mutant mice using proliferation marker Ki67 in SAG-treated GEs (Figure III-24 E). Surprisingly, I found a significant increase in the number of both $Ki67^{+}$ and apically dividing cells (Figure III-24 F, G) in the WT GE after treatment, whereas the amount of mitotic cells was significantly reduced in $Gdf15^{-/-}$ mice and the number of proliferating cells remained the same. When comparing these data with the response of the cells to exogenous GDF15 (see Chapter III-3.5), it seems that both responses are very similar, suggesting that decreased Shh signalling might be a part of the differences in proliferation in the mutant mice. Additionally, SAG decreased mitosis separately from cilia morphology, indicating that cilia morphology is not a consequence of changes in proliferation but that either lack of GDF15 impacts both cilia and proliferation at least to some degree independently, or the change in ciliary morphology and resulting functional defects alter Shh signalling which then in turn affects NSC proliferation.

Lastly, I wanted to know whether AC3 and HDAC6 overexpression might be a cause for the decrease in endogenous Shh signalling in $Gdf15^{-/-}$ mice, so I analysed levels of *Gli1* transcripts in the E18 GE after treatment with inhibitors NKY80 and TSA, as well as with GDF15 (Figure III-24 H). I found that as before, exposure to GDF15 did not change Gli1 mRNA levels in WT animals, while it slightly but significantly increased levels in the $Gdf15^{-/-}$ GE. Blocking AC3 with NKY80 increased levels in both genotypes, but not significantly, whereas HDAC6-inhibition by TSA caused a 4-fold increase in *Gli1* mRNA levels in $Gdf15^{-/-}$ mice. In WT mice, there was a similar increase, however due to the large inter-sample differences, this change was not statistically significant.

All in all, these results show that Shh signalling is altered in $Gdf15^{-/-}$ mice, and that this change can be rescued by exposure to exogenous GDF15 as well as by HDAC6 inhibition.

4.3 e) Gdf15$^{-/-}$ animals have more Prominin-1-expressing cells, which are reduced by HDAC6 inhibition and EGF application but not by exposure to SAG

Most apical cells in the V-SVZ and late embryonic GE express the transmembrane glycoprotein Prominin-1 (Prom), which localizes to the cell and ciliary membrane, especially the ciliary tip[69,70,72]. In Chapter III-3.6, I showed that GDF15 knockout persistently increases the number of ependymal cells and NSCs; therefore, the number of Prom-expressing (P^+) cells in the niche should also be increased. To assess this, I used flow cytometry to analyse the percentage of E18 GE cells that were labelled with a conjugated antibody against Prom (Figure III-25 A). As expected, this analysis showed that the Gdf15$^{-/-}$ GE contains a higher number of P^+ cells than that of WT animals (Figure III-25 B), i.e. 15.34 ± 1.4 % in mutant and 9.63 ± 0.9 % in WT mice, reflecting the increase in apical ciliated cells visible in whole mount preparations.

Lastly, to determine whether the above-investigated signalling pathways and enzymes (i.e. EGFR signalling, HDAC6 and Shh signalling) are involved in this increase in apical cell number, I treated the GEs of WT and Gdf15$^{-/-}$ animals with GDF15, EGF, HDAC6-inhibitor TSA and Shh-pathway activator SAG (Figure III-25 C). To ensure comparability despite day-to-day differences in staining intensity and inter-animal variability, for each animal I treated one hemisphere with one of the mentioned agents while leaving the other hemisphere in medium with the appropriate amount of solvent (4 mM HCl for GDF15, DMSO for TSA and SAG) as a control, which was then used to normalize the number of total P^+ cells (untreated = 100 %). Here I found that in Gdf15$^{-/-}$ animals, application of GDF15 and EGF both caused a significant decrease in the number of P^+ cells to about 85% of the untreated sample (GDF15: 85.73 ± 5.8 %; EGF: 83.2 ± 2.0 %), whereas this effect was even greater when HDAC6 was inhibited (TSA: 61.46 ± 9.5 %). GDF15 application similarly reduced the number of P^+ cells in the WT GE, whereas EGF slightly

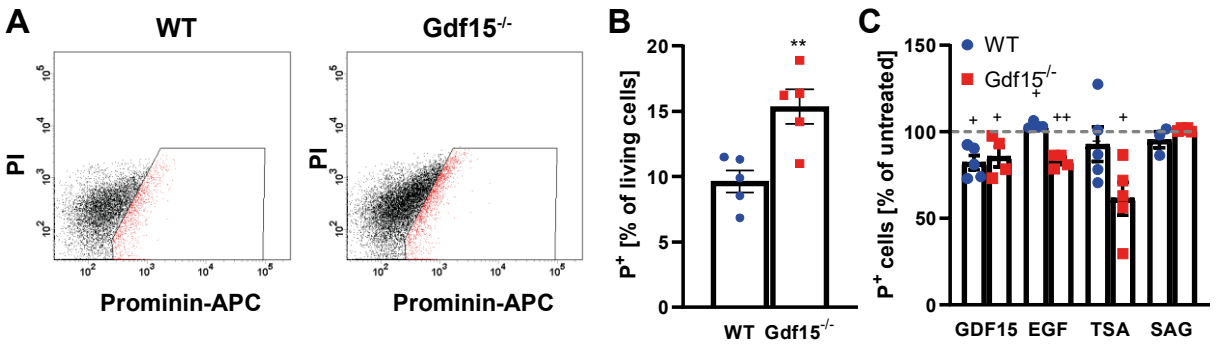

Figure III-25: Gdf15$^{-/-}$ animals have a higher number of Prominin-1 expressing cells.
(A) Representative FACS plots of WT and Gdf15$^{-/-}$ E18 GE cells labelled with an extracellularly binding APC-conjugated antibody against Prominin-1. Gate shows cells deemed positive for Prominin-1 (P^+, red dots). PI = propidium iodide, labelling dead cells. PI^+ cells were excluded from analysis.
(B) Quantification of P^+ cells in the WT and Gdf15$^{-/-}$ GE, displayed as percentage of total living (= PI^-) cells.
(C) Quantification of P^+ cells in the WT and Gdf15$^{-/-}$ GE after treatment with GDF15, EGF, TSA or SAG for 24 h, displayed as percentage of P^+ cells in samples incubated in medium with DMSO only as control (grey line).
$^+$indicates significance to respective control sample.

but consistently increased P^+ cells. Finally, TSA-treatment had no effect on the cells of WT animals, and SAG did not cause changes in either genotype; the lack of effect of the latter was expected, since I did not see a change in cycling $Ki67^+$ cells after application of Shh, suggesting no change in cell number (Chapter III-4.3 d).

All in all, these results confirm that while Shh signalling is affected in mutant mice, this defect is not the cause of the present phenotype; on the other hand, both EGFR signalling and HDAC6 activity seem to be involved in this mechanism. Additionally, these data highlight the complexity of the involved pathways due to the contrary response of WT and mutant cells to EGF and TSA.

4.3 f) Proteomic changes in primary cilia of Gdf15$^{-/-}$ mice

Above, I have presented evidence that the levels of HDAC6, AC3 and Gli1 are increased in the cells of $Gdf15^{-/-}$ animals. However, it is likely that the expression of many more, especially ciliary, proteins is changed in knock-out mice. Therefore, I used fluorescence-activated cell sorting (FACS) on isolated single cilia from the WT and $Gdf15^{-/-}$ E18 GE[72,168], identified by immunoreactivity to Arl13b and acT, to collect large amounts of primary cilia as well as immunonegative control samples (Ctrl; Figure III-26 A) and assess their protein content using liquid chromatography-mass spectrometry (LC-MS).

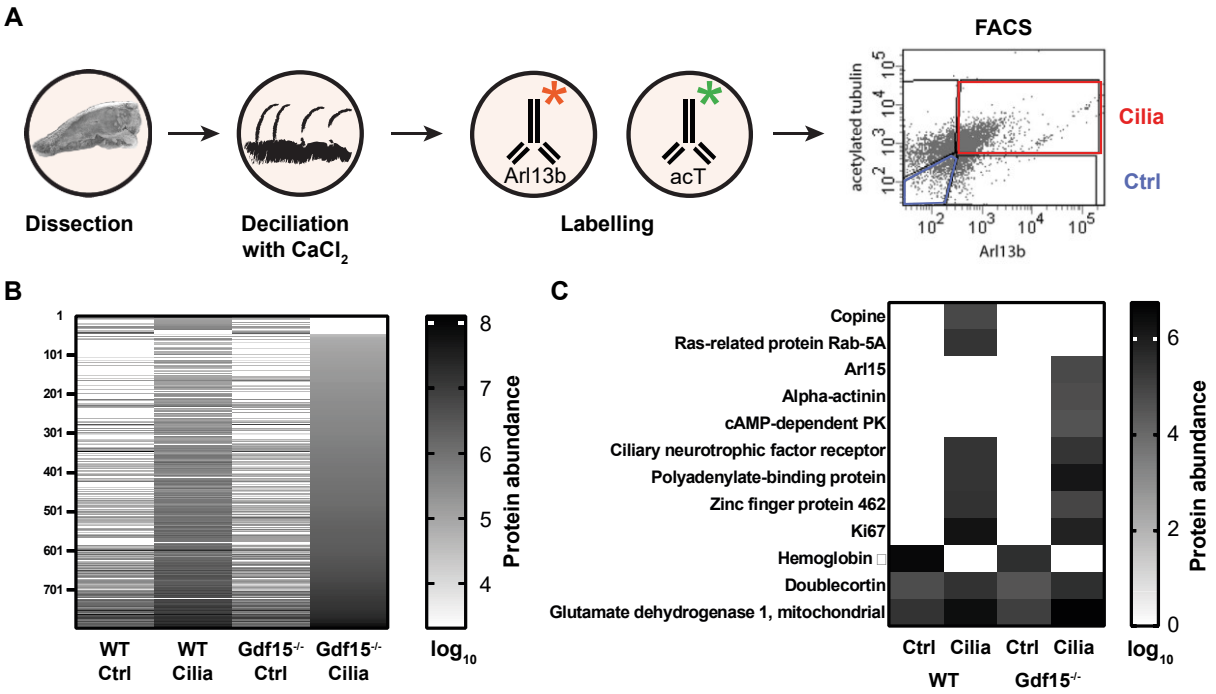

Figure III-26: Proteomic analysis of primary cilia after FACS.
(A) Schematic of workflow from GE samples to isolated cilia. After dissection of the GE, WT and $Gdf15^{-/-}$ tissue samples are deciliated by exposure to a high calcium concentration, and the medium supernatant containing the cilia is subsequently stained with fluorophore-conjugated antibodies against Arl13b and acT. The cilia are then sorted by FACS, and $Arl13b^+acT^+$ particles (Cilia) and $Arl13b^-acT^-$ particles (Ctrl) are collected. The samples are then digested in solution and analysed by LC-MS. Some graphic assets re-used from Monaco, et al. [72].
(B, C) Heat map showing the protein abundance (displayed in a log_{10} scale) of all 797 detected proteins (B) and selected proteins only (C).

After exclusion of contaminants (i.e. proteins of any species other than *Mus musculus*, as well as keratins) I found 797 different proteins across all samples, most of them only expressed in the cilia samples (Figure III-26 B). Of these proteins, 14 were only expressed in WT cilia but not in Gdf15$^{-/-}$ samples, among them Copine and Rab-5A, proteins involved in membrane trafficking, whereas 45 proteins could be found in Gdf15$^{-/-}$ cilia that were not present in the cilia of WT animals (Figure III-26 C). These proteins included Arl15, alpha-actinin and cAMP-dependent protein kinase, the latter suggesting higher levels of cAMP in Gdf15$^{-/-}$ cilia. Other proteins like ciliary neurotrophic factor receptor, expressed generally in neuronal cilia, as well as polyadenylate-binding protein, associated to mRNA, were present in both WT and Gdf15$^{-/-}$ cilia, and abundant proteins like doublecortin and mitochondrial glutamate dehydrogenase were present in all samples. Lastly, proteins considered contaminants, such as hemoglobins, were present exclusively in the Ctrl samples.

Interestingly, I also found an abundance of nuclear proteins such as zinc finger proteins and even Ki67 in ciliary samples, which could suggest that parts of nuclei were also isolated in these samples, likely due to high levels of acT in the perinuclear region. Furthermore, I surprisingly did not find proteins that I expected in ciliary samples, such as AC3, Arl13b, Prom, or any IFT proteins. However, the proteins I did find all shared the characteristic of being very highly expressed in most cells; therefore, it is possible that less expressed proteins might not be detected with the amount of sample collected.

To determine which protein pathways might be upregulated in Gdf15$^{-/-}$ cilia, I analysed proteins present in both WT and Gdf15$^{-/-}$ cilia samples, as well as those expressed in the mutant sample only, and performed pathway analysis on the proteins enriched in Gdf15$^{-/-}$ cilia samples using reactome.org[171] (Table III-1). This analysis revealed that most pathways enriched in Gdf15$^{-/-}$ cilia are mitosis- or cell cycle-related, particularly concerning G2/M-phase transition as well as centrosome organisation and maturation. Additionally, I found an enrichment in the AurA kinase pathway ("AURKA Activation by TPX2"), which could be expected from the overexpression of HDAC6 in the mutant mice[74] (see also Chapter III-4.3 a). Finally, pathways concerning Rho GTPase signalling were also increased; Rho GTPases are involved in the differentiation of apical ependymal cells and interact with Prom[182,183], both of which are also increased in Gdf15$^{-/-}$ mutant mice. Interestingly, I could not find any pathways significantly downregulated ($p<0.05$) in Gdf15$^{-/-}$ cilia samples.

All in all, these results show that several proliferation-dependent pathways are upregulated in Gdf15$^{-/-}$ cells, which is visible in their ciliary proteome.

Table III-1: Pathway analysis of proteins enriched in the cilia isolated from the E18 Gdf15$^{-/-}$ GE.

Pathway	p-value
Recruitment of NuMA to mitotic centrosomes	$2.22*10^{-16}$
Loss of proteins required for interphase microtubule organization from the centrosome	$9.44*10^{-15}$
Loss of Nlp from mitotic centrosomes	$9.44*10^{-15}$
AURKA Activation by TPX2	$1.27*10^{-14}$
Centrosome maturation	$2.89*10^{-14}$
Recruitment of mitotic centrosome proteins and complexes	$2.89*10^{-14}$
Regulation of PLK1 Activity at G2/M Transition	$4.75*10^{-14}$
G2/M Transition	$6.41*10^{-14}$
Mitotic G2-G2/M phases	$6.94*10^{-14}$
Cilium Assembly	$7.52*10^{-14}$
Mitotic Prometaphase	$7.82*10^{-14}$
Anchoring of the basal body to the plasma membrane	$1.02*10^{-13}$
Organelle biogenesis and maintenance	$1.67*10^{-12}$
M Phase	$1.49*10^{-11}$
Cell Cycle, Mitotic	$1.80*10^{-10}$
Cell Cycle	$1.05*10^{-09}$
HSP90 chaperone cycle for steroid hormone receptors (SHR) in the presence of ligand	$7.21*10^{-08}$
RHO GTPase Effectors	$1.21*10^{-06}$
Signaling by Rho GTPases	$2.85*10^{-06}$
Signaling by Rho GTPases, Miro GTPases and RHOBTB3	$2.22*10^{-16}$

IV. Discussion

1. Stem cell heterogeneity in the adult mouse brain

Stem cell identity and their contribution to adult neurogenesis in the V-SVZ has long been a subject of debate. Both GFAP-expressing so-called niche astrocytes and ependymal cells were identified as NSCs in the V-SVZ at the same time[25,184], and later on, apical Nestin$^+$ NSCs were thought to be the main contributors to neurogenesis, while cells at the basal side of the niche were identified mostly as apical-derived TAPs and neuroblasts or niche astrocytes incapable of neurogenesis[71,185,186]. However, more recent studies suggest that different pools of NSCs might be present in the V-SVZ[28,29,187].

In the first part of this thesis, I more closely characterized apical and basal NSCs in terms of Nestin and hGFAP reporter expression, as well as ciliation. Here I found that most G$^+$ cells were located at the basal side of the niche, were unciliated and did not express Nestin, whereas apical G$^+$ cells were in majority Nestin-immunopositive. Additionally, I found that basal G$^+$ cells, although containing a majority of quiescent NSCs, appeared to proliferate faster compared to apical cells after entering the cell cycle. This concurs with the current literature that apical NSCs are slowly dividing whereas most cycling cells are located at the basal side of the niche[29,188]. In a collaborative effort with other members of the Ciccolini group[2], I could also show, using clonal analysis and viral tagging, that apical NSCs do not contribute to neurogenesis in a significant way and that basal NSCs, as also suggested by their higher proliferation rate, are the main source of adult-born interneurons. The similarity of the characterization of apical and basal cells at P7 suggests that these basal NSCs are a separate population of NSCs already present at this early age and are not primarily derived from apical NSCs in adult animals, as previously thought[16,25].

Additionally, although basal NSCs proliferate more, as evidenced by the depletion of cells displaying nuclear H2B-GFP reporter expression after the application of doxycycline, some of these cells did in fact retain the reporter expression over 30 days, indicating quiescence. Due to the lack of endogenous GFAP expression in these cells[2], it is unlikely that the non-dividing cells could be terminally differentiated astrocytes. These data indicate that proliferating basal G$^+$ cells are in fact NSCs and not TAPs derived from asymmetric division of apical NSCs.

Nestin has long been used as a marker for NSCs; however, some, especially quiescent, NSCs were shown to not express the marker[11]. Supporting these findings, I here showed evidence that basal NSCs, which undergo quiescence and contribute to neurogenesis, do in majority not express this marker. In the SGZ, however, even quiescent radial NSCs were found to express Nestin[44,189], a characteristic that coincides with cilia expression in this niche[131,190]. Indeed, my results show that in the V-SVZ, the majority of ciliated cells were apical, Nestin-expressing cells, whereas basal Nestin$^-$ cells only rarely

extend primary cilia. Due to their role in cell cycle and quiescence, primary cilia might be involved in both the regulation of quiescence and the expression of Nestin in these apical cells via the transduction of signals received from the CSF. Hence, the differences in neurogenesis and quiescence observed in apical and basal cells might be due to location and the resulting differing microenvironments.

Interestingly, I found a decrease in the percentage of ciliated cells from P7 to 8w animals which seems counterintuitive based on the decrease in proliferation in adult animals. However, the adult V-SVZ also contains a higher number of ependymal cells, whose cilia are not labelled by AC3[72], and an overall lower number of apical NSCs, which suggests that the lower number of cilia is not due to lower percentage of ciliated NSCs, but less NSCs overall. Additionally, cilia presence itself was demonstrated to be a less reliable indicator of quiescence than primary cilia length[12], which I found to be increased in adult WT animals compared to E18 embryos.

Lastly, I showed evidence that in adult animals, cells in the ventral part of the V-SVZ are more likely to be ciliated than those in the dorsal or medial part, a trend which is already established one week after birth. Interestingly, it was previously shown that the ablation of primary cilia in the V-SVZ uniquely affects cells in this region[111], suggesting a vital functional role of cilia in these cells.

A summary of the findings from this part of the thesis together with the collaboration of other lab members is displayed in Figure IV-1. All in all, these results suggest that basal NSCs are a separate population of NSCs capable of undergoing quiescence and neurogenesis, and that differences between apical and basal NSCs may be due to their respective microenvironments and primary cilia presence.

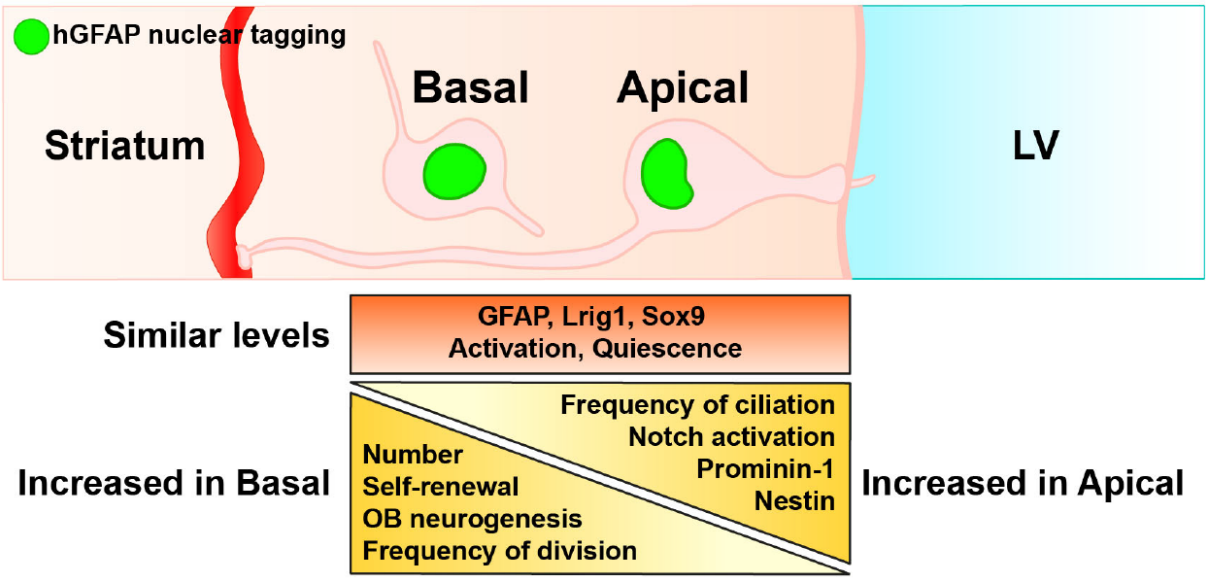

Figure IV-1: Schematic diagram summarizing main characteristics of apical and basal NSCs.
Both apical and basal NSCS are present in the adult V-SVZ. hGFAP promoter is active in both NSC groups. Apical and basal NSCs display similar levels of GFAP, Lrg1 and SOX9, but not of Nestin and Prominin-1 expression, which are prevalently observed in apical NSCs. Apical NSCs, like previously described radial glia-like/type B1 astrocytes, contact the lateral ventricle and often extend primary cilia. However, basal NSCs, similar to type B2 astrocytes in the V-SVZ, do not contact the lateral ventricle and rarely display primary cilia. Both NSC types undergo activation and quiescence and self-renewal in vivo. However, basal NSCs self-renew and proliferate more than apical NSCs in vitro and divide more frequently, and are the main contributors to OB neurogenesis than the apical counterpart in vivo. Apical and basal NSCs differ in the expression of genes associated with Notch signalling and the highest levels of activation are observed in apical NSCs.
Figure and legend from Baur, et al. [2].

2. The role of GDF15 in the V-SVZ

2.1 GFRAL is expressed in NSCs and TAPs in the V-SVZ but not in the hippocampus

Even though expression of GDF15 in the V-SVZ and choroid plexus has been found over two decades ago[153], the role of the protein in this niche has not yet been sufficiently explored, especially since no significant levels of GFRAL were detected in the V-SVZ at mRNA level when the receptor was discovered[157].

In this thesis, I showed evidence that GFRAL is indeed expressed only weakly at mRNA level, but sufficiently for detection at protein level. Additionally, I found that in apical cells, GFRAL co-localizes with Nestin, GFAP and EGFR, but basally not with CXCR4, suggesting expression by apical quiescent and activated NSCs, but not by basal cells including basal NSCs, TAPs or neuroblasts. Previous work by Carmen Carrillo García showed that GDF15 itself is expressed is NSCs in the niche at mRNA and protein level[164,175], suggesting autocrine signalling or paracrine signalling between neighbouring GDF15/GFRAL-expressing cells. Additionally, I found only very low GFRAL expression on protein level in the adult HP, which coincides with lower levels of GDF15 detected there at this age[175]. This may be due to GDF15 sequestered by the choroid plexus which is received by apical NSCs in the V-SVZ, whereas GDF15 signalling is reduced in the hippocampus in adult animals.

Lastly, I found that knock-out of GDF15 did not change the levels of GFRAL expression. This indicates that, as opposed to EGFR signalling, GDF15/GFRAL signalling does not trigger a positive or negative feedback loop, but its expression might rather be controlled by other factors. As $Gdf15^{-/-}$ cells kept in culture lose their unique properties and differences compared to the WT control after about 24-48 h *in vitro*[1,164], it is likely that the effect and expression of GDF15 and GFRAL is dependent on niche-specific signals, such as signalling molecules in the CSF or the movement of the CSF flow itself, or even cell-cell contacts. Indeed, previous work from this laboratory shows that cell-cell signalling such as notch signalling is vital for the regulation of activation and quiescence in apical and basal NSCs in the adult V-SVZ[2,93,191]. Additionally, the presence of the receptor in cilia, an organelle capable of sensing signals in the CSF as well as detecting the mechanical push of CSF flow[95,96,192], supports the hypothesis that primary cilia are an integral part of the GDF15 signalling mechanism in apical NSCs.

2.2 GDF15 regulates cell cycle speed and number of proliferating cells in the V-SVZ

Due to its role in NSCs in the hippocampus as well as the regulation of proliferation in cancer cells[158,160,164,193], I hypothesized that GDF15 may affect proliferation in NSCs in the V-SVZ. In the GE of E18 embryos, I found that lack of GDF15 increased the number of proliferating cells as well as cell cycle speed, and that application of endogenous GDF15 for 24 h decreased NSC proliferation in knock-out mice. Contrary to this, WT cells increased proliferation upon GDF15 application. This opposing role of GDF15 is in agreement with the fact that GDF15 is not merely a mitogen or an inhibitor of proliferation[164,175], but instead seems regulate the number of NSCs and their proliferation rate within a certain range. The latter hypothesis is supported by the fact that while the application of GDF15 had opposite effects on proliferation and apical mitosis in both genotypes, these parameters were brought to the same level after application, suggesting a steady state point that GDF15 is working towards.

However, contrary to the hippocampus, where GDF15 needs active CXCR4 to function[164], I found no such effect of the chemokine in the embryonic GE. CXCR4 was previously found to regulate growth factor-dependent proliferation[194], and inhibition of the receptor affects the ability of $EGFR^h$ cells to form clones[1]. Interestingly, in $Gdf15^{-/-}$ mice, where EGFR signalling is affected, inhibition of CXCR4 by AMD reduced proliferation and mitosis less than in WT mice, where AMD led to a complete inhibition of mitosis. When applied in combination with GDF15, GDF15 seemed to counteract the effect of AMD in WT mice, whereas the decrease of proliferation is enhanced in mutant mice. For this, there might be two reasons: Firstly, it is possible that the cell populations that need active CXCR4 to proliferate are different from those responding to GDF15 and that they are differently represented in the WT and mutant GE, or secondly, CXCR4 signalling is altered in mutant mice. Since in the $Gdf15^{-/-}$ GE, mitosis was only decreased in apical progenitors in response to CXCR4 inhibition, it is likely that some of the apical progenitors are CXCR4-dependent $EGFR^h$ cells, which are more represented in WT animals than in mutants due to the alterations in EGFR signalling. The interpretation that GDF15 and CXCR4 affect the proliferation of largely independent groups of progenitors is consistent with my observation that the expression of CXCR4 and GFRAL overlap at the apical but not at the basal side of the niche.

All in all, these findings suggest that GDF15 does not regulate the cycling speed of all progenitor cells in the GE, but more significantly affects a specific subset of apical progenitors.

2.3 GDF15 regulates number of ependymal and NSCs in late embryos and adult mice

EGFR signalling has been implied in the differentiation of ependymal cells, where it is regulated via numb trafficking[195]. Specifically, the reduction of apical EGFR surface expression was found to lead to ependymal cell differentiation, as EGFR kinase was found to suppress ciliogenesis[196]. Indeed, in Gdf15$^{-/-}$ animals, I found lower levels of surface EGFR and an increase in ependymal cells at P2 (Figure IV-2 shows an overview of changes in the Gdf15$^{-/-}$ V-SVZ). However, this effect is not associated to differentiation, as NSCs are not depleted in the mutant mice – on the contrary, apical NSCs were also increased. In previous studies, GDF15 knock-out was not found to increase numbers of any other differentiated cell types like neurons or oligodendrocytes[1,164,175]; rather, excess neuroblasts were compensated by cell death. This indicates that lack of GDF15 specifically promotes the proliferation of a common progenitor for apical NSCs and ependymal cells while not affecting neurogenesis. Combined with the fact that GDF15 primarily affects apical NSCs[197] and neurogenesis is maintained mainly by basal NSCS, this points to GDF15 being a regulator specific to apically dividing NSCs and their differentiation.

Additionally, I found that due to the increase of both NSCs and ependymal cells in the apical niche, overall cell number per area was increased in Gdf15$^{-/-}$ mice, resulting in smaller cell size, from E18 to adult mice. Interestingly, the total amount of ependymal cells and NSCs in the WT V-SVZ was found to decrease with time, with a concurrent increase in cell size, a process which begins already shortly before birth[198]. This process is also associated with the maturation of NSCs from radial glia, and the establishment of the pinwheel structure of the niche[10]. My results suggest that GDF15 regulates this maturation, as its expression coincides with this timeline and its ablation stops the decrease in ependymal cell number.

Lastly, while the increased proliferation in Gdf15$^{-/-}$ mice remains consistent for 24 h *ex vivo*, i.e. in whole explants of the GE in medium, the specific phenotype of Gdf15$^{-/-}$ cells displaying shorter cilia disappears after several days in dissociated cultures[1,175] (also shown in yet unpublished work from the Bachelor Thesis of Antonia Schürg), even if no GDF15 was added to the culture medium. This suggests that not only the presence or absence of the protein in the CSF is important for this phenotype, but also the cell-cell connections and niche integrity, such as apical-basal polarity. As GDF15 is also upregulated during injury[152,199], it is likely that the destruction of cell-cell contacts during injury might be involved in the action mechanism of GDF15. Consequently, this may also explain the opposing reactions in proliferation between WT and mutant cells after the application of GDF15, which may be altered in Gdf15$^{-/-}$ mice due to the higher density of cells accompanied by smaller cell size and therefore, increased cell-cell signalling compared to cell size.

2.4 GDF15 regulates primary cilia length in the embryonic GE and adult V-SVZ

Primary cilia are a well-known regulator of cell cycle and proliferation[108,129]. Indeed, ablation of GDF15 caused a significant decrease in primary cilia length and increase in thickness as well as in overall ciliation in the embryonic GE. As previously reported[12], I here also found an inverse correlation between proliferation and cilia length, and that addition of GDF15 to the culture medium rescued this phenotype, indicating a direct effect. This change in cilia length was accompanied by overexpression of HDAC6 and AC3, known regulators of cilia length[115,124,180]. The mechanisms underlying this phenomenon are more closely discussed in Chapter IV-3.2 and IV-3.3.

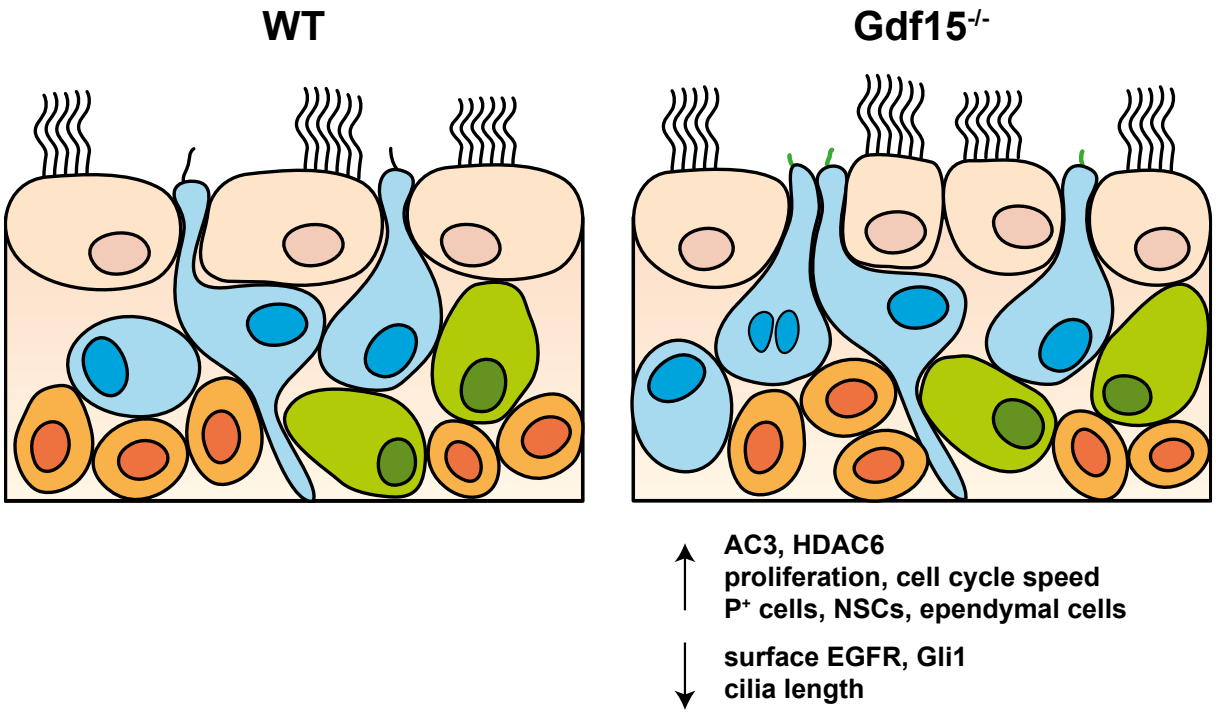

Figure IV-2: Effects of GDF15 ablation on the V-SVZ.
Compared to WT animals, the Gdf15$^{-/-}$ GE / V-SVZ contains more ependymal cells and NSCs with higher cell cycle speed and increased proliferation. Additionally, cells in the Gdf15$^{-/-}$ GE show increased levels of AC3 and HDAC6, accompanied by lover levels of surface EGFR and Gli1. Compared to the WT V-SVZ, primary cilia in the Gdf15$^{-/-}$ niche are shorter and thicker.

3. Mechanisms of GDF15 function

3.1 GDF15 affects EGFR signalling

Previous experiments showed that GDF15 is more highly expressed in E^h cells[164,175], and in this study I found considerable co-localization of EGFR and GFRAL. These data indicate that EGFR and GDF15 act on the same cell populations. That most proliferating progenitors express EGFR[1] and EGFR inhibitor reduced proliferation in $Gdf15^{-/-}$ animals indicates that EGFR function is still vital for proliferation in mutant mice. However, my data also show a reduction in surface EGFR expression as well as anomalies in signalling kinetics. Interestingly, the mRNA level of EGFR was not affected, showing that GDF15 does not regulate EGFR on a transcript level; and while protein immunoreactivity was lower in $Gdf15^{-/-}$ cells, the levels of phEGFR were not significantly affected by the ablation of GDF15. Taken together, these results indicate that while EGFR signalling may be altered, it is likely not lower than in WT controls. Indeed, my analysis of phERK did not show any differences in baseline ERK phosphorylation between WT and knock-out cells.

Although my results show that the increase in ependymal cells and NSCs in $Gdf15^{-/-}$ mice is likely due to higher proliferation and less due to increased ependymal differentiation, the trafficking of EGFR away from the apical membrane has been implied in the differentiation of ependymal cells[195]. Indeed, addition of EGF to an overnight GE whole tissue culture showed that EGF decreased the number of Prominin-1-expressing cells, i.e. apical NSCs and ependymal cells. To discriminate between the effect of EGFR signalling on proliferation and differentiation of ependymal cells, however, a similar experiment of pharmacological inhibition of EGFR would have to be performed in the presence of anti-proliferative drugs.

After activation, EGFR is internalized and degraded[86]; therefore, lower levels of surface EGFR might actually be an indicator of higher EGFR activation. As EGFR was also shown to inhibit ciliogenesis via its kinase activity[196], an increase in EGFR signalling could explain the decrease in cilia length. However, this cannot be the sole reason for the observed phenotype, as application of EGF or EGFR inhibitor did not affect cilia length or thickness. Additionally, differences in EGF protein expression in V-SVZ-cells or levels in the CSF would need to be analysed to determine if it is affected by GDF15 knock-out.

A downstream target of EGFR signalling is ERK, a regulator of proliferation and cell behaviour which is activated by multiple mitogens, growth factors, cytokines and GPCRs[200]. I found in this study that ERK phosphorylation by MEK is caused also by GDF15 application, which is supported by the current literature[155,157,160], and that this mechanism is needed for the effect for GDF15 on cilia. However, activation of the pathway by EGFR signalling was not sufficient, suggesting multiple converging pathways are necessary for this effect (a diagram showing the possible working mechanism of GDF15

is displayed in Figure IV-3). However, like EGFR, GFRAL also activates the PLCγ and PI3K-AKT pathways[155]; so far, no further downstream signalling has been identified. My results however suggest that GFRAL may have a direct interaction with proteins within the cilia which has not yet been discovered. A co-immunoprecipitation experiment could show whether GFRAL physically interacts with e.g. AC3 or HDAC6, or any of the GPCR associated with AC3, which my results indicate.

All in all, I found that GDF15 significantly affects EGFR trafficking and signalling; however, the underlying mechanism still remains unclear.

3.2 Ciliary GFRAL influences primary cilia morphology via local translation and signalling

In this thesis, I for the first time showed evidence that GFRAL is expressed not only in a sufficient level for signalling in the GE and adult V-SVZ, but also in primary cilia. Furthermore, I found that this is the case specifically in this neurogenic niche and not in the hippocampus, where cilia length is also not altered. This points towards ciliary GFRAL being necessary for the changes in cilia length. Indeed, I found that blocking transcription did not stop the effect of GDF15 on cilia length, suggesting that local protein transcription and signalling within the cilium were enough to affect this phenotype. While there are several known ciliary localization sequences (CLS)[103], none of them are present in the GFRAL protein; however, since only few CLS are present on different proteins, it is possible that GFRAL has its own unique CLS that has not yet been identified. Otherwise, it is also possible that GFRAL localizes to cilia via a direct interaction with another ciliary protein that may be expressed exclusively in the GE/V-SVZ, which could explain the absence from primary cilia in other brain regions.

While the increase in P^+ cells in the $Gdf15^{-/-}$ GE reflects the increase in apical cell number, the expression of Prom itself could be more closely investigated. Prom is not only expressed in apical cells and in tips of primary and ependymal cilia in the niche, but it was also found to bind selectively to Arl13b and HDAC6 to regulate primary cilia function and therefore, activation of stem cells[201]. Therefore, the overexpression of HDAC6 might also affect its relationship with and the activity of Prom. Interestingly, Prom is a protein with 8 different splice variants, some of which are expressed only in certain subregions of the brain; e.g. while splice variant s3 is expressed only in the DG, s6 is expressed only in the V-SVZ[202]. Interaction of specifically this splice variant with GFRAL could be a reason for ciliary expression of the receptor in the V-SVZ but not in the DG, and the following changes in ciliary phenotype being present only in the former region. A closer investigation of a possible interaction between Prom and GFRAL should therefore be investigated using co-immunoprecipitation.

GFRAL is not yet known to physically interact with either AC3 or HDAC6, however, it is likely that both these proteins are involved in this mechanism. Both proteins are overexpressed in the $Gdf15^{-/-}$ E18 GE and have been previously shown to be involved in control of cilia length[115,124,180]; additionally,

inhibition of HDAC6 was shown, due to its role in ciliogenesis and Wnt signalling, to affect the proliferation and differentiation of cancer cells[117-119]. Interestingly, like GDF15[158,160,193], HDAC6 activity both inhibits and increases tumour proliferation in different contexts. In my experiments, I also found that HDAC6 inhibition by TSA leads to opposite effects on cilia length in WT and mutant mice, while proliferation is only affected in the $Gdf15^{-/-}$ GE. I furthermore found differences in tubulin acetylation after HDAC6 inhibition, and different patterns or HDAC6 expression. As HDAC6 usually localizes to the basal body of the primary cilium[115,117,118], which was not readily visible from my immunolabelling, a difference in localization of the protein may affect cilia besides the overexpression itself. However, a more thorough study with another antibody or a tagged HDAC6 protein is needed to confirm these results.

Besides its role in ciliogenesis and ciliary signalling[124,126,127], especially in neurons, AC3 was also found to affect body weight[179,203] and its upregulation in HEK293 cells increased proliferation, invasion and clone-formation via the CREB pathway[125]. It was also found to be upregulated in gastric cancer[125,204]. Similarly, the overexpression of AC3 in the $Gdf15^{-/-}$ GE was here accompanied by increased proliferation, and AC3 expression was decreased by GDF15 and TSA application, particularly the latter. This suggests that GDF15 could regulate AC3 expression via HDAC6 to help regulate cilia length.

AC3 acts through its adenylate cyclase activity, increasing the concentration of cAMP inside the ciliary compartment and thereby activating PKA[126]. Therefore, it is likely that in $Gdf15^{-/-}$ animals, cAMP levels are increased; however, my attempts to quantify cellular or ciliary cAMP concentration using traditional assays were unsuccessful. Recent studies have used cilia-localized biosensors to analyse cAMP concentration[205,206]; using *in utero* electroporation or transgenic mouse lines, it would be possible for future researchers to analyse ciliary cAMP concentration in cilia of $Gdf15^{-/-}$ animals to determine whether the altered AC3 expression is associated with higher enzyme activity.

3.3 Ciliary signalling is altered in $Gdf15^{-/-}$ mice

Higher PKA activity due to higher cAMP concentration was previously shown to inhibit Gli2 and thereby, Shh signalling[148,207]. Indeed, I found lower base levels of Gli1 mRNA in the $Gdf15^{-/-}$ GE compared to WT controls, supporting this hypothesis. However, application of SAG was still able to increase Gli1 levels, indicating that Shh signalling can still be activated even if baseline activation is lower. Interestingly, SAG was able to affect proliferation without affecting primary cilia length, suggesting that the decrease in cilia length is not a by-product of changes in cell cycle but these parameters may be influenced separately by GDF15.

In this thesis, I focused on AC3 to determine the effect of adenylate cyclases on cilia morphology and used inhibitor NKY80 to block AC3 activity. However, NKY80 also shows high affinity for AC5 and AC6[208], membrane-bound adenylate cyclases which are both localized to primary cilia as well[209-211]. They were not only shown to be strongly expressed in the embryonic neural tube, a Shh target region[212], but also to directly suppress Shh signalling similar to AC3[209]. Therefore, it is likely that using NKY80 changed both ciliary length and Shh signalling not only based on its effect on AC3 but also on AC5 and AC6. It would therefore be interesting to investigate the expression of these proteins in the Gdf15$^{-/-}$ GE, and if the effect on their expression by inhibition of HDAC6 or GDF15 application is similar.

Another cilia-dependent signalling pathway which might be affected is Wnt signalling, where when canonical Wnt/β-catenin signalling is active, β-catenin is stabilized and translocates into the nucleus. In a pilot experiment, I therefore assessed β-catenin protein levels using western blot and immunofluorescence, and did not see a difference between WT and Gdf15$^{-/-}$ samples in either protein level or nuclear localization. However, recently discovered Wnt/STOP signalling is a cilia-dependent signalling pathway that does not affect β-catenin localization or stability[151]. It is therefore possible that this specific Wnt pathway might be affected in Gdf15$^{-/-}$ animals, contributing to the proliferation or cilia phenotype.

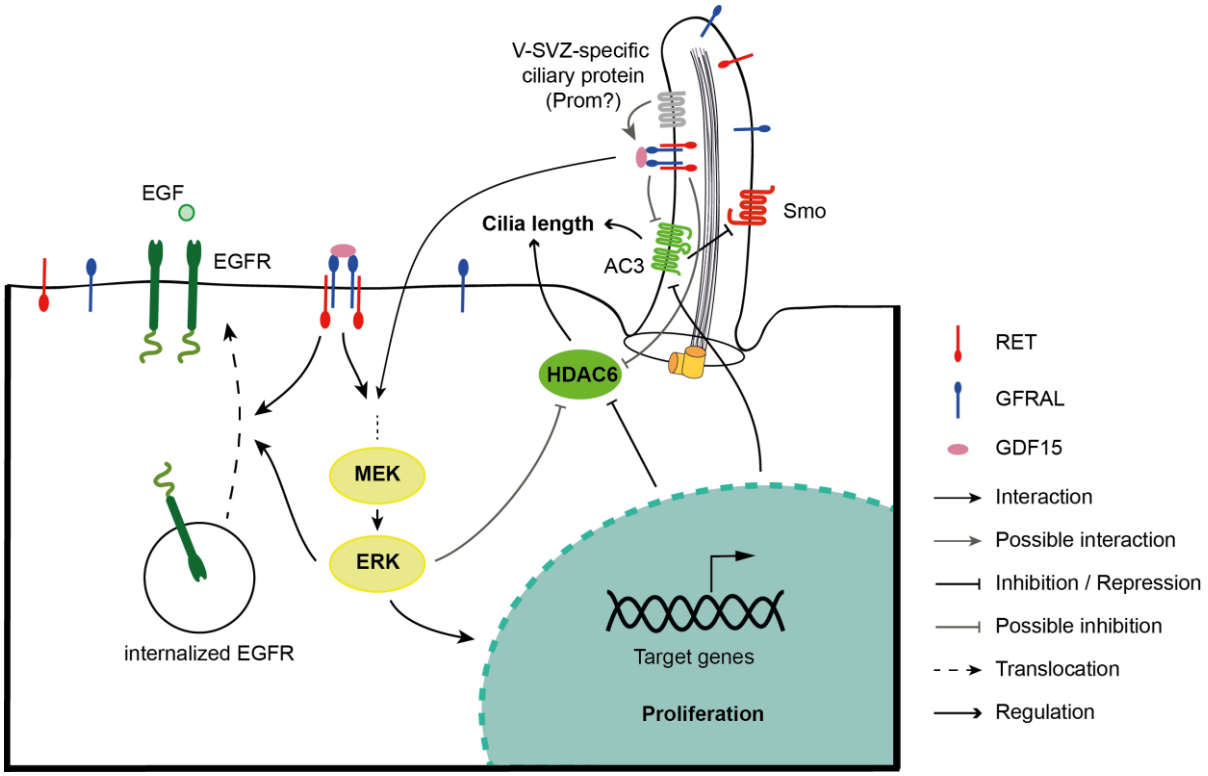

Figure IV-3: Possible mechanisms of GDF15 function in the GE and V-SVZ.
Ciliary GFRAL, possibly localized to the cilia via interaction with an unknown protein, interacts locally with HDAC6 and AC3 in a mechanism that requires MAPK/ERK signalling, as well as by transcriptional repression of these proteins, both of which regulate cilia length and affect proliferation. Activated GFRAL also might affect EGFR externalization, either directly or via MAPK/ERK signalling, contributing to the regulation of proliferation.

4. Conclusion and open questions

In this thesis, I investigated the heterogeneity of NSCs in the adult and postnatal V-SVZ, showing that apical NSCs are more likely to express Nestin and extend primary cilia, while identifying a more proliferative basal NSC population which contributes significantly to adult neurogenesis.

Furthermore, I could show for the first time that GDF15 receptor GFRAL is expressed in primary cilia of apical NSCs and that GDF15 affects primary cilia length and proliferation of NSCs in the GE and V-SVZ. I further identified EGFR, HDAC6 and AC3 as likely candidates for the promotion of this mechanism. However, the precise protein interactions that lead to this effect of GDF15 still remain largely unclear. Therefore, closer investigations of the interaction between HDAC6, AC3 and GFRAL are necessary, as well as the effect on EGFR surface expression. The specific mechanism that leads to GFRAL expression in the GE but not in other brain regions is also highly intriguing and warrants closer inspection. Lastly, HDAC6 was shown to affect Wnt signalling[74]; both non-canonical Wnt/PCP and Wnt/STOP signalling are dependent on primary cilia and may affect cell behaviour in the niche. These pathways still remain to be investigated, along with other downstream pathways of GFRAL such as the AKT and PLCγ pathways, as well as PDGFRa, which is expressed on cilia of NSCs throughout the niche[90,140,142,143] and may therefore be affected by GDF15.

All in all, this work lays the foundations to closer investigate the role of GDF15 in this important neurogenic niche and may contribute to future research regarding adult neurogenesis and cancer.

V. Acknowledgements

First, I would like to thank Dr. Francesca Ciccolini for the opportunity to perform this work in such an exciting field, for her trust in my abilities, continued scientific advice, encouragement to present my work at conferences and supporting me with publishing papers. I would also like to thank Prof. Dr. Hilmar Bading for taking the time to be my examiner again, as well as him and Dr. Gislene Pereira for their valuable comments on my work during TAC and lab meetings.

Furthermore, I would like to thank Gabriele Hölzl-Wenig and Claudia Mandl for their help with dissections, FACS sorting, animal breeding and orders, organisation, and generally for always lending a helping hand when I needed it. Thanks also goes to Andrea Hellwig for performing electron microscopy, as well as Sebastian Weber from the EMCF for his help with sample preparation.

I would also like to acknowledge the Core Facility for Mass Spectrometry and Proteomics (CFMP), especially Thomas Ruppert, Ute Bach and Marcin Luzarowski, for their help with mass spectrometry.

Furthermore, I would like to thank the entire Department of Neurobiology for providing a friendly work environment and constructive help with my experiments, especially Otto Bräunling, Anna Hertle and Ursula Weiß; I want to thank Bahar Aksan and Stefanie Zeuch for long, nice lunchtimes, and Jing Yan and Yumeng Wang for friendly chats in the office.

Last but not least I would like to thank my husband Florian for his continued support, endless patience, endurance, encouragement and snack supply, as well as my sister and parents, who supported me every step of the way.

VI. References

1 Baur, K. *et al.* Growth/differentiation factor 15 controls number of ependymal and neural stem cells in the ventricular/subventricular zone. *bioRxiv* (2022).

2 Baur, K. *et al.* A novel stem cell type at the basal side of the subventricular zone maintains adult neurogenesis. *EMBO Rep*, e54078 (2022). https://doi.org:10.15252/embr.202154078

3 Altman, J. Are new neurons formed in the brains of adult mammals? *Science* **135**, 1127-1128 (1962). https://doi.org:10.1126/science.135.3509.1127

4 Sokolov, E. N. & Nezlina, N. I. Long-term memory, neurogenesis, and signal novelty. *Neurosci Behav Physiol* **34**, 847-857 (2004). https://doi.org:10.1023/b:neab.0000038138.75801.85

5 Sharp, F. R., Liu, J. & Bernabeu, R. Neurogenesis following brain ischemia. *Brain Res Dev Brain Res* **134**, 23-30 (2002). https://doi.org:10.1016/s0165-3806(01)00286-3

6 Reynolds, B. A. & Weiss, S. Generation of neurons and astrocytes from isolated cells of the adult mammalian central nervous system. *Science* **255**, 1707-1710 (1992). https://doi.org:10.1126/science.1553558

7 Doetsch, F., Garcia-Verdugo, J. M. & Alvarez-Buylla, A. Cellular composition and three-dimensional organization of the subventricular germinal zone in the adult mammalian brain. *J Neurosci* **17**, 5046-5061 (1997).

8 Seri, B., Garcia-Verdugo, J. M., McEwen, B. S. & Alvarez-Buylla, A. Astrocytes give rise to new neurons in the adult mammalian hippocampus. *J Neurosci* **21**, 7153-7160 (2001).

9 Del Bigio, M. R. The ependyma: a protective barrier between brain and cerebrospinal fluid. *Glia* **14**, 1-13 (1995). https://doi.org:10.1002/glia.440140102

10 Mirzadeh, Z., Merkle, F. T., Soriano-Navarro, M., Garcia-Verdugo, J. M. & Alvarez-Buylla, A. Neural stem cells confer unique pinwheel architecture to the ventricular surface in neurogenic regions of the adult brain. *Cell Stem Cell* **3**, 265-278 (2008). https://doi.org:10.1016/j.stem.2008.07.004

11 Codega, P. *et al.* Prospective identification and purification of quiescent adult neural stem cells from their in vivo niche. *Neuron* **82**, 545-559 (2014). https://doi.org:10.1016/j.neuron.2014.02.039

12 Khatri, P. *et al.* Proliferation and cilia dynamics in neural stem cells prospectively isolated from the SEZ. *Sci Rep* **4**, 3803 (2014). https://doi.org:10.1038/srep03803

13 Chenn, A. & McConnell, S. K. Cleavage orientation and the asymmetric inheritance of Notch1 immunoreactivity in mammalian neurogenesis. *Cell* **82**, 631-641 (1995). https://doi.org:10.1016/0092-8674(95)90035-7

14 Kosodo, Y. *et al.* Asymmetric distribution of the apical plasma membrane during neurogenic divisions of mammalian neuroepithelial cells. *EMBO J* **23**, 2314-2324 (2004). https://doi.org:10.1038/sj.emboj.7600223

15 Huttner, W. B. & Kosodo, Y. Symmetric versus asymmetric cell division during neurogenesis in the developing vertebrate central nervous system. *Curr Opin Cell Biol* **17**, 648-657 (2005). https://doi.org:10.1016/j.ceb.2005.10.005

16 Obernier, K. *et al.* Adult Neurogenesis Is Sustained by Symmetric Self-Renewal and Differentiation. *Cell Stem Cell* **22**, 221-234 e228 (2018). https://doi.org:10.1016/j.stem.2018.01.003

17 Doetsch, F., Garcia-Verdugo, J. M. & Alvarez-Buylla, A. Regeneration of a germinal layer in the adult mammalian brain. *Proc Natl Acad Sci U S A* **96**, 11619-11624 (1999). https://doi.org:10.1073/pnas.96.20.11619

18 Cesetti, T. *et al.* Analysis of stem cell lineage progression in the neonatal subventricular zone identifies EGFR+/NG2- cells as transit-amplifying precursors. *Stem Cells* **27**, 1443-1454 (2009). https://doi.org:10.1002/stem.74

19 Doetsch, F., Petreanu, L., Caille, I., Garcia-Verdugo, J. M. & Alvarez-Buylla, A. EGF converts transit-amplifying neurogenic precursors in the adult brain into multipotent stem cells. *Neuron* **36**, 1021-1034 (2002).

20 Lim, D. A. & Alvarez-Buylla, A. The Adult Ventricular-Subventricular Zone (V-SVZ) and Olfactory Bulb (OB) Neurogenesis. *Cold Spring Harb Perspect Biol* **8** (2016). https://doi.org:10.1101/cshperspect.a018820

21 Lois, C. & Alvarez-Buylla, A. Long-distance neuronal migration in the adult mammalian brain. *Science* **264**, 1145-1148 (1994).

22 Lois, C., Garcia-Verdugo, J. M. & Alvarez-Buylla, A. Chain migration of neuronal precursors. *Science* **271**, 978-981 (1996). https://doi.org:10.1126/science.271.5251.978

23 Voigt, T. Development of glial cells in the cerebral wall of ferrets: direct tracing of their transformation from radial glia into astrocytes. *J Comp Neurol* **289**, 74-88 (1989). https://doi.org:10.1002/cne.902890106

24 Culican, S. M., Baumrind, N. L., Yamamoto, M. & Pearlman, A. L. Cortical radial glia: identification in tissue culture and evidence for their transformation to astrocytes. *J Neurosci* **10**, 684-692 (1990).

25 Doetsch, F., Caille, I., Lim, D. A., Garcia-Verdugo, J. M. & Alvarez-Buylla, A. Subventricular zone astrocytes are neural stem cells in the adult mammalian brain. *Cell* **97**, 703-716 (1999).

26 Laywell, E. D., Rakic, P., Kukekov, V. G., Holland, E. C. & Steindler, D. A. Identification of a multipotent astrocytic stem cell in the immature and adult mouse brain. *Proc Natl Acad Sci U S A* **97**, 13883-13888 (2000). https://doi.org:10.1073/pnas.250471697

27 Sun, W. *et al.* SOX9 Is an Astrocyte-Specific Nuclear Marker in the Adult Brain Outside the Neurogenic Regions. *J Neurosci* **37**, 4493-4507 (2017). https://doi.org:10.1523/JNEUROSCI.3199-16.2017

28 Mich, J. K. *et al.* Prospective identification of functionally distinct stem cells and neurosphere-initiating cells in adult mouse forebrain. *Elife* **3**, e02669 (2014). https://doi.org:10.7554/eLife.02669

29 Morizur, L. *et al.* Distinct Molecular Signatures of Quiescent and Activated Adult Neural Stem Cells Reveal Specific Interactions with Their Microenvironment. *Stem Cell Reports* **11**, 565-577 (2018). https://doi.org:10.1016/j.stemcr.2018.06.005

30 Götz, M., Nakafuku, M. & Petrik, D. Neurogenesis in the Developing and Adult Brain-Similarities and Key Differences. *Cold Spring Harb Perspect Biol* **8** (2016). https://doi.org:10.1101/cshperspect.a018853

31 Turrero Garcia, M. & Harwell, C. C. Radial glia in the ventral telencephalon. *FEBS Lett* **591**, 3942-3959 (2017). https://doi.org:10.1002/1873-3468.12829

32 Anthony, T. E., Klein, C., Fishell, G. & Heintz, N. Radial glia serve as neuronal progenitors in all regions of the central nervous system. *Neuron* **41**, 881-890 (2004). https://doi.org:10.1016/s0896-6273(04)00140-0

33 Turrero García, M. & Harwell, C. C. Radial glia in the ventral telencephalon. *FEBS Letters* **591**, 3942-3959 (2017). https://doi.org:10.1002/1873-3468.12829

34 Tan, X. *et al.* Vascular Influence on Ventral Telencephalic Progenitors and Neocortical Interneuron Production. *Dev Cell* **36**, 624-638 (2016). https://doi.org:10.1016/j.devcel.2016.02.023

35 Misson, J. P., Edwards, M. A., Yamamoto, M. & Caviness, V. S., Jr. Identification of radial glial cells within the developing murine central nervous system: studies based upon a new immunohistochemical marker. *Brain Res Dev Brain Res* **44**, 95-108 (1988).

36 Tramontin, A. D., Garcia-Verdugo, J. M., Lim, D. A. & Alvarez-Buylla, A. Postnatal development of radial glia and the ventricular zone (VZ): a continuum of the neural stem cell compartment. *Cereb Cortex* **13**, 580-587 (2003). https://doi.org:10.1093/cercor/13.6.580

37 Miyama, S., Takahashi, T., Goto, T., Bhide, P. G. & Caviness, V. S., Jr. Continuity with ganglionic eminence modulates interkinetic nuclear migration in the neocortical pseudostratified ventricular epithelium. *Exp Neurol* **169**, 486-495 (2001). https://doi.org:10.1006/exnr.2001.7676

38 Florio, M. & Huttner, W. B. Neural progenitors, neurogenesis and the evolution of the neocortex. *Development* **141**, 2182-2194 (2014). https://doi.org:10.1242/dev.090571

39 Pilz, G. A. *et al.* Amplification of progenitors in the mammalian telencephalon includes a new radial glial cell type. *Nat Commun* **4**, 2125 (2013). https://doi.org:10.1038/ncomms3125

40 Kriegstein, A. R. & Gotz, M. Radial glia diversity: a matter of cell fate. *Glia* **43**, 37-43 (2003). https://doi.org:10.1002/glia.10250

41 Kriegstein, A. & Alvarez-Buylla, A. The glial nature of embryonic and adult neural stem cells. *Annu Rev Neurosci* **32**, 149-184 (2009). https://doi.org:10.1146/annurev.neuro.051508.135600

42 Alves, J. A., Barone, P., Engelender, S., Froes, M. M. & Menezes, J. R. Initial stages of radial glia astrocytic transformation in the early postnatal anterior subventricular zone. *J Neurobiol* **52**, 251-265 (2002). https://doi.org:10.1002/neu.10087

43 Fuentealba, L. C. *et al.* Embryonic Origin of Postnatal Neural Stem Cells. *Cell* **161**, 1644-1655 (2015). https://doi.org:10.1016/j.cell.2015.05.041

44 Kempermann, G., Jessberger, S., Steiner, B. & Kronenberg, G. Milestones of neuronal development in the adult hippocampus. *Trends Neurosci* **27**, 447-452 (2004). https://doi.org:10.1016/j.tins.2004.05.013

45 Yuzwa, S. A. *et al.* Developmental Emergence of Adult Neural Stem Cells as Revealed by Single-Cell Transcriptional Profiling. *Cell Rep* **21**, 3970-3986 (2017). https://doi.org:10.1016/j.celrep.2017.12.017

46 Capilla-Gonzalez, V., Cebrian-Silla, A., Guerrero-Cazares, H., Garcia-Verdugo, J. M. & Quinones-Hinojosa, A. Age-related changes in astrocytic and ependymal cells of the subventricular zone. *Glia* **62**, 790-803 (2014). https://doi.org:10.1002/glia.22642

47 Daynac, M., Morizur, L., Chicheportiche, A., Mouthon, M. A. & Boussin, F. D. Age-related neurogenesis decline in the subventricular zone is associated with specific cell cycle regulation changes in activated neural stem cells. *Sci Rep* **6**, 21505 (2016). https://doi.org:10.1038/srep21505

48 Luo, J., Daniels, S. B., Lennington, J. B., Notti, R. Q. & Conover, J. C. The aging neurogenic subventricular zone. *Aging Cell* **5**, 139-152 (2006). https://doi.org:10.1111/j.1474-9726.2006.00197.x

49 Conover, J. C. & Shook, B. A. Aging of the subventricular zone neural stem cell niche. *Aging Dis* **2**, 49-63 (2011).

50 Luo, J., Shook, B. A., Daniels, S. B. & Conover, J. C. Subventricular zone-mediated ependyma repair in the adult mammalian brain. *J Neurosci* **28**, 3804-3813 (2008). https://doi.org:10.1523/JNEUROSCI.0224-08.2008

51 Lugert, S. *et al.* Quiescent and active hippocampal neural stem cells with distinct morphologies respond selectively to physiological and pathological stimuli and aging. *Cell Stem Cell* **6**, 445-456 (2010). https://doi.org:10.1016/j.stem.2010.03.017

52 Scott, C. E. *et al.* SOX9 induces and maintains neural stem cells. *Nat Neurosci* **13**, 1181-1189 (2010). https://doi.org:10.1038/nn.2646

53 Malatesta, P. *et al.* Neuronal or glial progeny: regional differences in radial glia fate. *Neuron* **37**, 751-764 (2003). https://doi.org:10.1016/s0896-6273(03)00116-8

54 Ciccolini, F. & Svendsen, C. N. Fibroblast growth factor 2 (FGF-2) promotes acquisition of epidermal growth factor (EGF) responsiveness in mouse striatal precursor cells: identification of neural precursors responding to both EGF and FGF-2. *J Neurosci* **18**, 7869-7880 (1998).

55 Casarosa, S., Fode, C. & Guillemot, F. Mash1 regulates neurogenesis in the ventral telencephalon. *Development* **126**, 525-534 (1999). https://doi.org:10.1242/dev.126.3.525

56 Yun, K. *et al.* Modulation of the notch signaling by Mash1 and Dlx1/2 regulates sequential specification and differentiation of progenitor cell types in the subcortical telencephalon. *Development* **129**, 5029-5040 (2002). https://doi.org:10.1242/dev.129.21.5029

57 Scholzen, T. & Gerdes, J. The Ki-67 protein: from the known and the unknown. *J Cell Physiol* **182**, 311-322 (2000). https://doi.org:10.1002/(SICI)1097-4652(200003)182:3<311::AID-JCP1>3.0.CO;2-9

58 Tapia, C. *et al.* Two mitosis-specific antibodies, MPM-2 and phospho-histone H3 (Ser28), allow rapid and precise determination of mitotic activity. *Am J Surg Pathol* **30**, 83-89 (2006). https://doi.org:10.1097/01.pas.0000183572.94140.43

59 Stumm, R. K. *et al.* A dual role for the SDF-1/CXCR4 chemokine receptor system in adult brain: isoform-selective regulation of SDF-1 expression modulates CXCR4-dependent neuronal plasticity and cerebral leukocyte recruitment after focal ischemia. *J Neurosci* **22**, 5865-5878 (2002). https://doi.org:20026609

60 Stumm, R. K. *et al.* CXCR4 regulates interneuron migration in the developing neocortex. *J Neurosci* **23**, 5123-5130 (2003).

61 Belmadani, A. *et al.* The chemokine stromal cell-derived factor-1 regulates the migration of sensory neuron progenitors. *J Neurosci* **25**, 3995-4003 (2005). https://doi.org:10.1523/JNEUROSCI.4631-04.2005

62 Dziembowska, M. *et al.* A role for CXCR4 signaling in survival and migration of neural and oligodendrocyte precursors. *Glia* **50**, 258-269 (2005). https://doi.org:10.1002/glia.20170

63 Cui, L. *et al.* Stromal cell-derived factor-1 and its receptor CXCR4 in adult neurogenesis after cerebral ischemia. *Restor Neurol Neurosci* **31**, 239-251 (2013). https://doi.org:10.3233/RNN-120271

64 Bajetto, A. *et al.* Stromal cell-derived factor-1alpha induces astrocyte proliferation through the activation of extracellular signal-regulated kinases 1/2 pathway. *J Neurochem* **77**, 1226-1236 (2001).

65 Ho, S. Y. *et al.* SDF-1/CXCR4 Signaling Maintains Stemness Signature in Mouse Neural Stem/Progenitor Cells. *Stem Cells Int* **2017**, 2493752 (2017). https://doi.org:10.1155/2017/2493752

66 Bagri, A. *et al.* The chemokine SDF1 regulates migration of dentate granule cells. *Development* **129**, 4249-4260 (2002).

67 Lu, M., Grove, E. A. & Miller, R. J. Abnormal development of the hippocampal dentate gyrus in mice lacking the CXCR4 chemokine receptor. *Proc Natl Acad Sci U S A* **99**, 7090-7095 (2002). https://doi.org:10.1073/pnas.092013799

68 Gusel'nikova, V. V. & Korzhevskiy, D. E. NeuN As a Neuronal Nuclear Antigen and Neuron Differentiation Marker. *Acta Naturae* **7**, 42-47 (2015).

69 Weigmann, A., Corbeil, D., Hellwig, A. & Huttner, W. B. Prominin, a novel microvilli-specific polytopic membrane protein of the apical surface of epithelial cells, is targeted to plasmalemmal protrusions of non-epithelial cells. *Proc Natl Acad Sci U S A* **94**, 12425-12430 (1997). https://doi.org:10.1073/pnas.94.23.12425

70 Coskun, V. *et al.* CD133+ neural stem cells in the ependyma of mammalian postnatal forebrain. *Proc Natl Acad Sci U S A* **105**, 1026-1031 (2008). https://doi.org:10.1073/pnas.0710000105

71 Beckervordersandforth, R. *et al.* In vivo fate mapping and expression analysis reveals molecular hallmarks of prospectively isolated adult neural stem cells. *Cell Stem Cell* **7**, 744-758 (2010). https://doi.org:10.1016/j.stem.2010.11.017

72 Monaco, S. *et al.* A Flow Cytometry-Based Approach for the Isolation and Characterization of Neural Stem Cell Primary Cilia. *Front Cell Neurosci* **12** (2019). https://doi.org:10.3389/fncel.2018.00519

73 Bachor, T. P. *et al.* Early ciliary and prominin-1 dysfunctions precede neurogenesis impairment in a mouse model of type 2 diabetes. *Neurobiol Dis* **108**, 13-28 (2017). https://doi.org:10.1016/j.nbd.2017.07.010

74 Pugacheva, E. N., Jablonski, S. A., Hartman, T. R., Henske, E. P. & Golemis, E. A. HEF1-dependent Aurora A activation induces disassembly of the primary cilium. *Cell* **129**, 1351-1363 (2007). https://doi.org:10.1016/j.cell.2007.04.035

75 Abdi, K. *et al.* Uncovering inherent cellular plasticity of multiciliated ependyma leading to ventricular wall transformation and hydrocephalus. *Nat Commun* **9**, 1655 (2018). https://doi.org:10.1038/s41467-018-03812-w

76 Gritti, A. *et al.* Epidermal and fibroblast growth factors behave as mitogenic regulators for a single multipotent stem cell-like population from the subventricular region of the adult mouse

forebrain. *J Neurosci* **19**, 3287-3297 (1999). https://doi.org:10.1523/JNEUROSCI.19-09-03287.1999

77 Ciccolini, F. Identification of two distinct types of multipotent neural precursors that appear sequentially during CNS development. *Mol Cell Neurosci* **17**, 895-907 (2001). https://doi.org:10.1006/mcne.2001.0980

78 Cochard, L. M. *et al.* Manipulation of EGFR-Induced Signaling for the Recruitment of Quiescent Neural Stem Cells in the Adult Mouse Forebrain. *Front Neurosci* **15**, 621076 (2021). https://doi.org:10.3389/fnins.2021.621076

79 Wee, P. & Wang, Z. Epidermal Growth Factor Receptor Cell Proliferation Signaling Pathways. *Cancers (Basel)* **9** (2017). https://doi.org:10.3390/cancers9050052

80 Caric, D. *et al.* EGFRs mediate chemotactic migration in the developing telencephalon. *Development* **128**, 4203-4216 (2001). https://doi.org:10.1242/dev.128.21.4203

81 Lavoie, H. & Therrien, M. Regulation of RAF protein kinases in ERK signalling. *Nat Rev Mol Cell Biol* **16**, 281-298 (2015). https://doi.org:10.1038/nrm3979

82 Jang, H. J. *et al.* PLCgamma1: Potential arbitrator of cancer progression. *Adv Biol Regul* **67**, 179-189 (2018). https://doi.org:10.1016/j.jbior.2017.11.003

83 Tomas, A., Futter, C. E. & Eden, E. R. EGF receptor trafficking: consequences for signaling and cancer. *Trends Cell Biol* **24**, 26-34 (2014). https://doi.org:10.1016/j.tcb.2013.11.002

84 Goh, L. K., Huang, F., Kim, W., Gygi, S. & Sorkin, A. Multiple mechanisms collectively regulate clathrin-mediated endocytosis of the epidermal growth factor receptor. *J Cell Biol* **189**, 871-883 (2010). https://doi.org:10.1083/jcb.201001008

85 Ogiso, H. *et al.* Crystal structure of the complex of human epidermal growth factor and receptor extracellular domains. *Cell* **110**, 775-787 (2002). https://doi.org:10.1016/s0092-8674(02)00963-7

86 Vieira, A. V., Lamaze, C. & Schmid, S. L. Control of EGF receptor signaling by clathrin-mediated endocytosis. *Science* **274**, 2086-2089 (1996). https://doi.org:10.1126/science.274.5295.2086

87 Furuta, Y., Piston, D. W. & Hogan, B. L. Bone morphogenetic proteins (BMPs) as regulators of dorsal forebrain development. *Development* **124**, 2203-2212 (1997). https://doi.org:10.1242/dev.124.11.2203

88 Hirota, Y. *et al.* Roles of Wnt Signaling in the Neurogenic Niche of the Adult Mouse Ventricular-Subventricular Zone. *Neurochem Res* **41**, 222-230 (2016). https://doi.org:10.1007/s11064-015-1766-z

89 Ihrie, R. A. *et al.* Persistent sonic hedgehog signaling in adult brain determines neural stem cell positional identity. *Neuron* **71**, 250-262 (2011). https://doi.org:10.1016/j.neuron.2011.05.018

90 Chojnacki, A., Mak, G. & Weiss, S. PDGFRalpha expression distinguishes GFAP-expressing neural stem cells from PDGF-responsive neural precursors in the adult periventricular area. *J Neurosci* **31**, 9503-9512 (2011). https://doi.org:10.1523/JNEUROSCI.1531-11.2011

91 Demoulin, J. B. & Essaghir, A. PDGF receptor signaling networks in normal and cancer cells. *Cytokine Growth Factor Rev* **25**, 273-283 (2014). https://doi.org:10.1016/j.cytogfr.2014.03.003

92 Farahani, R. M. & Xaymardan, M. Platelet-Derived Growth Factor Receptor Alpha as a Marker of Mesenchymal Stem Cells in Development and Stem Cell Biology. *Stem Cells Int* **2015**, 362753 (2015). https://doi.org:10.1155/2015/362753

93 Luque-Molina, I. *et al.* The Orphan Nuclear Receptor TLX Represses Hes1 Expression, Thereby Affecting NOTCH Signaling and Lineage Progression in the Adult SEZ. *Stem Cell Reports* **13**, 132-146 (2019). https://doi.org:10.1016/j.stemcr.2019.05.004

94 Afzelius, B. A. Cilia-related diseases. *J Pathol* **204**, 470-477 (2004). https://doi.org:10.1002/path.1652

95 Yoder, B. K., Hou, X. & Guay-Woodford, L. M. The polycystic kidney disease proteins, polycystin-1, polycystin-2, polaris, and cystin, are co-localized in renal cilia. *J Am Soc Nephrol* **13**, 2508-2516 (2002).

96 Yoder, B. K. Role of primary cilia in the pathogenesis of polycystic kidney disease. *J Am Soc Nephrol* **18**, 1381-1388 (2007). https://doi.org:10.1681/ASN.2006111215

97 Plotnikova, O. V., Golemis, E. A. & Pugacheva, E. N. Cell cycle-dependent ciliogenesis and cancer. *Cancer Res* **68**, 2058-2061 (2008). https://doi.org:10.1158/0008-5472.CAN-07-5838

98 Han, Y. G. *et al.* Dual and opposing roles of primary cilia in medulloblastoma development. *Nat Med* **15**, 1062-1065 (2009). https://doi.org:10.1038/nm.2020

99 Roth, Y., Kimhi, Y., Edery, H., Aharonson, E. & Priel, Z. Ciliary motility in brain ventricular system and trachea of hamsters. *Brain Res* **330**, 291-297 (1985).

100 Siyahhan, B. *et al.* Flow induced by ependymal cilia dominates near-wall cerebrospinal fluid dynamics in the lateral ventricles. *J R Soc Interface* **11**, 20131189 (2014). https://doi.org:10.1098/rsif.2013.1189

101 Sorokin, S. P. Reconstructions of centriole formation and ciliogenesis in mammalian lungs. *J Cell Sci* **3**, 207-230 (1968).

102 Beisson, J. & Wright, M. Basal body/centriole assembly and continuity. *Curr Opin Cell Biol* **15**, 96-104 (2003).

103 Malicki, J. & Avidor-Reiss, T. From the cytoplasm into the cilium: bon voyage. *Organogenesis* **10**, 138-157 (2014). https://doi.org:10.4161/org.29055

104 Kinnebrew, M. *et al.* Cholesterol accessibility at the ciliary membrane controls hedgehog signaling. *Elife* **8** (2019). https://doi.org:10.7554/eLife.50051

105 Larkins, C. E., Aviles, G. D., East, M. P., Kahn, R. A. & Caspary, T. Arl13b regulates ciliogenesis and the dynamic localization of Shh signaling proteins. *Mol Biol Cell* **22**, 4694-4703 (2011). https://doi.org:10.1091/mbc.E10-12-0994

106 Garcia-Gonzalo, F. R. & Reiter, J. F. Open Sesame: How Transition Fibers and the Transition Zone Control Ciliary Composition. *Cold Spring Harb Perspect Biol* **9** (2017). https://doi.org:10.1101/cshperspect.a028134

107 Ford, M. J. *et al.* A Cell/Cilia Cycle Biosensor for Single-Cell Kinetics Reveals Persistence of Cilia after G1/S Transition Is a General Property in Cells and Mice. *Dev Cell* **47**, 509-523 e505 (2018). https://doi.org:10.1016/j.devcel.2018.10.027

108 Plotnikova, O. V., Pugacheva, E. N. & Golemis, E. A. Primary cilia and the cell cycle. *Methods Cell Biol* **94**, 137-160 (2009). https://doi.org:10.1016/S0091-679X(08)94007-3

109 Han, Y. G. & Alvarez-Buylla, A. Role of primary cilia in brain development and cancer. *Curr Opin Neurobiol* **20**, 58-67 (2010). https://doi.org:10.1016/j.conb.2009.12.002

110 Goto, H., Inoko, A. & Inagaki, M. Cell cycle progression by the repression of primary cilia formation in proliferating cells. *Cell Mol Life Sci* **70**, 3893-3905 (2013). https://doi.org:10.1007/s00018-013-1302-8

111 Tong, C. K. *et al.* Primary cilia are required in a unique subpopulation of neural progenitors. *Proc Natl Acad Sci U S A* **111**, 12438-12443 (2014). https://doi.org:10.1073/pnas.1321425111

112 Hao, K., Chen, Y., Yan, X. & Zhu, X. Cilia locally synthesize proteins to sustain their ultrastructure and functions. *Nat Commun* **12**, 6971 (2021). https://doi.org:10.1038/s41467-021-27298-1

113 Robert, A. *et al.* The intraflagellar transport component IFT88/polaris is a centrosomal protein regulating G1-S transition in non-ciliated cells. *J Cell Sci* **120**, 628-637 (2007). https://doi.org:10.1242/jcs.03366

114 Akella, J. S. *et al.* MEC-17 is an alpha-tubulin acetyltransferase. *Nature* **467**, 218-222 (2010). https://doi.org:10.1038/nature09324

115 Hubbert, C. *et al.* HDAC6 is a microtubule-associated deacetylase. *Nature* **417**, 455-458 (2002). https://doi.org:10.1038/417455a

116 North, B. J., Marshall, B. L., Borra, M. T., Denu, J. M. & Verdin, E. The human Sir2 ortholog, SIRT2, is an NAD+-dependent tubulin deacetylase. *Mol Cell* **11**, 437-444 (2003). https://doi.org:10.1016/s1097-2765(03)00038-8

117 Gradilone, S. A. *et al.* HDAC6 inhibition restores ciliary expression and decreases tumor growth. *Cancer Res* **73**, 2259-2270 (2013). https://doi.org:10.1158/0008-5472.CAN-12-2938

118 Shi, P. *et al.* HDAC6 Signaling at Primary Cilia Promotes Proliferation and Restricts Differentiation of Glioma Cells. *Cancers (Basel)* **13** (2021). https://doi.org:10.3390/cancers13071644

119 Xiang, W. *et al.* HDAC6 inhibition suppresses chondrosarcoma by restoring the expression of primary cilia. *Oncol Rep* **38**, 229-236 (2017). https://doi.org:10.3892/or.2017.5694

120 Luo, J. *et al.* The type 3 adenylyl cyclase is required for the survival and maturation of newly generated granule cells in the olfactory bulb. *PLoS One* **10**, e0122057 (2015). https://doi.org:10.1371/journal.pone.0122057

121 Antal, M. C. *et al.* Adenylate Cyclase Type III Is Not a Ubiquitous Marker for All Primary Cilia during Development. *PLoS One* **12**, e0170756 (2017). https://doi.org:10.1371/journal.pone.0170756

122 Bishop, G. A., Berbari, N. F., Lewis, J. & Mykytyn, K. Type III adenylyl cyclase localizes to primary cilia throughout the adult mouse brain. *J Comp Neurol* **505**, 562-571 (2007). https://doi.org:10.1002/cne.21510

123 Sterpka, A. & Chen, X. Neuronal and astrocytic primary cilia in the mature brain. *Pharmacol Res* **137**, 114-121 (2018). https://doi.org:10.1016/j.phrs.2018.10.002

124 Ou, Y. *et al.* Adenylate cyclase regulates elongation of mammalian primary cilia. *Exp Cell Res* **315**, 2802-2817 (2009). https://doi.org:10.1016/j.yexcr.2009.06.028

125 Hong, S. H. *et al.* Upregulation of adenylate cyclase 3 (ADCY3) increases the tumorigenic potential of cells by activating the CREB pathway. *Oncotarget* **4**, 1791-1803 (2013). https://doi.org:10.18632/oncotarget.1324

126 Qiu, L., LeBel, R. P., Storm, D. R. & Chen, X. Type 3 adenylyl cyclase: a key enzyme mediating the cAMP signaling in neuronal cilia. *Int J Physiol Pathophysiol Pharmacol* **8**, 95-108 (2016).

127 Stoufflet, J. *et al.* Primary cilium-dependent cAMP/PKA signaling at the centrosome regulates neuronal migration. *Sci Adv* **6** (2020). https://doi.org:10.1126/sciadv.aba3992

128 Chen, X. *et al.* Ablation of Type III Adenylyl Cyclase in Mice Causes Reduced Neuronal Activity, Altered Sleep Pattern, and Depression-like Phenotypes. *Biol Psychiatry* **80**, 836-848 (2016). https://doi.org:10.1016/j.biopsych.2015.12.012

129 Eggenschwiler, J. T. & Anderson, K. V. Cilia and developmental signaling. *Annu Rev Cell Dev Biol* **23**, 345-373 (2007). https://doi.org:10.1146/annurev.cellbio.23.090506.123249

130 Bijlsma, M. F., Damhofer, H. & Roelink, H. Hedgehog-stimulated chemotaxis is mediated by smoothened located outside the primary cilium. *Sci Signal* **5**, ra60 (2012). https://doi.org:10.1126/scisignal.2002798

131 Breunig, J. J. *et al.* Primary cilia regulate hippocampal neurogenesis by mediating sonic hedgehog signaling. *Proc Natl Acad Sci U S A* **105**, 13127-13132 (2008). https://doi.org:10.1073/pnas.0804558105

132 Corbit, K. C. *et al.* Vertebrate Smoothened functions at the primary cilium. *Nature* **437**, 1018-1021 (2005). https://doi.org:10.1038/nature04117

133 Rohatgi, R., Milenkovic, L. & Scott, M. P. Patched1 regulates hedgehog signaling at the primary cilium. *Science* **317**, 372-376 (2007). https://doi.org:10.1126/science.1139740

134 Milenkovic, L. *et al.* Single-molecule imaging of Hedgehog pathway protein Smoothened in primary cilia reveals binding events regulated by Patched1. *Proc Natl Acad Sci U S A* **112**, 8320-8325 (2015). https://doi.org:10.1073/pnas.1510094112

135 Haycraft, C. J. *et al.* Gli2 and Gli3 localize to cilia and require the intraflagellar transport protein polaris for processing and function. *PLoS Genet* **1**, e53 (2005). https://doi.org:10.1371/journal.pgen.0010053

136 Huangfu, D. & Anderson, K. V. Signaling from Smo to Ci/Gli: conservation and divergence of Hedgehog pathways from Drosophila to vertebrates. *Development* **133**, 3-14 (2006). https://doi.org:10.1242/dev.02169

137 Tukachinsky, H., Lopez, L. V. & Salic, A. A mechanism for vertebrate Hedgehog signaling: recruitment to cilia and dissociation of SuFu-Gli protein complexes. *J Cell Biol* **191**, 415-428 (2010). https://doi.org:10.1083/jcb.201004108

138 Caspary, T., Larkins, C. E. & Anderson, K. V. The graded response to Sonic Hedgehog depends on cilia architecture. *Dev Cell* **12**, 767-778 (2007). https://doi.org:10.1016/j.devcel.2007.03.004

139 Frasca, A. *et al.* MECP2 mutations affect ciliogenesis: a novel perspective for Rett syndrome and related disorders. *EMBO Mol Med* **12**, e10270 (2020). https://doi.org:10.15252/emmm.201910270

140 Christensen, S. T., Morthorst, S. K., Mogensen, J. B. & Pedersen, L. B. Primary Cilia and Coordination of Receptor Tyrosine Kinase (RTK) and Transforming Growth Factor beta (TGF-beta) Signaling. *Cold Spring Harb Perspect Biol* **9** (2017). https://doi.org:10.1101/cshperspect.a028167

141 Demoulin, J. B. & Montano-Almendras, C. P. Platelet-derived growth factors and their receptors in normal and malignant hematopoiesis. *Am J Blood Res* **2**, 44-56 (2012).

142 Jackson, E. L. *et al.* PDGFR alpha-positive B cells are neural stem cells in the adult SVZ that form glioma-like growths in response to increased PDGF signaling. *Neuron* **51**, 187-199 (2006). https://doi.org:10.1016/j.neuron.2006.06.012

143 Schneider, L. *et al.* PDGFRalphaalpha signaling is regulated through the primary cilium in fibroblasts. *Curr Biol* **15**, 1861-1866 (2005). https://doi.org:10.1016/j.cub.2005.09.012

144 Händel, M. *et al.* Selective targeting of somatostatin receptor 3 to neuronal cilia. *Neuroscience* **89**, 909-926 (1999).

145 Mykytyn, K. & Askwith, C. G-Protein-Coupled Receptor Signaling in Cilia. *Cold Spring Harb Perspect Biol* **9** (2017). https://doi.org:10.1101/cshperspect.a028183

146 Kong, J. H., Siebold, C. & Rohatgi, R. Biochemical mechanisms of vertebrate hedgehog signaling. *Development* **146** (2019). https://doi.org:10.1242/dev.166892

147 Briscoe, J. & Therond, P. P. The mechanisms of Hedgehog signalling and its roles in development and disease. *Nat Rev Mol Cell Biol* **14**, 416-429 (2013). https://doi.org:10.1038/nrm3598

148 Tuson, M., He, M. & Anderson, K. V. Protein kinase A acts at the basal body of the primary cilium to prevent Gli2 activation and ventralization of the mouse neural tube. *Development* **138**, 4921-4930 (2011). https://doi.org:10.1242/dev.070805

149 Wheway, G., Nazlamova, L. & Hancock, J. T. Signaling through the Primary Cilium. *Front Cell Dev Biol* **6**, 8 (2018). https://doi.org:10.3389/fcell.2018.00008

150 Acebron, S. P., Karaulanov, E., Berger, B. S., Huang, Y. L. & Niehrs, C. Mitotic wnt signaling promotes protein stabilization and regulates cell size. *Mol Cell* **54**, 663-674 (2014). https://doi.org:10.1016/j.molcel.2014.04.014

151 Zhang, K. *et al.* Primary cilia are WNT-transducing organelles whose biogenesis is controlled by a WNT-PP1 axis. *Dev Cell* **58**, 139-154 e138 (2023). https://doi.org:10.1016/j.devcel.2022.12.006

152 Strelau, J. *et al.* GDF-15/MIC-1 a novel member of the TGF-beta superfamily. *J Neural Transm Suppl*, 273-276 (2000). https://doi.org:10.1007/978-3-7091-6301-6_18

153 Schober, A. *et al.* Expression of growth differentiation factor-15/ macrophage inhibitory cytokine-1 (GDF-15/MIC-1) in the perinatal, adult, and injured rat brain. *J Comp Neurol* **439**, 32-45 (2001). https://doi.org:10.1002/cne.1333

154 Fairlie, W. D. *et al.* Epitope mapping of the transforming growth factor-beta superfamily protein, macrophage inhibitory cytokine-1 (MIC-1): identification of at least five distinct epitope specificities. *Biochemistry* **40**, 65-73 (2001). https://doi.org:10.1021/bi001064p

155 Mullican, S. E. *et al.* GFRAL is the receptor for GDF15 and the ligand promotes weight loss in mice and nonhuman primates. *Nat Med* **23**, 1150-1157 (2017). https://doi.org:10.1038/nm.4392

156 Yang, L. *et al.* GFRAL is the receptor for GDF15 and is required for the anti-obesity effects of the ligand. *Nat Med* **23**, 1158-1166 (2017). https://doi.org:10.1038/nm.4394

157 Emmerson, P. J. *et al.* The metabolic effects of GDF15 are mediated by the orphan receptor GFRAL. *Nat Med* **23**, 1215-1219 (2017). https://doi.org:10.1038/nm.4393

158 Lu, X. *et al.* EZH2-Mediated Epigenetic Suppression of GDF15 Predicts a Poor Prognosis and Regulates Cell Proliferation in Non-Small-Cell Lung Cancer. *Mol Ther Nucleic Acids* **12**, 309-318 (2018). https://doi.org:10.1016/j.omtn.2018.05.016

159 Bauskin, A. R. *et al.* The propeptide mediates formation of stromal stores of PROMIC-1: role in determining prostate cancer outcome. *Cancer Res* **65**, 2330-2336 (2005). https://doi.org:10.1158/0008-5472.CAN-04-3827

160 Li, S., Ma, Y. M., Zheng, P. S. & Zhang, P. GDF15 promotes the proliferation of cervical cancer cells by phosphorylating AKT1 and Erk1/2 through the receptor ErbB2. *J Exp Clin Cancer Res* **37**, 80 (2018). https://doi.org:10.1186/s13046-018-0744-0

161 Siddiqui, J. A. *et al.* Pathophysiological role of growth differentiation factor 15 (GDF15) in obesity, cancer, and cachexia. *Cytokine Growth Factor Rev* **64**, 71-83 (2022). https://doi.org:10.1016/j.cytogfr.2021.11.002

162 Li, F., Ruan, X. & Min, L. Targeting both sides of the GDF15-GFRAL-RET receptor complex: A new approach to achieve body weight homeostasis. *Genes Dis* **4**, 183-184 (2017). https://doi.org:10.1016/j.gendis.2017.11.004

163 Suriben, R. *et al.* Antibody-mediated inhibition of GDF15-GFRAL activity reverses cancer cachexia in mice. *Nat Med* **26**, 1264-1270 (2020). https://doi.org:10.1038/s41591-020-0945-x

164 Carrillo-Garcia, C. *et al.* Growth/differentiation factor 15 promotes EGFR signalling, and regulates proliferation and migration in the hippocampus of neonatal and young adult mice. *Development* **141**, 773-783 (2014). https://doi.org:10.1242/dev.096131

165 Strelau, J. *et al.* Progressive postnatal motoneuron loss in mice lacking GDF-15. *J Neurosci* **29**, 13640-13648 (2009). https://doi.org:10.1523/JNEUROSCI.1133-09.2009

166 Ciccolini, F. & Svendsen, C. N. Neurotrophin responsiveness is differentially regulated in neurons and precursors isolated from the developing striatum. *J Mol Neurosci* **17**, 25-33 (2001). https://doi.org:10.1385/JMN:17:1:25

167 Ciccolini, F., Mandl, C., Holzl-Wenig, G., Kehlenbach, A. & Hellwig, A. Prospective isolation of late development multipotent precursors whose migration is promoted by EGFR. *Dev Biol* **284**, 112-125 (2005). https://doi.org:10.1016/j.ydbio.2005.05.007

168 Baur, K., Holzl-Wenig, G. & Ciccolini, F. A flow cytometry-based approach for the study of primary cilia. *Methods Cell Biol* **175**, 17-31 (2023). https://doi.org:10.1016/bs.mcb.2022.07.018

169 Hughes, C. S. *et al.* Ultrasensitive proteome analysis using paramagnetic bead technology. *Mol Syst Biol* **10**, 757 (2014). https://doi.org:10.15252/msb.20145625

170 Schindelin, J. *et al.* Fiji: an open-source platform for biological-image analysis. *Nat Methods* **9**, 676-682 (2012). https://doi.org:10.1038/nmeth.2019

171 Gillespie, M. *et al.* The reactome pathway knowledgebase 2022. *Nucleic Acids Res* **50**, D687-D692 (2022). https://doi.org:10.1093/nar/gkab1028

172 Fabregat, A. *et al.* Reactome diagram viewer: data structures and strategies to boost performance. *Bioinformatics* **34**, 1208-1214 (2018). https://doi.org:10.1093/bioinformatics/btx752

173 Kefaloyianni, E. *et al.* ADAM17 substrate release in proximal tubule drives kidney fibrosis. *JCI Insight* **1** (2016). https://doi.org:10.1172/jci.insight.87023

174 Bottner, M., Suter-Crazzolara, C., Schober, A. & Unsicker, K. Expression of a novel member of the TGF-beta superfamily, growth/differentiation factor-15/macrophage-inhibiting cytokine-1 (GDF-15/MIC-1) in adult rat tissues. *Cell Tissue Res* **297**, 103-110 (1999). https://doi.org:10.1007/s004410051337

175 Carrillo García, C. *Role of growth/differentiation factor (GDF) 15 in the regulation of embryonic neural precursors*, Heidelberg, Univ., Diss., 2008, (2008).

176 Stratton, J. A., Shah, P., Sinha, S., Crowther, E. & Biernaskie, J. A tale of two cousins: Ependymal cells, quiescent neural stem cells and potential mechanisms driving their functional divergence. *FEBS J* **286**, 3110-3116 (2019). https://doi.org:10.1111/febs.14930

177 Kokovay, E. *et al.* Adult SVZ lineage cells home to and leave the vascular niche via differential responses to SDF1/CXCR4 signaling. *Cell Stem Cell* **7**, 163-173 (2010). https://doi.org:10.1016/j.stem.2010.05.019

178 Arellano, J. I., Guadiana, S. M., Breunig, J. J., Rakic, P. & Sarkisian, M. R. Development and distribution of neuronal cilia in mouse neocortex. *J Comp Neurol* **520**, 848-873 (2012). https://doi.org:10.1002/cne.22793

179 Cao, H., Chen, X., Yang, Y. & Storm, D. R. Disruption of type 3 adenylyl cyclase expression in the hypothalamus leads to obesity. *Integr Obes Diabetes* **2**, 225-228 (2016). https://doi.org:10.15761/IOD.1000149

180 Cao, M., Li, G. & Pan, J. Regulation of cilia assembly, disassembly, and length by protein phosphorylation. *Methods Cell Biol* **94**, 333-346 (2009). https://doi.org:10.1016/S0091-679X(08)94017-6

181 Patnaik, S. R. *et al.* Bardet-Biedl Syndrome proteins regulate cilia disassembly during tissue maturation. *Cell Mol Life Sci* **76**, 757-775 (2019). https://doi.org:10.1007/s00018-018-2966-x

182 Hori, A. *et al.* Prominin-1 Modulates Rho/ROCK-Mediated Membrane Morphology and Calcium-Dependent Intracellular Chloride Flux. *Sci Rep* **9**, 15911 (2019). https://doi.org:10.1038/s41598-019-52040-9

183 Pan, J., You, Y., Huang, T. & Brody, S. L. RhoA-mediated apical actin enrichment is required for ciliogenesis and promoted by Foxj1. *J Cell Sci* **120**, 1868-1876 (2007). https://doi.org:10.1242/jcs.005306

184 Johansson, C. B. *et al.* Identification of a neural stem cell in the adult mammalian central nervous system. *Cell* **96**, 25-34 (1999). https://doi.org:10.1016/s0092-8674(00)80956-3

185 Obernier, K. & Alvarez-Buylla, A. Neural stem cells: origin, heterogeneity and regulation in the adult mammalian brain. *Development* **146** (2019). https://doi.org:10.1242/dev.156059

186 Steiner, B. *et al.* Type-2 cells as link between glial and neuronal lineage in adult hippocampal neurogenesis. *Glia* **54**, 805-814 (2006). https://doi.org:10.1002/glia.20407

187 Dulken, B. W., Leeman, D. S., Boutet, S. C., Hebestreit, K. & Brunet, A. Single-Cell Transcriptomic Analysis Defines Heterogeneity and Transcriptional Dynamics in the Adult Neural Stem Cell Lineage. *Cell Rep* **18**, 777-790 (2017). https://doi.org:10.1016/j.celrep.2016.12.060

188 Furutachi, S. *et al.* Slowly dividing neural progenitors are an embryonic origin of adult neural stem cells. *Nat Neurosci* **18**, 657-665 (2015). https://doi.org:10.1038/nn.3989

189 Encinas, J. M., Vaahtokari, A. & Enikolopov, G. Fluoxetine targets early progenitor cells in the adult brain. *Proc Natl Acad Sci U S A* **103**, 8233-8238 (2006). https://doi.org:10.1073/pnas.0601992103

190 Amador-Arjona, A. *et al.* Primary cilia regulate proliferation of amplifying progenitors in adult hippocampus: implications for learning and memory. *J Neurosci* **31**, 9933-9944 (2011). https://doi.org:10.1523/JNEUROSCI.1062-11.2011

191 Luque-Molina, I. *et al.* Bone Morphogenetic Protein Promotes Lewis X Stage-Specific Embryonic Antigen 1 Expression Thereby Interfering with Neural Precursor and Stem Cell Proliferation. *Stem Cells* **35**, 2417-2429 (2017). https://doi.org:10.1002/stem.2701

192 Ward, C. J. *et al.* Cellular and subcellular localization of the ARPKD protein; fibrocystin is expressed on primary cilia. *Hum Mol Genet* **12**, 2703-2710 (2003). https://doi.org:10.1093/hmg/ddg274

193 Meier, J. C. *et al.* Knockdown of platinum-induced growth differentiation factor 15 abrogates p27-mediated tumor growth delay in the chemoresistant ovarian cancer model A2780cis. *Cancer Med* **4**, 253-267 (2015). https://doi.org:10.1002/cam4.354

194 Li, M. *et al.* Chemokine receptor CXCR4 signaling modulates the growth factor-induced cell cycle of self-renewing and multipotent neural progenitor cells. *Glia* **59**, 108-118 (2011). https://doi.org:10.1002/glia.21080

195 Abdi, K. *et al.* EGFR Signaling Termination via Numb Trafficking in Ependymal Progenitors Controls Postnatal Neurogenic Niche Differentiation. *Cell Rep* **28**, 2012-2022 e2014 (2019). https://doi.org:10.1016/j.celrep.2019.07.056

196 Kasahara, K. *et al.* EGF receptor kinase suppresses ciliogenesis through activation of USP8 deubiquitinase. *Nat Commun* **9**, 758 (2018). https://doi.org:10.1038/s41467-018-03117-y

197 Ortiz-Alvarez, G. *et al.* Adult Neural Stem Cells and Multiciliated Ependymal Cells Share a Common Lineage Regulated by the Geminin Family Members. *Neuron* **102**, 159-172 e157 (2019). https://doi.org:10.1016/j.neuron.2019.01.051

198 Redmond, S. A. *et al.* Development of Ependymal and Postnatal Neural Stem Cells and Their Origin from a Common Embryonic Progenitor. *Cell Rep* **27**, 429-441 e423 (2019). https://doi.org:10.1016/j.celrep.2019.01.088

199 Emmerson, P. J., Duffin, K. L., Chintharlapalli, S. & Wu, X. GDF15 and Growth Control. *Front Physiol* **9**, 1712 (2018). https://doi.org:10.3389/fphys.2018.01712

200 Lavoie, H., Gagnon, J. & Therrien, M. ERK signalling: a master regulator of cell behaviour, life and fate. *Nat Rev Mol Cell Biol* **21**, 607-632 (2020). https://doi.org:10.1038/s41580-020-0255-7

201 Singer, D. *et al.* Prominin-1 controls stem cell activation by orchestrating ciliary dynamics. *EMBO J* **38** (2019). https://doi.org:10.15252/embj.201899845

202 Fargeas, C. A., Huttner, W. B. & Corbeil, D. Nomenclature of prominin-1 (CD133) splice variants - an update. *Tissue Antigens* **69**, 602-606 (2007). https://doi.org:10.1111/j.1399-0039.2007.00825.x

203 Wang, H. *et al.* Evaluation of the association between the AC3 genetic polymorphisms and obesity in a Chinese Han population. *PLoS One* **5**, e13851 (2010). https://doi.org:10.1371/journal.pone.0013851

204 Zou, J., Wu, K., Lin, C. & Jie, Z. G. LINC00319 acts as a microRNA-335-5p sponge to accelerate tumor growth and metastasis in gastric cancer by upregulating ADCY3. *Am J Physiol Gastrointest Liver Physiol* **318**, G10-G22 (2020). https://doi.org:10.1152/ajpgi.00405.2018

205 Mukherjee, S. *et al.* A novel biosensor to study cAMP dynamics in cilia and flagella. *Elife* **5** (2016). https://doi.org:10.7554/eLife.14052

206 Arena, D. T. & Hofer, A. M. Imaging the cAMP Signaling Microdomain of the Primary Cilium Using Targeted FRET-Based Biosensors. *Methods Mol Biol* **2483**, 77-92 (2022). https://doi.org:10.1007/978-1-0716-2245-2_5

207 Happ, J. T. *et al.* A PKA inhibitor motif within SMOOTHENED controls Hedgehog signal transduction. *Nat Struct Mol Biol* **29**, 990-999 (2022). https://doi.org:10.1038/s41594-022-00838-z

208 Onda, T. *et al.* Type-specific regulation of adenylyl cyclase. Selective pharmacological stimulation and inhibition of adenylyl cyclase isoforms. *J Biol Chem* **276**, 47785-47793 (2001). https://doi.org:10.1074/jbc.M107233200

209 Vuolo, L., Herrera, A., Torroba, B., Menendez, A. & Pons, S. Ciliary adenylyl cyclases control the Hedgehog pathway. *J Cell Sci* **128**, 2928-2937 (2015). https://doi.org:10.1242/jcs.172635

210 Arora, K., Lund, J. R., Naren, N. A., Zingarelli, B. & Naren, A. P. AC6 regulates the microtubule-depolymerizing kinesin KIF19A to control ciliary length in mammals. *J Biol Chem* **295**, 14250-14259 (2020). https://doi.org:10.1074/jbc.RA120.013703

211 Choi, Y. H. *et al.* Polycystin-2 and phosphodiesterase 4C are components of a ciliary A-kinase anchoring protein complex that is disrupted in cystic kidney diseases. *Proc Natl Acad Sci U S A* **108**, 10679-10684 (2011). https://doi.org:10.1073/pnas.1016214108

212 Dessaud, E., McMahon, A. P. & Briscoe, J. Pattern formation in the vertebrate neural tube: a sonic hedgehog morphogen-regulated transcriptional network. *Development* **135**, 2489-2503 (2008). https://doi.org:10.1242/dev.009324

VII. Appendix

1. Solutions: Flow cytometry

Dissection sucrose solution
150 mM Sucrose
125 mM NaCl
3.5 mM KCl
1.2 mM NaH_2PO_4 x H_2O
2.4 mM $CaCl_2$ x 2 H_2O
1.3 mM $MgCl_2$ x 6 H_2O
2 mM HEPES
6.65 mM D-(+)-glucose

NSA complete medium (100 ml)
98 ml Euromed medium (Euroclone/Biozol, # ECM0883L)
1 ml GlutaMAX (Gibco, #35050061)
1 ml Penicillin/Streptomycin (Gibco, #15140)

Sort Medium (10 ml)
5 ml NSA complete medium
5 ml Leibowitz L15 medium (Gibco, #31415)
200 µl B27 supplement (Invitrogen, #17504044)
100 µl FCS (Gibco, #10720)
133 µl D-(+)-glucose 45% (Sigma-Aldrich, #G8769)
100 µl DNase (0.1% in ddH_2O, Sigma-Aldrich #D4513)

High Calcium sort medium
Sort medium
+ 10 mM $CaCl_2$

2. Protocol: Flow cytometry on cells from E18 embryos

- Dissect the SVZ in dissection sucrose
- Put tissue in Eppendorf tubes with 100 µl sort medium
- Dissociation: 100 µl tip, pipetting up and down 15x
- Add medium to a total of 300 µl

Control samples

- Autofluorescence
    - 30µl cell suspension + 270µl sort medium
- EGF block
    - 30µl in 1 ml sort medium containing 20 ng/ml EGF medium for 30 min at 37°
    - Spin down at 1000 rpm for 10 min
    - Resuspend in 150 µl
    - Add 150µl 1:500 EGF 488 in sort medium, incubate 30 min
- EGF 488
    - 30µl + 120µl sort medium
    - Add 150µl 1:500 EGF 488 in sort medium, incubate 30 min

Sort samples

- Prominin staining
    - Add medium to cell suspension so you have 200µl per animal
    - Add prominin 1:100 (so 2µl in 200µl if you have 1 animal)
    - Plate 100µl/well in 96 well plate
      This is to make sure the cells do not lie on top of each other
    - Incubate for 1h at 4°C
    - Centrifuge at 1000rpm for 5 min, discard supernatant, add 100µl sort medium, **repeat**
    - Add 100µl in first well, resuspend, transfer into the next and so on
    - (Take 30µl for prominin **control** (+270µl sort medium, measure in FACS))
    - Add sort medium to a final volume of 200µl per animal
- EGF staining
    - Add 1:500 EGF 488 solution 1:1 to the prominin stained samples (final dilution 1:1000)
    - Incubate for 30min at 4°C, measure/sort directly with FACS!

3. Protocol: Immunostaining on brain sections

Fixation

- Fix in 4% PFA in PBS for 48 h at 4°C
- Cryoprotection: put whole brains in 30% sucrose in PBS for 48 h
- Slice at Cryostat in 20 µm sections
- Adult: Rinse in PBS, put sections in 48-well plate with 500 µl PBS + 0.01% azide; store at 4°C
- E18: Mount sections directly onto "Superfrost" coated glass slides; store in slide box at -20°C

Staining

- IdU staining only:
    - Incubate in 2N HCl at 37°C for 30 min in damp chamber
    - Take off solution and neutralize in 0.1 M sodium tetraborate pH 8.5 for 30 min at RT
- Permeabilization: Incubate in 0.5% NP-40/PBS for 10 min at RT
- Background reduction: incubate in glycine 100 mM for 30 min at RT
- Blocking: Incubate in 5% FCS/PBS for 1.5h
- Add primary antibody in PBS, incubate overnight at 4°C

- Wash 3 x 10 min in PBS at RT
- Incubate secondary antibody with 1:500 DAPI in 5% FCS/PBS for 2h at RT in the dark
- Wash 3 x 10 min in PBS at RT in the dark
- Rinse in ddH2O
- Adult only: mount on "Superfrost" glass slide in drop of ddH_2O, take off water and let dry
- Add drop of Mowiol 4-88 (Merck, #81381) and put coverslip on
- Let dry stored horizontally overnight at RT or for longer at 4°C in the dark
- When dry, store at 4°C in slide box

4. Protocol: Immunostaining on whole mounts

Fixation

- Fix in 3% PFA / 4% Sucrose in PBS for 2-4h at RT or at 4°C overnight (recommended)
- Store indefinitely at 4°C in PBS + 0.01 % sodium azide

Staining

- Permeabilization: Incubate in 0.5% NP-40/PBS for 15 min at RT
- Background reduction: incubate in glycine 100 mM for 30 min at RT
- Blocking: Incubate in 5% FCS/PBS with 0.1% NP-40 for 1.5h
- Add primary antibody in 0.1% NP-40/PBS, incubate overnight at 4°C

- Wash 3 x 15 min in PBS at RT
- Incubate secondary antibody with 1:500 DAPI in 5% FCS/PBS, 0.1% NP-40 for 2h at RT in the dark
- Wash 3 x 15 min in PBS at RT in the dark
- Rinse in ddH2O
- Mount on coverslips in Mowiol 4-88 (Merck, #81381), let dry at RT for 2h
- Mount on glass slides in Mowiol
- Let dry overnight at RT in the dark
- When dry, store at 4°C in the dark

5. Protocol: Single Tube Solid Phase Sample Preparation (SP^3)

This protocol was provided by the CFMP Heidelberg.

Note: All reagents, solutions and vessels should be of high purity and keratin free to obtain optimal results. Used buffers are based on 100 mM TEAB. Never let beads without liquid, otherwise they can get dry (except in steps where that is required). It is recommended removing liquid from a tube and immediately adding fresh liquid.

Starting material:
10 µg of protein in 100 µl buffer. SP3 is done in 1.5 ml Eppis, using 1000 µL of liquid for binding to beads.

Reagents & Solutions

- Sera-Mag Speed Beads A and Sera-Mag Speed Beads B
- 100 mM TEAB pH 8.5
- 100% acetonitrile (ACN)
- 20x TCEP (57,4 mg/ml) in 50 mM TEAB = 200 mM TCEP
- 20x CAA (74,8 mg/ml) in 50 mM TEAB = 800 mM CAA
- 10% SDS
- TFA stock solution
  40% Trifluoroacetic acid in H_2O
- Lysis-buffer: 100 mM TEAB / 1%SDS / 10 mM TCEP/ 40 mM CAA
- Binding-buffer: 40% Lysis-buffer containing proteins / 60% ACN
- Wash buffer: Same as the binding buffer w/o SDS, TCEP and CAA, means in this case 60% ACN and 40% 100 mM TEAB.
- 80% Ethanol in dH_2O.
- Lys-C stock solution
  200 ng/µl solution (in 0.01% TFA), store at -20°C
- Trypsin stock solution
  200 ng/µl solution (in 0.01% TFA), store at -20°C

Procedure
Bead Preparation
Use 2µL of bead mix for sub microgramme-20µg of protein amount.

1. To prepare beads, remove from fridge and keep at room temperature for 10 minutes, suspend well using a vortex to ensure you have a homogenous slurry. Combine 20 µL of Sera-Mag A and 20 µL of Sera-Mag B. Critical: Store the beads in the fridge. Never freeze the beads.
2. Add 160 µL of dH_2O.
3. Place the tube with beads on a magnetic rack and let beads settle for about 2 minutes, subsequently remove and discard supernatant.
4. Rinse beads with 200µL of water by pipette mixing (take off magnetic stand, put back on before removing supernatant). Repeat this twice.
5. Store beads in 20µL of dH_2O (100 µg/µl total bead concentration) in the fridge for up to 2 weeks.
6. Use 2µL of bead-mix per sample; make sure the beads are well resuspended in the solution (pipette mix) before adding to a sample.

Reduction & Alkylation

We use 10mM TCEP and 40mM CAA (final concentration) for reduction/alkylation.
Set up samples as follows:

100 µl starting material
+ 20 µl 20x TCEP
+ 20 µl 20x CAA
+ 40 µl 10% SDS
+ 220 µl 100 mM TEAB

400 µl total volume

Incubate at 95°C for 5 minutes, then 25 minutes at 70°C in the shaker for reduction/alkylation. Cool down to room temperature.

SP3 Protein Clean-up and digestion

1. Add 600µl ACN to each sample and then 2µl SP3-beads. Mix
2. Incubate for 20 minutes at room temperature in the shaker.
3. Centrifuge briefly to bring all beads and liquid from the lid of the vial, then place on the magnetic rack and incubate for 2 minutes. Remove and collect supernatant, store as SP3 FT1 in -20°C.
4. Add 200µl wash buffer, mix by pipetting.
5. Sonicate for 7 minutes in the ultrasound bath.
6. Incubate for 20 minutes at room temperature in the shaker.
7. Spin samples to bring all beads and liquid from the lid of a vial. Place on the magnetic rack, incubate for another 2 minutes at room temperature. Remove supernatant. It is stored as SP3 FT2 at -20°C.
8. Add 200µl of 80% ethanol in Biosolve-H_2O, mix by pipetting and incubate for 2 minutes on the magnetic rack. Remove and discard supernatant.
9. Repeat step 8.
10. Add 180µL of 100% ACN, mix by pipetting and incubate for 2 minutes on the magnetic rack. Remove and discard supernatant.
11. Dry beads in 37 °C incubator for some minutes. Ensure beads change from a wet dark rust color to a dry light rust color, to ensure all acetonitrile has really evaporated.
12. Add 100µL of 100mM TEAB to beads.
13. Sonicate for 7 min and quickly spin down.
14. Add 1 µl proteinase Lys-C (200ng/µl). Mix by pipetting, thereby removing residues of the beads from the wall and incubate for 4h at 37°C in the shaker.
15. Add 1µl trypsin (200ng/µl). Mix by pipetting and incubate over night at 37°C in the shaker.

Next day

16. Allow the digest to cool down to RT. Spin samples in the centrifuge to bring all beads and liquid from the lid of a vial.
17. Stop the digestion by adding 3µl 40%TFA. Verify that pH is < 2. Place on the magnetic rack and incubate for another 2 minutes at room temperature.
18. Transfer supernatant to fresh Eppis.

Proceed with Stage tip desalting of supernatant and LC-MS analysis.

6. Protocol: mRNA reverse transcription

Per sample (20 µl) in a PCR tube:

- 2 µl Oligo(dT)15 primers + 18 µl purified RNA
- Mix well, spin down
- put in PCR machine: 3 min at 80°C
- Prepare reverse transcription Master Mix (per sample):

1x	Reagent	5x	10x	15x	20x	25x	30x	35x	40x	45x	50x
8 µl	**H_2O RNase-free**	40	80	120	160	200	240	280	320	360	400
8 µl	**5x M-MLV buffer**	40	80	120	160	200	240	280	320	360	400
2 µl	**dNTPs 10 mM**	10	20	30	40	50	60	70	80	90	100
2 µl	**M-MLV RT**	10	20	30	40	50	60	70	80	90	100
20 µl	**TOTAL**	100	200	300	400	500	600	700	800	900	1000

- Add 20 µl reverse transcription Master Mix per tube
- Mix, spin down
- put in PCR machine: 1 h at 42°C, 3 min at 80°C
- Freeze at -20°C until qPCR

7. Solutions: Western Blot

RIPA-buffer
150 mM NaCl
50 mM Tris-HCl pH 8.0
1% Triton X-100
0.1% SDS
(0.5% sodium deoxycholate) added fresh every time

Upper Buffer
0.5 M Tris-HCl pH 6.8

Lower Buffer
1.5 M Tris-HCl pH 8.8

Running Buffer
25 mM Tris
190 mM glycine
0.1% SDS

Transfer Buffer
20 mM Tris
150 mM Glycine
0.1% SDS
20% Methanol

TBS (10x)
24.23 g Tris-HCl pH 7.6
80.06 g NaCl

TBS-T (1L)
100 ml TBS (10x)
1 ml Tween-20

8. Protocol: Western Blot

Sample Preparation for cells

- *Prepare RIPA buffer: add sodium deoxycholate for a final concentration of 0.5%; add protease inhibitor to 1x final concentration*
- Dissect the V-SVZ in dissection sucrose
- Put tissue in Eppendorf tubes with 100 µl medium (sort medium or NSA+B27)
- Dissociation
    - 200 µl tip, 15x for prenatal
    - Filter through cell strain tube (blue lid)
- Add medium to a total of 3 ml per animal and mix well
- Distribute cell suspension into up to 6 Eppendorf tubes for each animal (500µl/eppi)
- Add 1:1 **warm** medium containing 1:500 EGF (stock 20 µg/ml; final concentration 1:1000 / 20 ng/µl) and incubate it at 37°C for 7 minutes
- Centrifuge cells for 8-10 minutes at 2000 rpm, take off supernatant
- Resuspend cells in 30 µl fresh RIPA buffer containing 1x protease inhibitor, vortex thoroughly and freeze at -20°C until western blot

Sample Preparation for whole tissue

- Dissect the V-SVZ in dissection sucrose
- Incubate overnight in 1 ml NSA + 2 % B27
- *Prepare RIPA buffer: add sodium deoxycholate for a final concentration of 0.5%; add protease inhibitor to 1x final concentration*
- Put entire V-SVZ in to 300 µl freshly prepared RIPA buffer
- Pipette up and down to dissolve, vortex, and freeze at -20°C until western blot

SDS-PAGE

- Cast gel according to notes in the hood
- Preparing the samples
    - Add 4x sample buffer
    - Spin down to mix
    - Boil at 95°C for 5 min in heat block
- Running the gel:
    - Put gels in running apparatus (small plates on the inside)
    - Fill up the chamber with 1x Running buffer
    - Load 10 µg protein (one well in 15 well comb can fit around 25 µl sample)
    - Ladder: use 4 µl
    - Add 2-4µl pure sample buffer for empty wells
    - Run gel at 30 mA per gel (i.e. 60 mA for 2 gels, 90 mA for 3 gels, …) for 1h 20min ON ICE (use ice especially when running more than one gel to avoid overheating)

Transfer

- Cut whatman paper in gel-sized pieces (4 per gel)
- Cut membrane in gel-size
- Transfer Buffer: 100 ml 10x buffer + 200 ml methanol + 700 ml ddH2O
- Soak sponges in transfer buffer

- Put in following order: Plastic net - Cathode (contact on the left) - Plastic net - 3 sponges - 2 filter papers – Gel – Membrane - 2 filter papers (smooth out at this point to avoid bubbles) - 3 sponges - Plastic net - Anode (contact on the right) – net - cover
- Fill up with transfer buffer (around 800 ml total)
- Squish everything together and put in transfer box
- Run at 20 V for 1.5-2 h

Staining

- Optional: Visualization with Ponceau solution
    - Rinse well with ddH_2O
    - Put membrane in Ponceau solution
    - Shake at RT for 5 min
    - Wash repeatedly in ddH_2O until red bands are visible
    - Scan at ChemiDoc with Ponceau setting
- Block with 5% Milk / TBS-T for 1 h at RT
- Primary antibodies: dilute in TBS-T + 0.01% azide, incubate at 4°C overnight on shaker

- Wash 3x 5 min in TBS-T
- Incubate with secondary antibody conjugated with HRP in 5% Milk / TBS-T for 1h at RT (use secondary for weaker protein first if detecting multiple proteins)
- Wash 3x 5 min in TBS-T
- Rinse with water
- Mix ECL solutions (1:1, about 400µl / membrane)
- Put membrane in cut-open autoclave bag or on a plastic lid, add ECL
- Detect at ChemiDoc